OXYGEN ABSORPTION IN THREE PHASE FLUIDIZED BEDS

by 7214

MICHAEL PAUL NEWCOMER

B. S., Kansas State University, 1968

A MASTER'S THESIS

submitted in partial fulfillment of the

requirements for the degree

MASTER OF SCIENCE

Department of Chemical Engineering

KANSAS STATE UNIVERSITY

Manhattan, Kansas

1971

Approved by:

L. T. Fan

Major Professor

THIS BOOK CONTAINS NUMEROUS PAGES WITH THE ORIGINAL PRINTING BEING SKEWED DIFFERENTLY FROM THE TOP OF THE PAGE TO THE BOTTOM.

THIS IS AS RECEIVED FROM THE CUSTOMER.

ABSTRACT

The mass transfer characteristics of three phase fluidized beds for the absorption of oxygen in water were investigated in this work. Overall volumetric mass transfer coefficients were experimentally measured for the various types of three phase fluidized beds studied, and it was found that the mass transfer performance of three phase fluidized beds is very dependent on the particle properties of the bed. Large particles of high density material produce the best fluidized bed mass transfer performance.

Overall volumetric mass transfer coefficients were experimentally measured for an equivalent conventional bubble column, and it was found that the mass transfer performance of all types of three phase fluidized beds studied is superior to that of the conventional bubble column. It was concluded that the three phase fluidized bed may have considerable practicle value as a new efficient means of promoting oxygen transfer.

Overall volumetric mass transfer coefficients were determined based on two flow (mixing) models, the plug flow model and the dispersion model. The plug flow model assumes that axial liquid phase dispersion is zero, while the dispersion model relaxes this assumption. Therefore, for application of the dispersion model, axial liquid phase dispersion characteristics for the systems studied were experimentally determined. Mass transfer coefficients based on the plug flow and dispersion models were compared, with the expected result that dispersion model coefficients were larger than plug flow model coefficients.

Since it was determined experimentally that appreciable liquid dispersion existed in the systems studied, the mass transfer coefficient based on the dispersion model is a better approximation to the true mass transfer

coefficient than that based on the plug flow model. Thus, the empirical correlations obtained from the results of this work were developed from the dispersion model.

Empirical correlations were developed for the purpose of predicting liquid phase dispersion and mass transfer characteristics of three phase fluidized beds, and also for predicting mass transfer to pressure drop performance of three phase fluidized beds as compared to the conventional bubble column. The empirical correlations obtained were used for the hypothetical design of a three phase fluidized bed for the absorption of oxygen in water, and this design was compared to the hypothetical design of an equivalent conventional bubble column.

TABLE OF CONTENTS

LIST OF FIGURES

INTRODUCTION

A. Objective

The primary objective of this research was to investigate the mass transfer characteristics of three phase fluidized beds for the absorption of oxygen in water, and to compare the results obtained to those obtained in the corresponding conventional bubble columns. The secondary objective of this work was to extend the results obtained to the design of large scale fluidized bed systems for the absorption of oxygen in water.

Recently there has been a great deal of interest in the production of protein from hydrocarbons and in the field of sewage treatment. The most basic problem which these two areas have in common is the absorption of oxygen by a liquid phase, therefore, new efficient means of promoting oxygen transfer are quite desirable. The three phase fluidized bed has been investigated in order to determine its applicability to the oxygen transfer problem.

A great deal of design work has been done by application of two limiting cases, the plug flow model and the perfectly mixed model. The three phase fluidized bed cannot be adequately described by either of these models, but is instead an intermediate case, best described by the dispersion model. Therefore, the three phase fluidized bed provides a very good example of how the dispersion model can be applied to the design of a mass transfer system.

B. Literature Survey

A search of the literature did not produce any previous work done specifically on oxygen absorption in three phase fluidized beds. Maxon and Johnson [7, 13] have reported some experimental work done on carbon dioxide

absorption in a three phase fluidized bed. Their work involved the absorption of carbon dioxide in water with both 0.22 mm. sand particles and 0.50-0.80 mm. glass particles as the fluidized bed material. According to them, the absorption rate increased with increasing liquid velocity for all particle sizes and decreased with increasing particle size for all liquid velocities. The absorption rates were lower than those obtained in an equivalent gas-liquid system with no particles present. This was explained as being due to a higher rate of bubble coalescence and, consequently, a lower gas-liquid interfacial area in the three phase fluidized bed.

Levich [7, 12] has reported some experimental work done on gas-liquid interfacial area and bubble size in a three phase fluidized bed. According to Levich, for the air-water system with 6.0 mm. glass particles as the fluidized bed material, the bubble size decreased and the gas-liquid interfacial area increased with increasing height above the fluidized bed inlet. Bubble breakup occurred at a higher rate in beds of low expansion. From these results, Levich has suggested that beds of larger particles may be of practical value because of the improved gas absorption which, presumably, may be obtained.

In the area of liquid dispersion, Chen and Douglas [3] have reported that for gas-liquid contact in a countercurrent turbulent bed contactor, the axial liquid phase dispersion coefficient increases with both increasing gas and liquid rates. In their work, the gas and liquid rates were of the same order of magnitude in terms of $lb_m/hr\text{-}ft^2$.

THEORETICAL

Two models of flow (mixing) which can be used to describe the mass transfer characteristics of the three phase fluidized bed absorption system are the plug flow model and the dispersion model. In this work, overall volumetric mass transfer coefficients for both the plug flow model and dispersion model are based on a unit volume of a fluidized bed. The equations describing the two models with the indicated basis are derived in the Appendix.[1]

For the plug flow model

$$\Gamma_e = \text{EXP}\ [-(R)_{PF}] \tag{1}$$

For the dispersion model

$$\Gamma_e = \frac{4\beta \text{EXP}(Pe_L/2)}{(1+\beta)^2\ \text{EXP}(\beta Pe_L/2) - (1-\beta)^2\ \text{EXP}(-\beta Pe_L/2)} \tag{2}$$

$$\beta = \sqrt{1 + 4(R)_{DM}/Pe_L} \tag{3}$$

where

Γ_e = $\bar{C}_e/\bar{C}_i$, dimensionless

$\bar{C}_e$ = $C^* - C_e$, lbmole O_2/lbmole H_2O

$\bar{C}_i$ = $C^* - C_i$, lbmole O_2/lbmole H_2O

C^* = liquid phase O_2 concentration at the gas-liquid interface, lbmole O_2/lbmole H_2O

[1]See Appendix, Section I.

C_e = liquid phase O_2 concentration at the fluidized bed exit, lbmole O_2/lbmole H_2O

C_i = liquid phase O_2 concentration at the fluidized bed inlet, lbmole O_2/lbmole H_2O

$(R)_{PF}$ = $(K_La)_{PF}M_mZ/L'$, dimensionless absorption number for the plug flow model

$(R)_{DM}$ = $(K_La)_{DM}M_mZ/L'$, dimensionless absorption number for the dispersion model

$(K_La)_{PF}$ = overall volumetric mass transfer coefficient for the plug flow model, based on a unit volume of fluidized bed, lbmole/hr-ft^3-ΔC

$(K_La)_{DM}$ = overall volumetric mass transfer coefficient for the dispersion model, based on a unit volume of fluidized bed, lbmole/hr-ft^3-ΔC

Pe_L = $L'Z/\rho_mD$, dimensionless axial liquid phase Peclet number

L' = superficial liquid mass velocity based on the cross sectional area of the fluidized bed, lb_m/hr-ft^2

Z = total fluidized bed length, ft

M_m = liquid molecular weight, lb_m/lbmole

ρ_m = liquid density, lb_m/ft^3

D = apparent axial liquid phase dispersion coefficient, ft^2/hr

It should be noted that D is defined as the apparent axial liquid phase dispersion coefficient, because we have more than just the liquid phase present in the three phase fluidized bed. Details are shown in the Appendix.[1] Dimensional analysis of Pe_L shows that our definition is equivalent to

[1]See Appendix, Section I.

$Pe_L = uZ/D_m$, where u is the liquid velocity and D_m[1] is the axial liquid phase dispersion coefficient. Thus, our definition of Pe_L is consistent with the definition found in the literature [5, 10].

The assumptions made in the development of Equations (1), (2) and (3) are

1. Steady state operation prevails.
2. The $O_2 - H_2O$ solution is very dilute. Therefore $L'_{in} = L'_{out} = L'$.
3. The principal resistance to mass transfer resides in the liquid phase.
4. The gas-liquid interface is in equilibrium. The interface is at the temperature of the liquid and the prevailing system pressure.
5. All mass transfer takes place in the fluidized bed.
6. The rate of dispersion in the radial direction is infinite and the dispersion coefficient in the axial direction is finite and constant.
7. Wall effects have a negligible influence on the performance of the fluidized bed.

Assumption number 5 is a written statement of Danckwerts' boundary condition [5] at the fluidized bed exit. This exit boundary condition assumes that mass transfer (absorption) ceases at the fluidized bed exit, thus, $\frac{dC}{dx} = 0$ at $x = Z$. Although this is not exactly correct, experimental measurements have shown that $\frac{dC}{dx} \cong 0$ at $x = Z$.[2] Thus, the assumption is justified.

Assumption number 6 implies that no radial concentration gradients exist in the fluidized bed. Experimental measurements indicate that this

[1] See Appendix, Section I.

[2] See Experimental Section.

assumption is justified.[1]

In regard to assumption number 7, wall effects will be negligible as long as the ratio (D_t/D_p) is large, where D_t is the column diameter and D_p is the particle diameter. Experimental work done in packed beds [1] indicates that wall effects can be neglected for $(D_t/D_p) > 6$. In this work, $(D_t/D_p) > 10$ for all types of fluidized beds. Thus, neglecting wall effects would appear to be justified.

For the determination of overall volumetric mass transfer coefficients for the plug flow model, Equation (1) is directly applicable. A sample calculation is shown in the Appendix.[2] For the determination of overall volumetric mass transfer coefficients for the dispersion model, Equation (2) and Equation (3) are applicable when the value of the axial liquid phase Peclet number (Pe_L) is known. Pe_L is determined from liquid phase tracer studies, and the equations describing the tracer model employed are developed in the Appendix.[3]

For an impulse input of tracer [10, 11]

$$\sigma^2 = \frac{1}{\tau C_o} \int_o^\infty [t/\tau - 1]^2 \, C(t)\,dt = 2(1/Pe_L) - 2(1/Pe_L)^2 \, [1-EXP(-Pe_L)] \quad (4)$$

where

$C(t)$ = exit liquid phase tracer concentration as a function of time, gm/ml

C_o = bulk liquid phase tracer concentration at $t = 0$ based on the liquid holdup, gm/ml

[1] See Experimental Section.

[2] See Appendix, Section IV.

[3] See Appendix, Section III.

t = time, sec

τ = mean liquid residence time based on the liquid holdup, sec

σ^2 = variance of the C(t) distribution, dimensionless

The assumptions made in the development of Equation (4) are

1. The tracer input is a perfect impulse function.
2. The system is closed. There is no liquid dispersion for $x < 0$ and $x > Z$.
3. The rate of dispersion in the radial direction is infinite and the dispersion coefficient in the axial direction is finite and constant.

For the tracer studies model, assumption number 2 merits some discussion. The assumption of a closed system implies that the liquid phase is in plug flow in the column sections above and below the fluidized bed. Referring to Figure 3, this assumption is undoubtedly quite good for the entrance section below the bed support. However, the validity of the assumption for the exit section above the fluidized bed is questionable. One would suspect that the turbulent flow of gas bubbles in the exit section might cause some liquid dispersion. Assuming that $D = 0$ in the entrance section and allowing for the possibility that $D \neq 0$ in the exit section, the analogous form of Equation (4) becomes [11]

$$\sigma^2 = 2(1/Pe_L) - 2(1/Pe_L)^2 \left[1-\alpha-3/2\alpha^2 + (\alpha-1)EXP(-Pe_L)\right] \qquad (5)$$

where

$\alpha = D_e/D$, dimensionless

D_e = apparent axial liquid phase dispersion coefficient in the exit section, ft^2/hr

D = apparent axial liquid phase dispersion coefficient in the fluidized bed, ft^2/hr

Comparison of Equation (4) and Equation (5) shows that when $D_e = 0$ ($\alpha=0$), Equation (5) reduces to Equation (4). We also see that for a fixed value of $\alpha \leq 1$, as $\sigma^2 \to 1$, the respective values of Pe_L calculated from Equation (4) and Equation (5) deviate further and further. The largest experimental value of σ^2 determined was $\sigma^2 = 0.74$. For $\sigma^2 = 0.74$, Equation (4) predicts the value of Pe_L to be 1.0. At the same experimental conditions for which $Pe_L = 1.0$ for the fluidized bed, the value of Pe_L was found to be 4.8 for the plain bubble column,[1] as determined from Equation (4). Assuming that the value of D_e for the exit section above the fluidized bed is close to the value of D in the plain bubble column at the same operating conditions, we can estimate that $D_e/D = \alpha \cong 1.0/4.8 = 0.208$ for the situation where Pe_L was found to be 1.0 for the fluidized bed from Equation (4). Using this estimate, for $\alpha = 0.208$ and $\sigma^2 = 0.74$, Equation (5) predicts a value for Pe_L of 1.8. Thus, at the worst possible conditions for agreement between Equation (4) and Equation (5) ($\sigma^2 \to 1$, $Pe_L \to 0$) Equation 4 predicts a value of $Pe_L = 1.0$ and Equation (5) predicts a value of $Pe_L = 1.8$ for the fluidized bed. This discrepancy is within the range of experimental deviation encountered.[2] Thus, the use of Equation (4) to calculate experimental values of Pe_L is justified.

Pe_L is determined from Equation (4), and a graphical solution of Equation (4) is shown in Figure 1 for the range of variance encountered. β is determined from Equation (2), and a graphical solution of Equation (2) is

[1] See Figure 14.

[2] See Figure 9 through Figure 13.

shown in Figure 2a through Figure 2c. The overall volumetric mass transfer coefficient for the dispersion model is determined by application of Equations (2), (3) and (4). A sample calculation is shown in the Appendix.[1]

The equation describing the perfectly mixed model is also derived in the Appendix,[2] but it is a poor model for the particular system under consideration and will not be considered further. Additionally, equations are derived in the Appendix[3] for the case where the overall volumetric mass transfer coefficient is based on a unit volume of liquid. The mass transfer coefficient determined on this basis is not suited well to design procedures and will not be considered further.

[1]See Appendix, Section V.

[2]See Appendix, Section I.

[3]See Appendix, Section II.

THIS BOOK CONTAINS NUMEROUS PAGES WITH DIAGRAMS THAT ARE CROOKED COMPARED TO THE REST OF THE INFORMATION ON THE PAGE.

THIS IS AS RECEIVED FROM CUSTOMER.

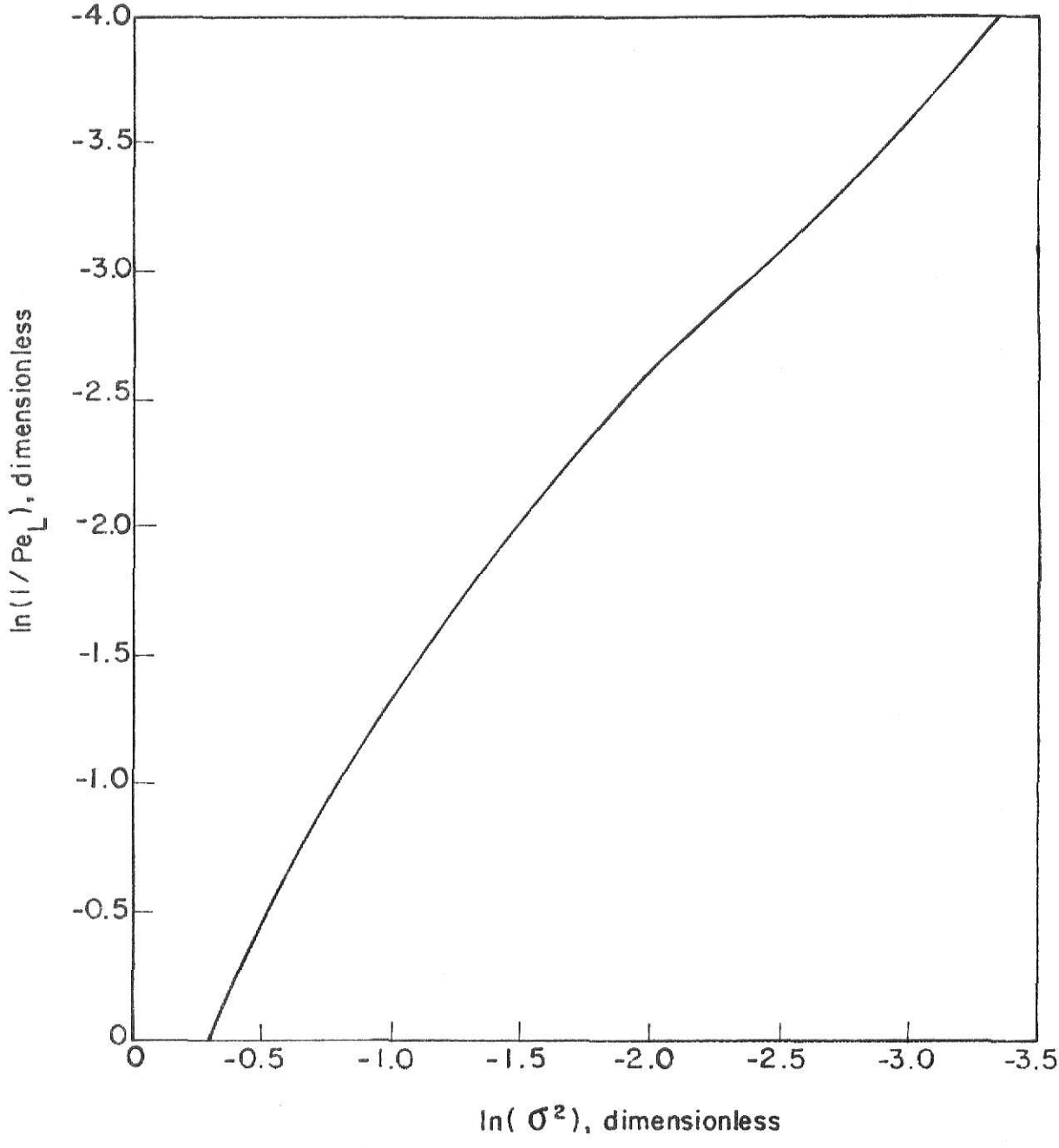

Fig. 1. Graphical solution to Equation (4).

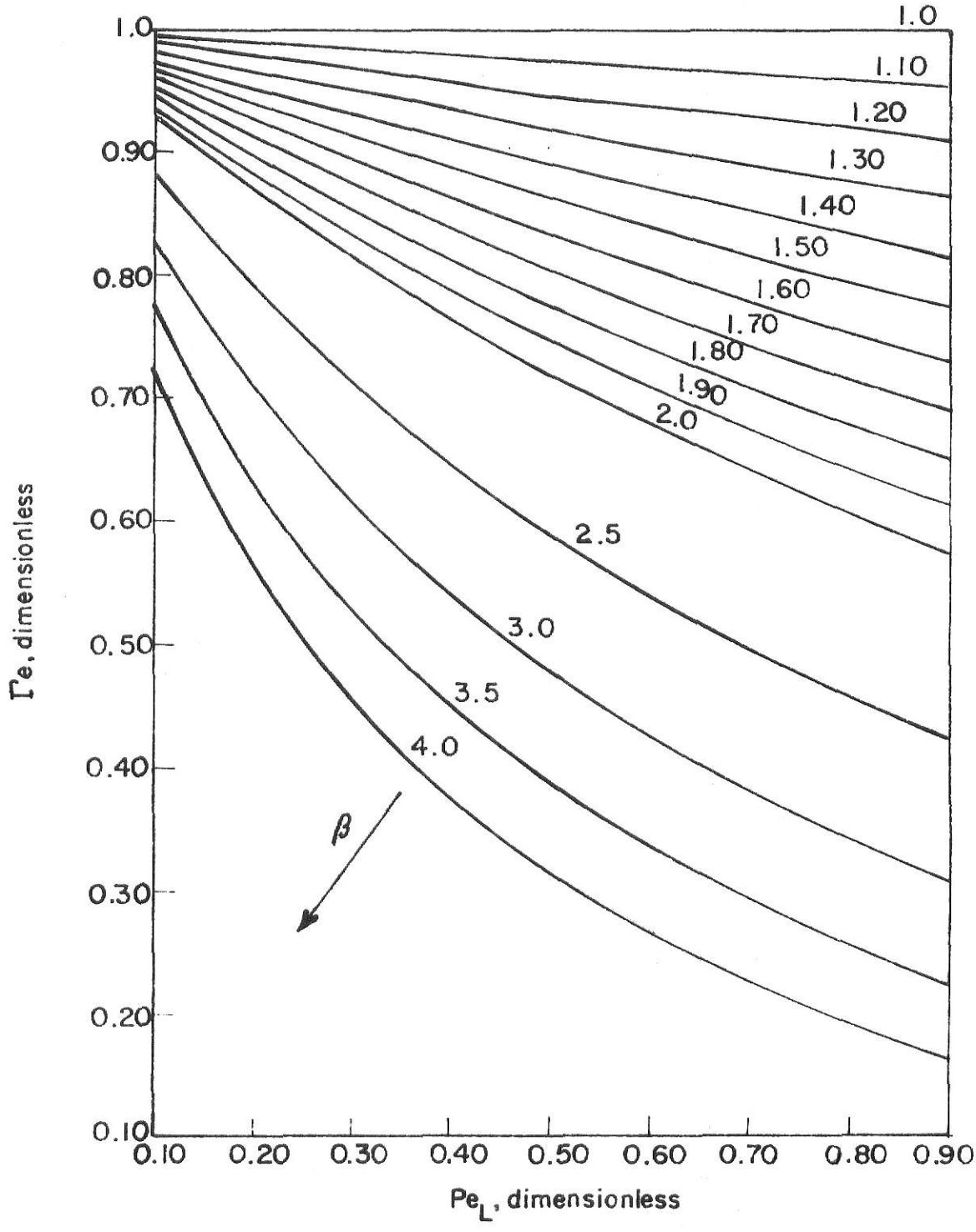

Fig. 2a. Graphical solution to Equation (2) for $Pe_L < 1.0$.

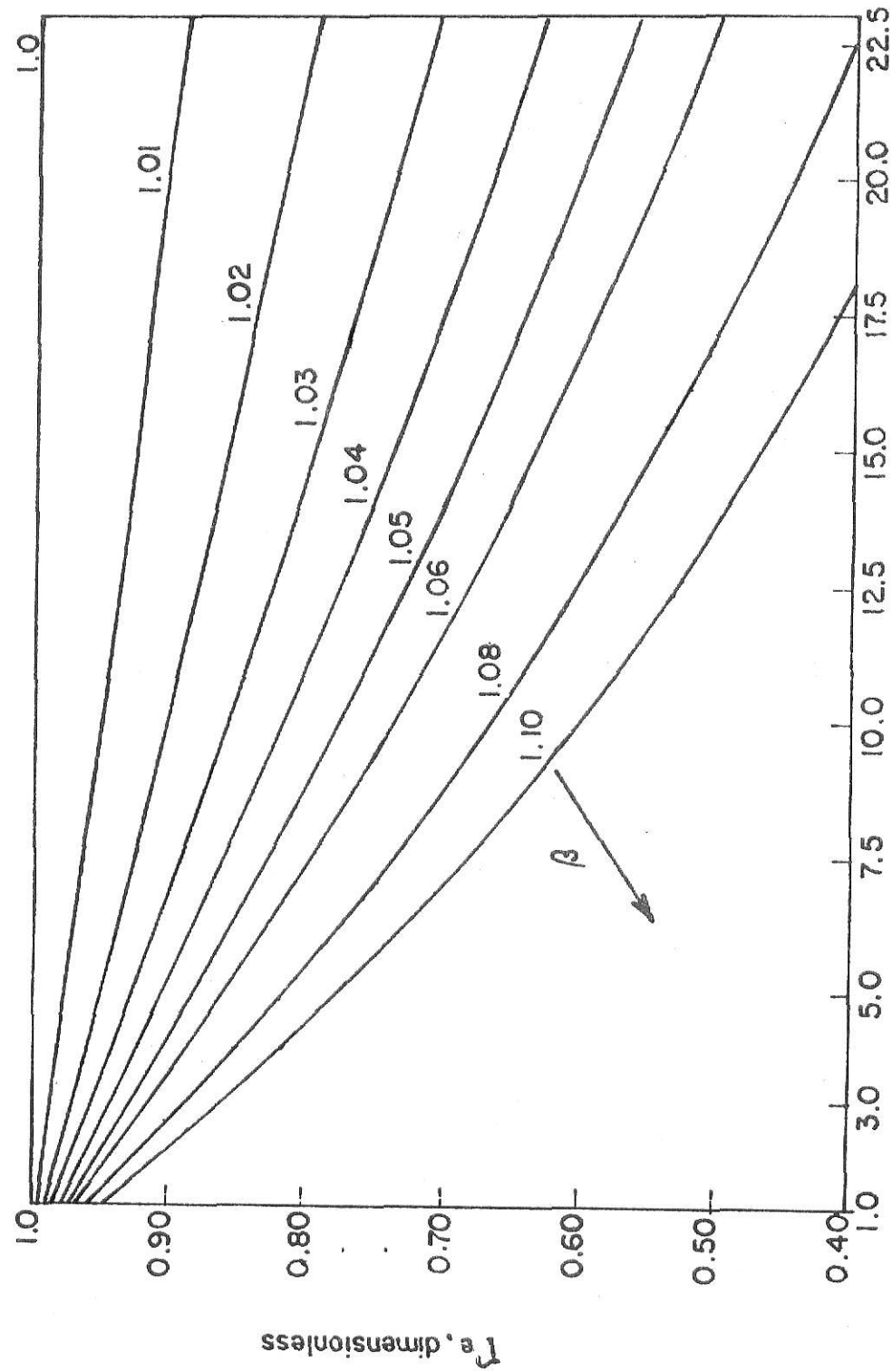

Fig. 2b. Graphical solution to Equation (2) for $Pe_L \geq 1.0$, $\beta \leq 1.10$.

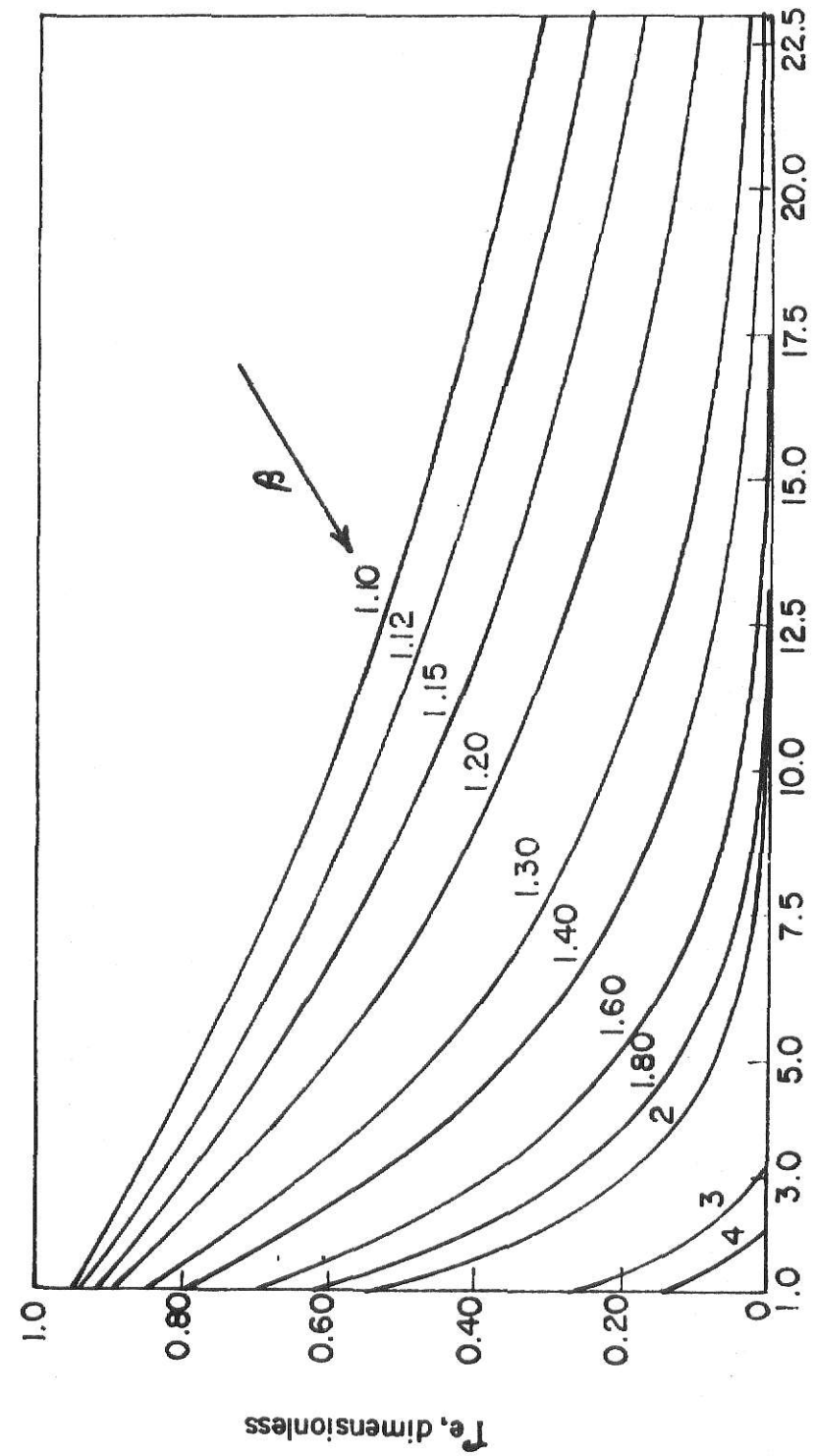

Fig. 2c. Graphical solution to Equation (2) for $Pe_L \geq 1.0$, $\beta \geq 1.10$.

EXPERIMENTAL

The basic experimental apparatus is shown in Figure 3. A 2.0" I.D. glass column was used to house the three phase fluidized bed and a fine mesh copper screen was used as the bed support. The three phase fluidized beds investigated were composed of various size and density spherical particles. Copper, stainless steel, and glass spheres were utilized at sizes from 1/16" to 3/16" in diameter and densities from 0.0938 lb_m/in^3 to 0.322 lb_m/in^3.

The liquid flow rate to the column was controlled with a liquid rotameter in conjunction with an overhead constant head tank. Two different liquid rotameters were used, one was calibrated for low liquid rates and the other for high liquid rates. The gas flow rate to the column was controlled with a gas rotameter in conjunction with a compressed oxygen bottle. The gas inlet to the column was a 1/2" diameter pipe. This was done in order to produce relatively large bubbles, so that the bubble breakup effectiveness of the fluidized bed could be determined. Also, the gas inlet was placed within 1" of the bed support in order to eliminate any premixing of the two phases.

Pressure gauges were installed at the column inlet and outlet in order to measure average column operating pressures for equilibrium calculations. For measurement of fluidization onset velocities, the pressure gauges were removed and a mercury manometer was utilized to measure pressure drop quite accurately. Liquid sampling points were provided at the column inlet and outlet in order to measure dissolved oxygen concentration and temperature of the liquid phase. The liquid sample at the column outlet was obtained by extending a 1/8" plastic tube down from the top of the column to the top of the expanded bed. It was found that no dissolved oxygen concentration change

could be detected between the top of the expanded bed and the top of the column, when the distance was 5" or less. For a distance of greater than 5", only a very small dissolved oxygen concentration change could be detected. Also, dissolved oxygen concentrations were measured across the column cross section, and no radial concentration gradients were detected.

Dissolved oxygen concentrations were measured with a lead-silver conductance cell "oxygen analyzer." Liquid temperatures were measured with a mercury thermometer for the purpose of equilibrium calculations. All experimental data was taken at an average liquid temperature of 18.5°C, the range of deviation being ±0.5°C.

Tracer studies were carried out on the liquid phase in order to access the degree of liquid dispersion over the range of experimental operating conditions. Sodium chloride solution was used as the tracer material, and was injected into the three phase fluidized bed as an impulse through a 1/16" stainless steel tube. A ground glass syringe was used to inject the tracer. The tracer exit concentration as a function of time at the top of the expanded bed was measured with a salinity probe in conjunction with a conductance meter and recorder printout.

Experimental values of the axial liquid phase Peclet number (Pe_L) are reported over the range of experimental gas rates, $14.3 \leq G' \leq 43.0$. Initially, Pe_L was measured over this range of experimental gas rates while holding the liquid rate constant. It was found that Pe_L did not vary to any significant extent with gas rate, the variation being on the same order of magnitude as the experimental deviation found in measurement of Pe_L at identical liquid and gas rates on successive runs. Thus, all experimental measurements of Pe_L were taken at the median gas rate, and considered to be

the same over the range of experimental gas rates, $14.3 \leq G' \leq 43.0$.

At this point it would be well to briefly discuss the rationale behind the ranges of liquid and gas rates investigated experimentally. The experimental liquid rates were chosen in order to operate the fluidized beds at fairly small bed expansions, i.e., less than 50%. At a large bed expansion, the particles are a relatively large distance apart and the fluidized bed approaches the operation of a plain bubble column. This was to be avoided since the effect of the fluidized bed on mass transfer was to be determined. The experimental gas rates were chosen by visual observation. A G' of 14.3 corresponds to a smooth even flow of gas bubbles through the column. A G' of 43.0 corresponds to a very turbulent flow of gas bubbles through the column. For $G' < 14.3$, a pulsating flow of gas bubbles was produced. For $G' > 43.0$ considerable gas "slugging" [8, 9] was produced. Both phenomena are to be avoided in order to obtain reliable experimental data.

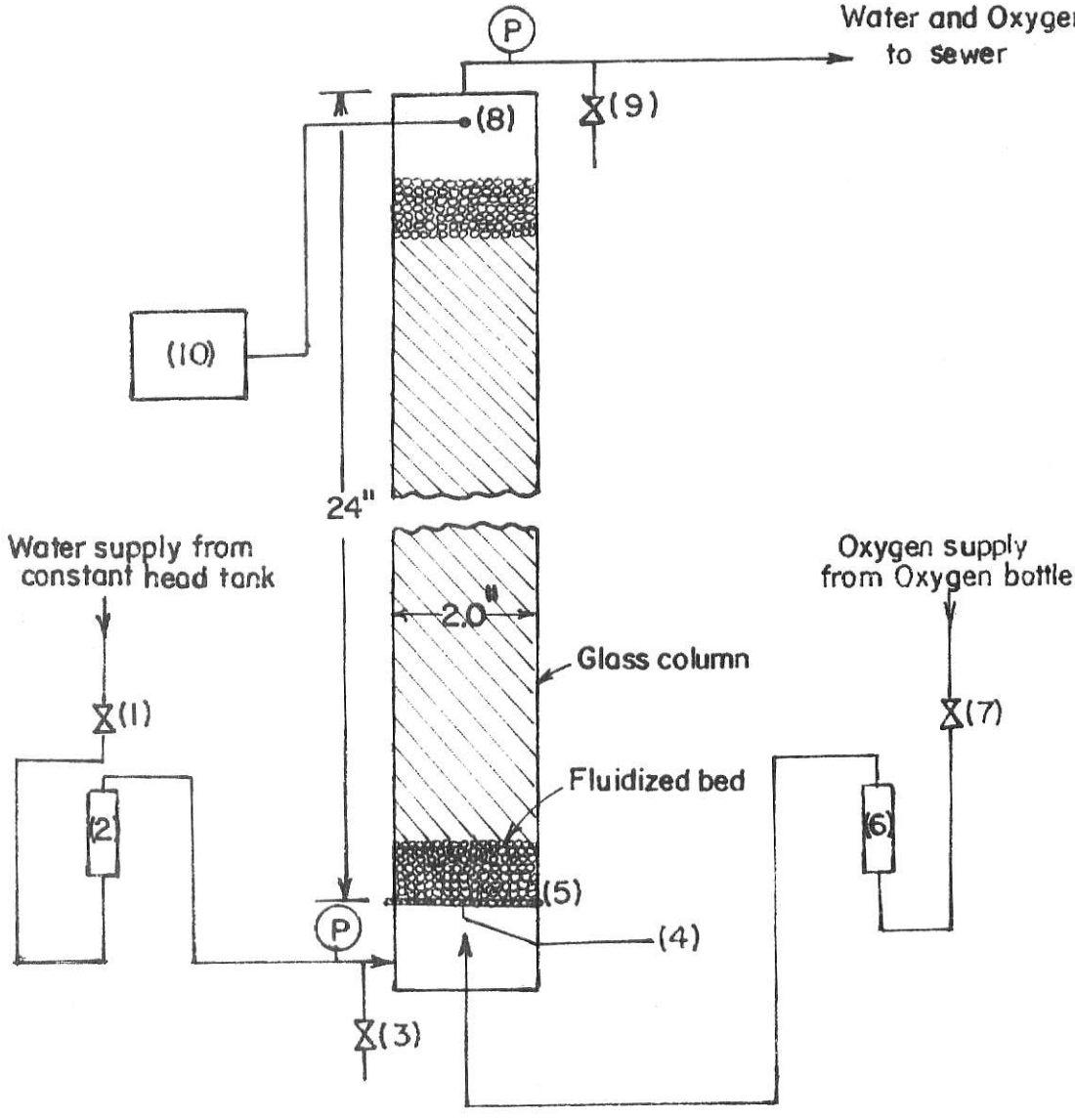

(1) Liquid flow control valve
(2) Liquid rotameter
(3) Inlet liquid sampling valve
(4) Tracer inlet tube
(5) Copper screen bed support
(6) Gas rotameter
(7) Gas flow control valve
(8) Tracer outlet probe
(9) Exit liquid sampling valve
(10) Conductance meter and recorder

Fig.3. Experimental apparatus schematic.

RESULTS AND DISCUSSION

A. Mass Transfer, Axial Liquid Phase Dispersion, Pressure Drop, and Bed Expansion Characteristics of the Systems Studied.

Experimentally measured overall volumetric mass transfer coefficients based on the plug flow model $(K_L a)_{PF}$ are shown in Figure 4 through Figure 8. Fluidized bed mass transfer coefficients are presented as a function of $(L'-L'_{min})$ with G' as a parameter. Mass transfer coefficients for the plain bubble column are presented as a function of L' with G' as a parameter. A sample calculation of the plug flow model mass transfer coefficient $(K_L a)_{PF}$ is shown in the Appendix.[1]

Experimentally measured axial liquid phase Peclet numbers (Pe_L) are shown in Figure 9 through Figure 14. Fluidized bed Peclet numbers are presented as a function of $(L'-L'_{min})$ over the range of experimental gas rates, $14.3 \leq G' \leq 43.0$.[2] Peclet numbers for the plain bubble column are presented as a function of L' over the range of experimental gas rates. A sample calculation of Pe_L is shown in the Appendix.[3] From Figure 9 through Figure 14, we see that Pe_L decreases with increasing liquid rate. From the definition of Pe_L,[4] it is obvious that the apparent axial liquid phase dispersion coefficient (D) increases rapidly with liquid rate. Chen and Douglas [3] have reported that for gas-liquid contact in a countercurrent turbulent bed contactor, the axial liquid phase dispersion coefficient increases with both increasing gas and liquid rates. Obviously, we have obtained the same result

[1] See Appendix, Section IV.

[2] See Experimental Section.

[3] See Appendix, Section V.

[4] See Theoretical Section.

for increasing liquid rates, however, we found that gas rate had little effect on the dispersion coefficient under the conditions employed in this work.[1] There are two probable reasons for this. First, in the experimental work by Chen and Douglas [3], the gas and liquid rates were of the same order of magnitude in terms of $lb_m/hr\text{-}ft^2$. In our work, the gas rates were extremely small compared to the liquid rates. Second, Chen and Douglas [3] used countercurrent contact. We used cocurrent contact, and would therefore expect small gas rates to have a negligible effect on liquid phase dispersion coefficients.

Using the results shown in Figure 14, values of D for the various systems were determined as a function of L' and it was found that for $L' > 10.0$ $lb_m/hr\text{-}ft^2$, liquid dispersion in the fluidized beds was significantly higher than that in the plain bubble column. This is to be expected, since we know that at high flow rates there can be considerable backmixing of the liquid phase, caused by the turbulent motion of the fluidized particles. For $L' < 10.0$ $lb_m hr\text{-}ft^2$, it was found that liquid dispersion in the fluidized beds and that in the plain bubble column were essentially the same.

Experimentally measured mass transfer coefficients based on the dispersion model $(K_L a)_{DM}$ are shown in Figure 15 through Figure 19. Here again, fluidized bed mass transfer coefficients are presented as a function of $[L'-L'_{min.}]$ with G' as a parameter, while mass transfer coefficients for the plain bubble column are presented as a function of L' with G' as a parameter. A sample calculation of the dispersion model mass transfer coefficient $(K_L a)_{DM}$ is given in the Appendix.[2]

[1] See Experimental Section.

[2] See Appendix, Section V.

From Figure 4 through Figure 8 and Figure 15 through Figure 19, we see that the mass transfer coefficient ($K_L a$) increases with increasing gas rate, while holding the liquid rate constant. This is to be expected, due to the increase in gas-liquid interfacial area as the gas rate is increased at constant liquid rate. We also see that the fluidized bed mass transfer coefficient varies with the liquid rate, while holding the gas rate constant. The degree of variation seems to depend on the type of fluidized bed. For the plain bubble column, the mass transfer coefficient also varies with the liquid rate, while holding the gas rate constant. However, in general it is less dependent on liquid rate than for the fluidized beds.

Measured pressure drop data are shown in Figure 20 through Figure 24, and are presented as a function of L' and G'. The pressure drop data shown in Figure 20 through Figure 23 has been corrected for the contribution of the column, and therefore represents the actual pressure drop behavior of the particle bed.

For a bed of particles, pressure drop increases rapidly with flow rate until the onset of fluidization is reached. Theoretically, this corresponds to the point at which the bed pressure drop attains a constant value as the flow rate is increased. Actually, the bed pressure drop does not attain an absolute constant value, but instead increases very slowly with flow rate after the onset of fluidization. The method used for determination of (L'_{min}) from pressure drop data is indicated in Figure 20 through Figure 23. This method is the standard procedure for determination of fluidization onset velocities [9].

It must be pointed out here that (L'_{min}) is the minimum liquid mass velocity required for fluidization at zero gas rate, $G' = 0$. This value of

L' was used as the base point for all liquid rates, in order that experimentally measured values of Pe_L and $(K_L a)$ correspond to the fluidized state.

From Figure 20 through Figure 23, we see that as G' is increased, the value of L' required for fluidization is decreased. Since the magnitude of G' is exceedingly small compared to the magnitude of L' (L'+G'≅L'), we need to explain this phenomena. In order to estimate minimum fluidization velocities, a correlation given by Leva [9] can be used

$$G_{mf} = 688\ D_p^{1.82}[\rho_F(\rho_p - \rho_F)]^{0.94}/\mu^{0.88} \qquad (6)$$

where

G_{mf} = minimum fluidization velocity required, $lb_m/hr\text{-}ft^2$

D_p = particle diameter, inches

ρ_F = fluid density, lb_m/ft^3

ρ_p = particle density, lb_m/ft^3

μ = fluid viscosity, cp.

Once G_{mf} is determined from Equation (6), if $D_p G_{mf}/\mu > 10$, a correction factor must be applied to G_{mf} as shown in Figure 3-15 of Leva [9]. Using the correlation of Equation (6) for 0.0625" copper spheres, the value of G_{mf} required for fluidization by only gas (0_2) was estimated to be 0.15×10^4 $lb_m/hr\text{-}ft^2$, and the value of G_{mf} required for fluidization by only liquid (H_20) was estimated to be 3.68×10^4 $lb_m/hr\text{-}ft^2$. We see that G_{mf} for the gas fluidized bed is much smaller than G_{mf} for the liquid fluidized bed. Thus, it requires a much smaller mass velocity of gas to produce fluidization than liquid. This fact would seem to verify the results of Figure 20 through Figure 23; even though G' is exceedingly small compared to L', it has a significant effect upon the value of L' required for fluidization.

The fluidization pressure drop for the three phase fluidized bed is

given by[1]

$$\Delta P = [\frac{W}{A}][\frac{\rho_p-\rho_m}{\rho_p}][\frac{\varepsilon_m}{1-\varepsilon_p}] + [\frac{W}{A}][\frac{\rho_p-\rho_g}{\rho_p}][\frac{\varepsilon_g}{1-\varepsilon_p}] \quad (7)$$

where

ΔP = pressure drop, lb_f/ft^2

W = weight of the particle bed, lb_f

A = fluidized bed cross sectional area, ft^2

ρ_p = particle density, lb_m/ft^3

ρ_m = liquid density, lb_m/ft^3

ρ_g = gas density, lb_m/ft^3

ε_m = volume fraction occupied by liquid, dimensionless

ε_p = volume fraction occupied by particles, dimensionless

ε_g = volume fraction occupied by gas, dimensionless

By making the assumption that $(\rho_p-\rho_g) \cong \rho_p$, and using the fact that $\varepsilon_m + \varepsilon_p + \varepsilon_g = 1$, Equation (7) is readily reduced to the following form

$$\Delta P = [\frac{W}{A}][1 - (\rho_m/\rho_p) + (\rho_m/\rho_p)\ (\frac{\varepsilon_g}{1-\varepsilon_p})] \quad (8)$$

We see from Equation (8) that as ε_g is increased, ΔP will increase accordingly. If ΔP increases monotonically with G', we can conclude that ε_g increases monotonically with G'.

For fluidization by only gas (0_2), $\varepsilon_m = 0$ and Equation (8) reduces to

$$\Delta P = W/A \quad (9)$$

For example, using Equation (9) for gas fluidization, the fluidized bed of

[1]See Appendix, Section VI.

0.0625" copper spheres with a settled bed length of 15.5"[1] yields a value for ΔP of 6.50 in. Hg. As shown in Figure 21, the value of ΔP for liquid fluidization was found to be approximately 4.10 in. Hg. Comparison of these two values for ΔP indicates that ΔP, and consequently ε_g, increases monotonically as G' is increased. This further verifies the results of Figure 20 through Figure 23. Thus, Equation (8) provides a simple method for estimating the gas phase volume fraction ε_g of a three phase fluidized bed from a pressure drop measurement, which is easily obtained.

Bed expansion characteristics for each type of fluidized bed are shown in Figure 25 through Figure 28. The bed expansion as a percentage of the settled bed length $(\frac{Z-Z_s}{Z_s})$ is presented as a function of $(L'-L'_{min})$ with G' as a parameter. We see that the bed expansion increases rapidly with liquid rate at a constant gas rate. As was the case for the pressure drop data, we again find that even though G' is exceedingly small compared to L' (L'+G'≅L') it has a substantial effect upon the bed expansion. We need to explain this phenomena.

The bed expansion for the three phase fluidized bed is given by[2]

$$\left(\frac{Z-Z_s}{Z_s}\right) = \left[\frac{kW}{1-\varepsilon_p}\right]\left[\frac{L'\varepsilon_m}{\rho_m} + \frac{G'\varepsilon_g}{\rho_g}\right] \qquad (10)$$

where

Z = total fluidized bed length, ft

Z_s = settled particle bed length, ft

k = proportionality constant, hr/lb_f-ft

[1] See Figure 26.

[2] See Appendix, Section VII.

W = weight of the particle bed, lb_f

L' = superficial liquid mass velocity, $lb_m/hr\text{-}ft^2$

G' = superficial gas mass velocity, $lb_m/hr\text{-}ft^2$

ρ_m = liquid density, lb_m/ft^3

ρ_g = gas density, lb/ft^3

ε_m = volume fraction occupied by liquid, dimensionless

ε_g = volume fraction occupied by gas, dimensionless

ε_p = volume fraction occupied by particles, dimensionless

Inspection of Equation (10) indicates that even though $L'\varepsilon_m >> G'\varepsilon_g$, the two terms $(L'\varepsilon_m/\rho_m)$ and $(G'\varepsilon_g/\rho_g)$ may be of the same order of magnitude because $\rho_m >> \rho_g$. For example, in the sample calculation for Pe_L,[1] it was found that for $L' = 10.20 \times 10^4$ and $G' = 28.6$, $\varepsilon_m \cong 0.48$ and $\varepsilon_g \cong 0.23$. For $\rho_m = 62.3$ and $\rho_g = 0.084$, $(L'\varepsilon_m/\rho_m) = 787.$ and $(G'\varepsilon_g/\rho_g) = 78.3$. Thus, even though G' is exceedingly small compared to L', it has a substantial effect upon the bed expansion, as indicated in Figure 25 through Figure 28.

All data shown in Figure 25 through Figure 28 indicates that the bed expansion increases with G' while holding L' constant. Several investigators [4, 14, 15, 17] have reported that for some types of three phase fluidized bed systems, the bed expansion decreases with increasing gas rate while holding the liquid rate constant, passing through a minimum point before increasing again. They have found this phenomena to be most common in fluidized beds of small particles with low liquid rates, and a large gas bubble size at the injection point. Our experimental systems do not exhibit this type of behavior.

The results shown in Figure 25 through Figure 28 are necessary for the

[1] See Appendix, Section V.

determination of Z at each experimental operating condition, and hence are necessary for the calculation of $(K_L a)$[1] and comparison of fluidized bed with plain bubble column pressure drop.

[1]See Appendix, Sections IV and V.

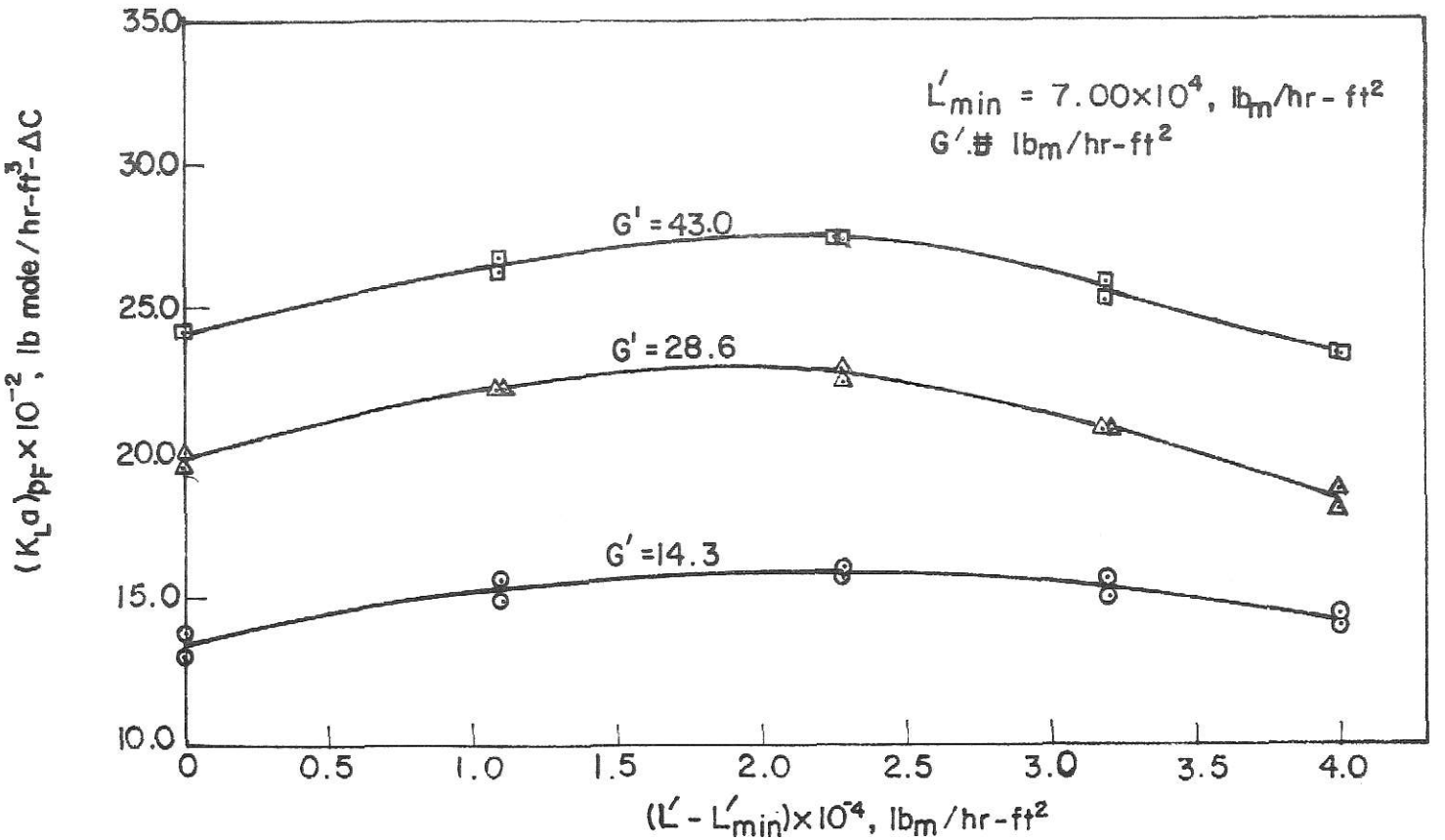

Fig.4. Fluidized bed mass transfer coefficient for 0.125" copper spheres based on the plug flow model.

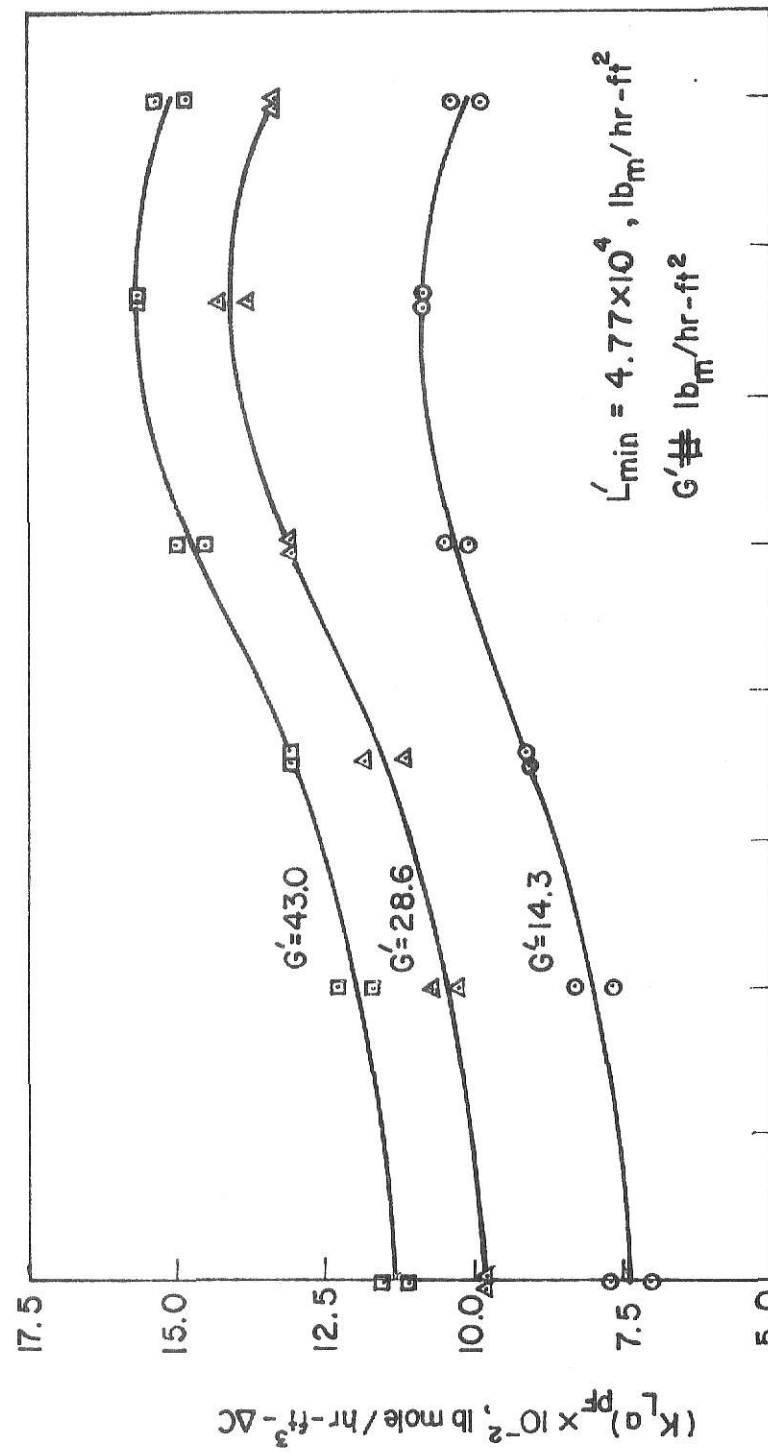

Fig.5. Fluidized bed mass transfer coefficient for 0.0625" copper spheres based on the plug flow model.

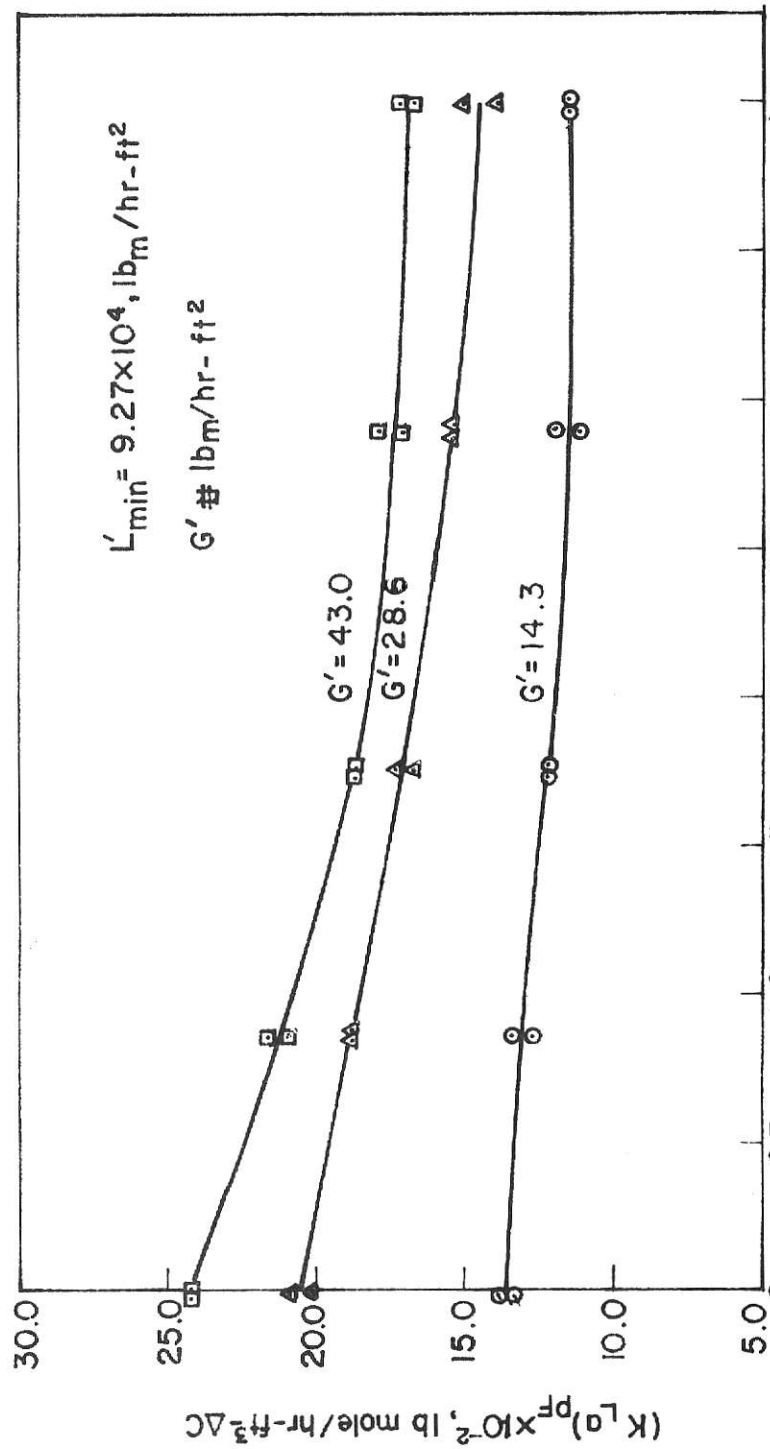

Fig. 6. Fluidized bed mass transfer coefficient for 0.1875" stainless steel spheres based on the plug flow model.

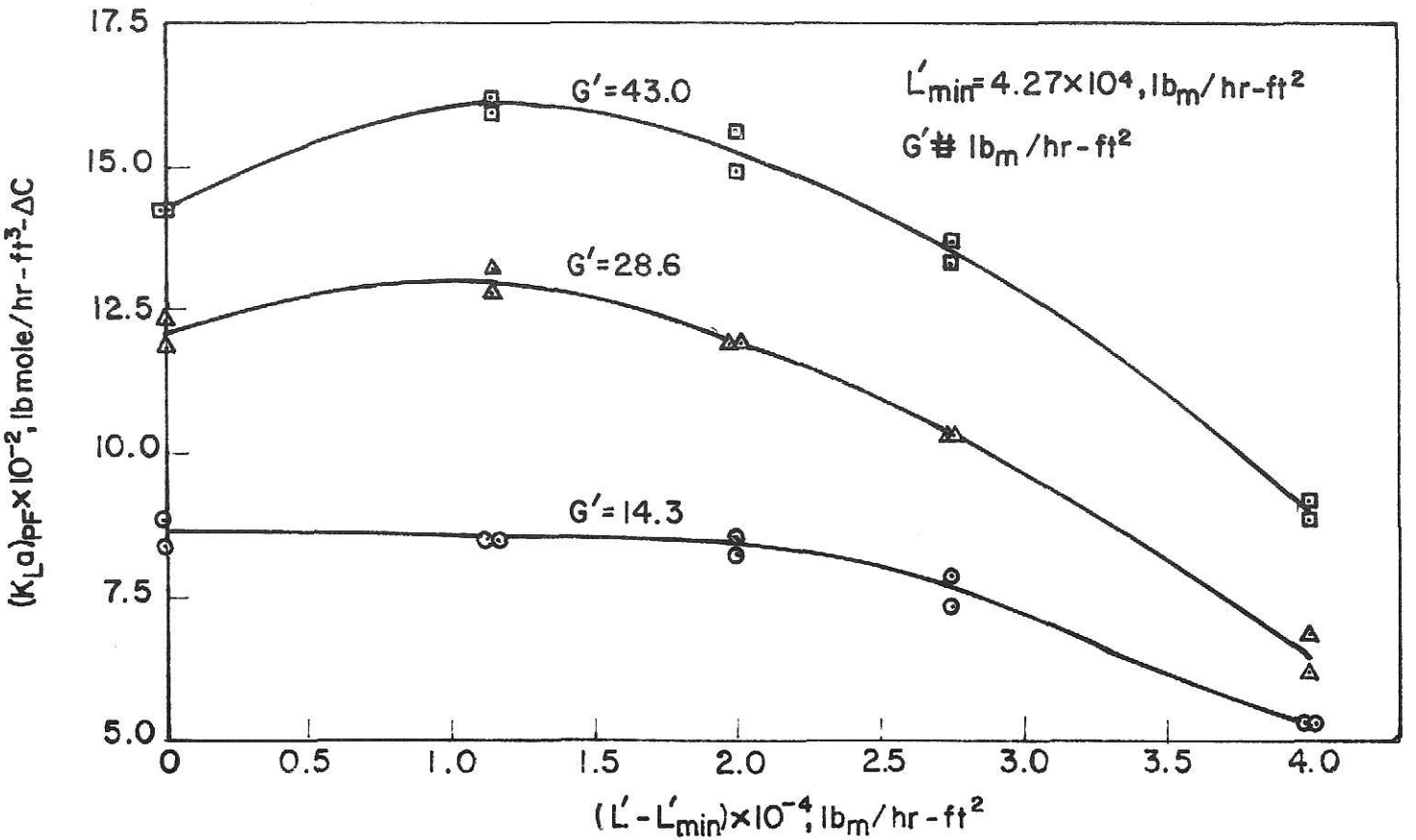

Fig.7. Fluidized bed mass transfer coefficient for 0.1875" glass spheres based on the plug flow model.

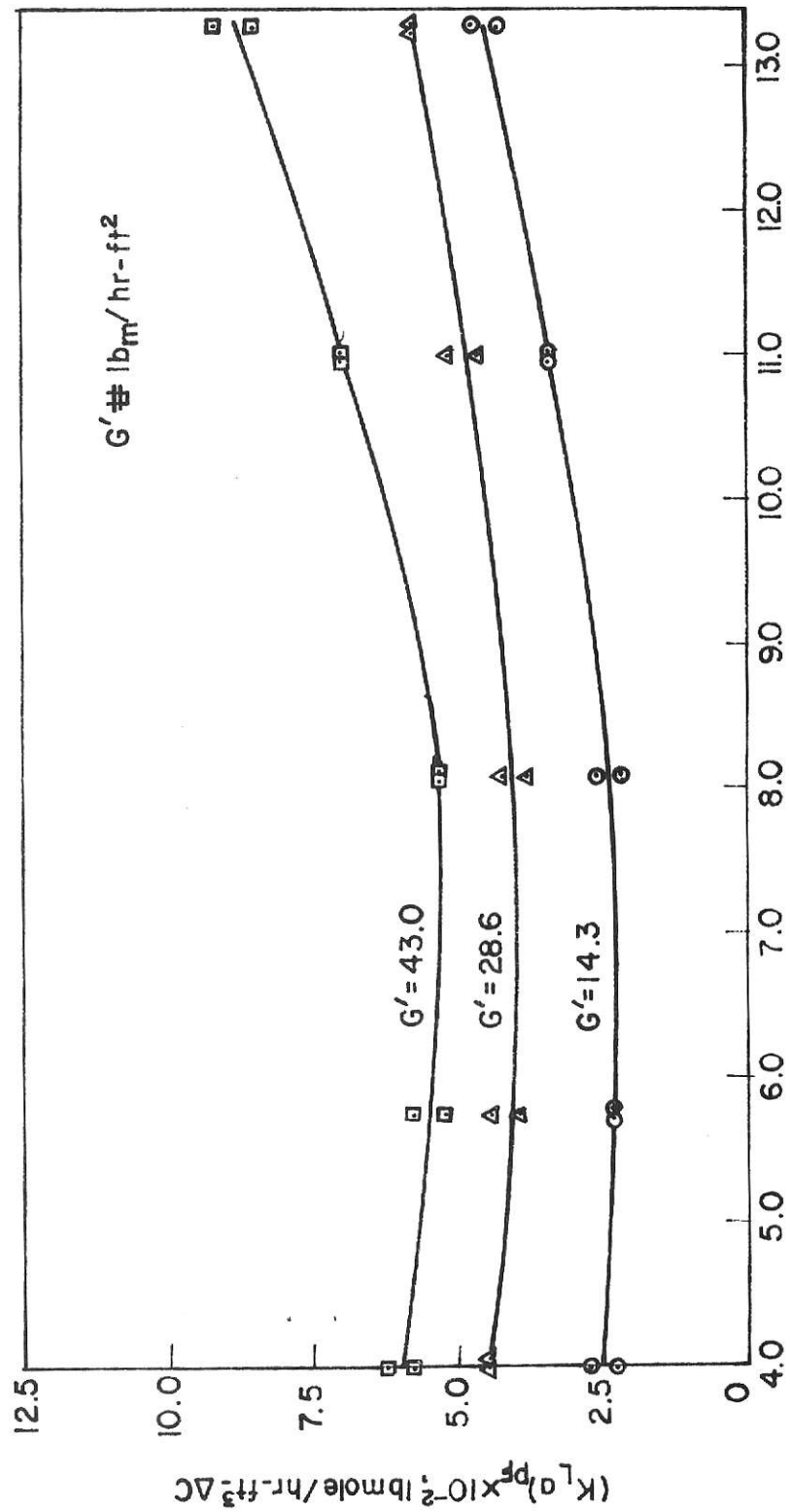

Fig.8. Mass transfer coefficient for plain bubble column based on the plug flow model.

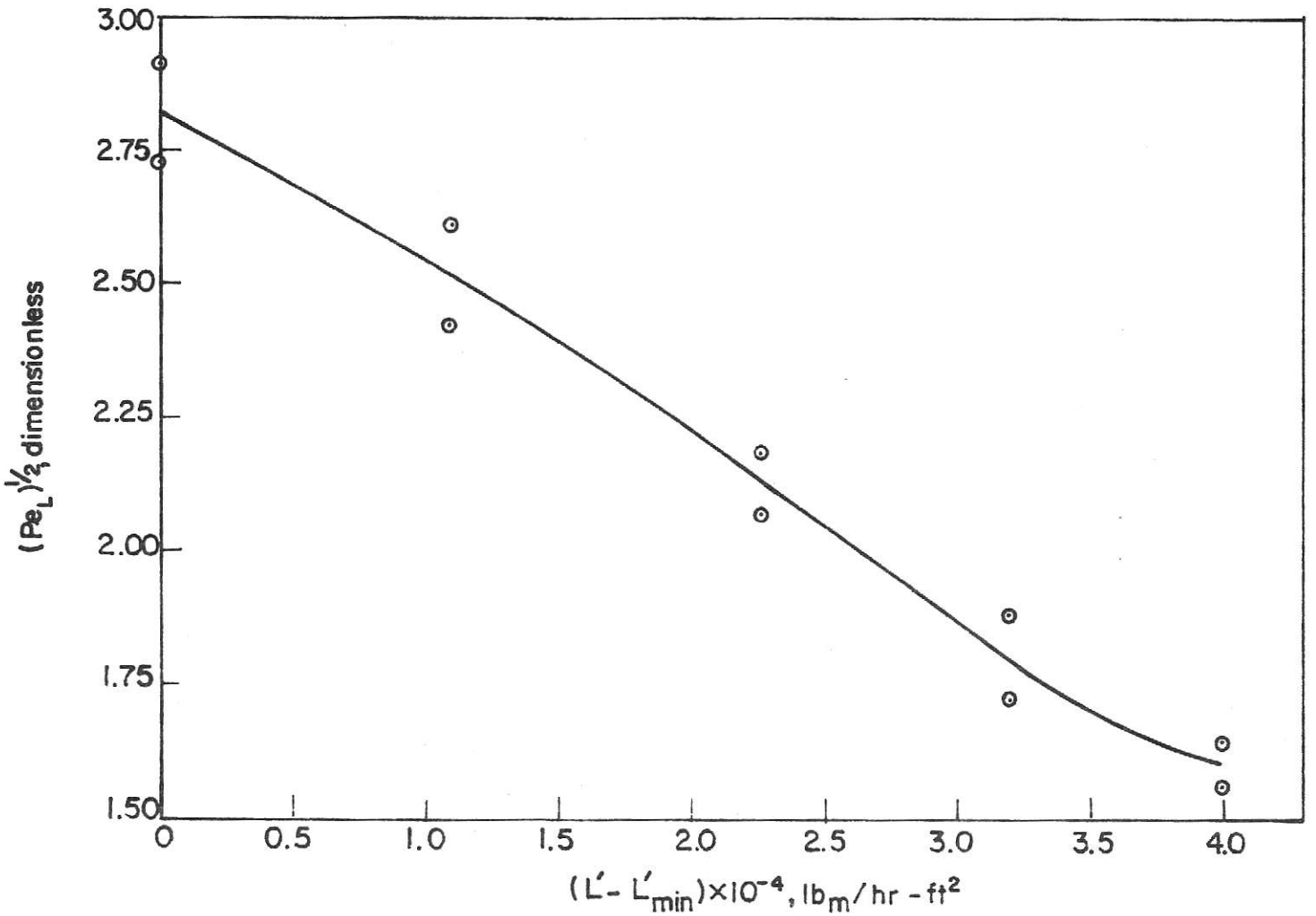

Fig. 9. Axial liquid phase Peclet number for 0.125" copper spheres for $14.3 \leq G' \leq 43.0$, $lb_m/hr - ft^2$.

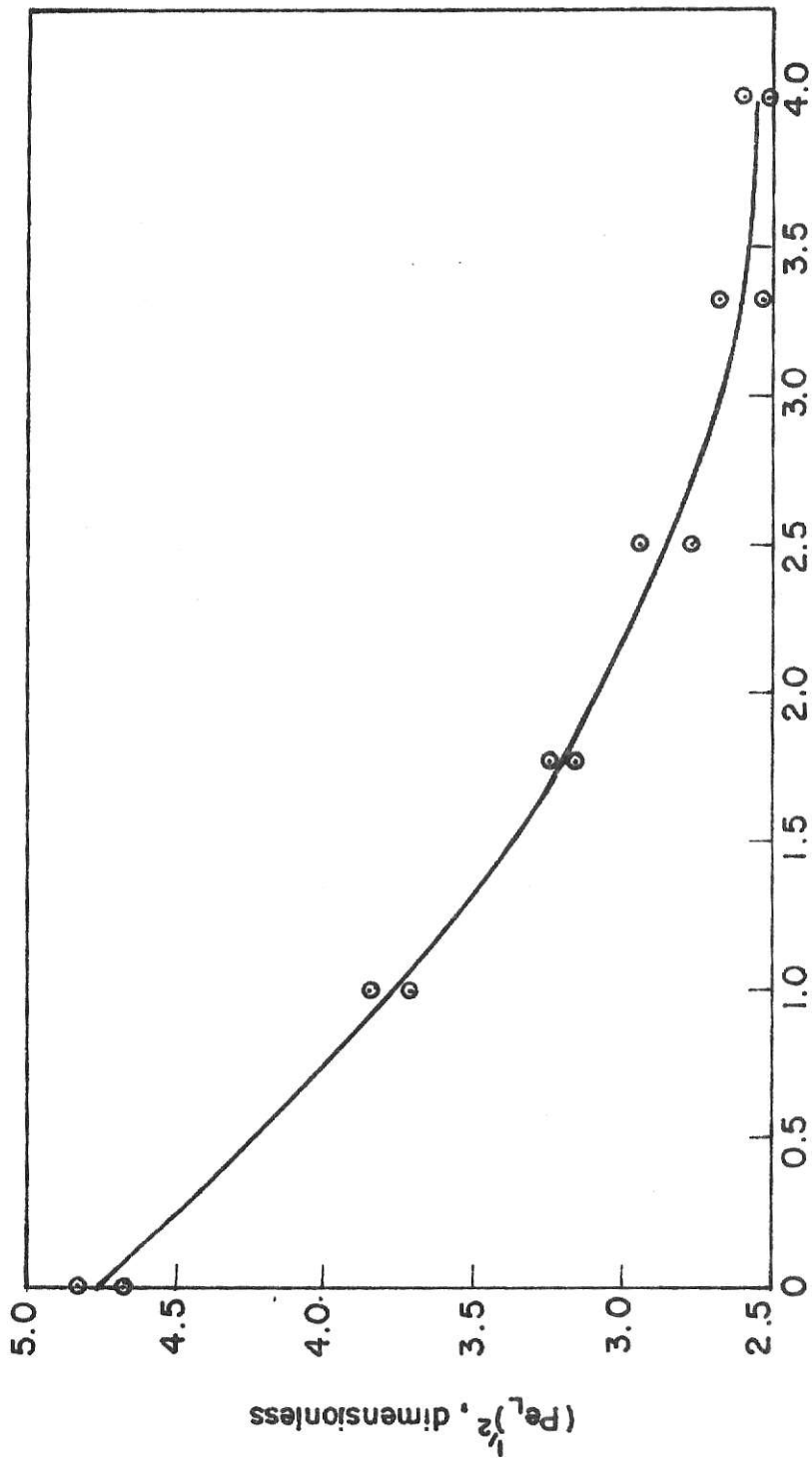

Fig.10. Axial liquid phase Peclet number for 0.0625" copper spheres for $14.3 \leq G' \leq 43.0$, $lb_m/hr\text{-}ft^2$.

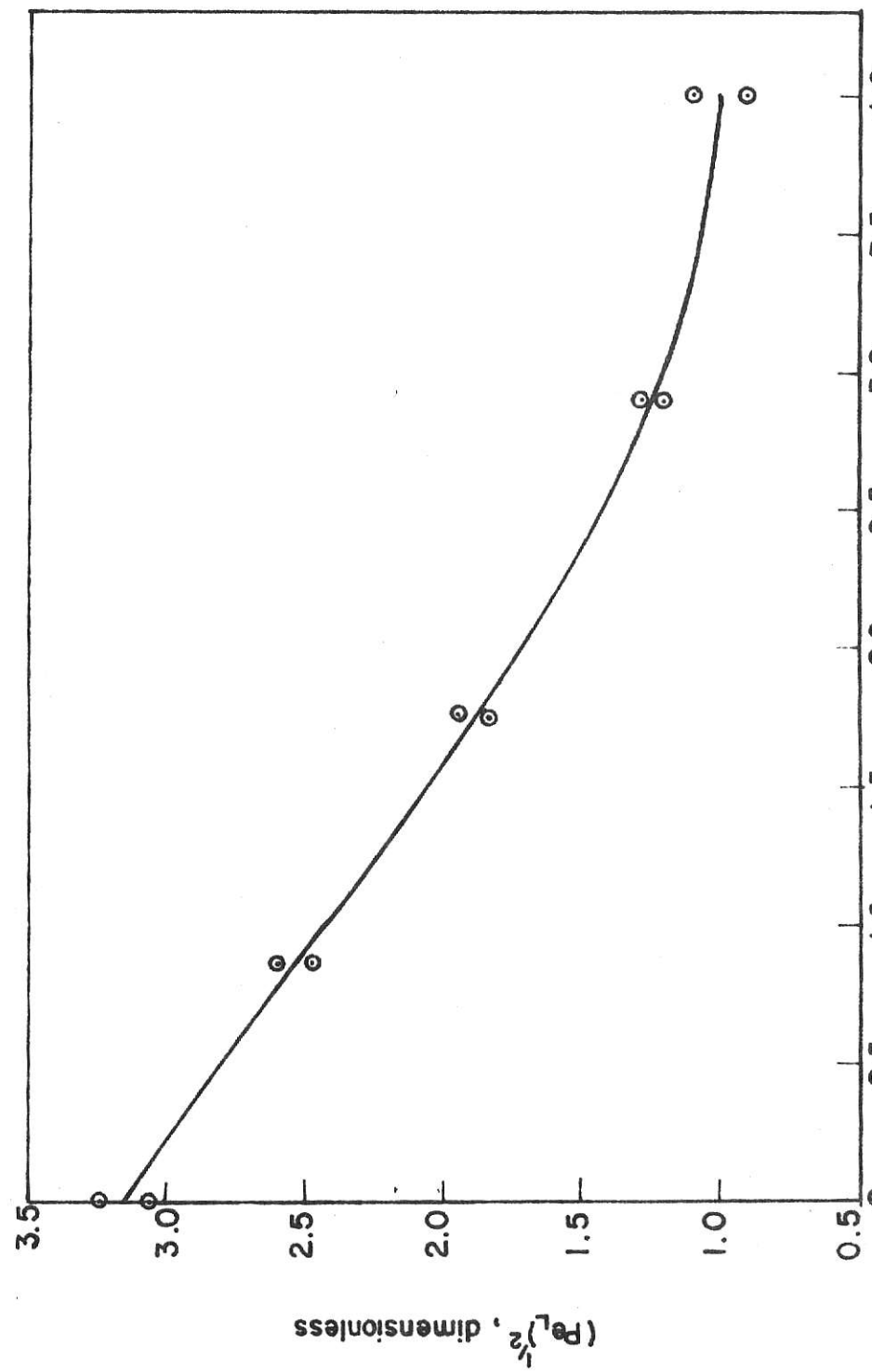

Fig. 11. Axial liquid phase Peclet number for 0.1875" stainless steel spheres for $14.3 \leq G' \leq 43.0$, $lb_m/hr\text{-}ft^2$.

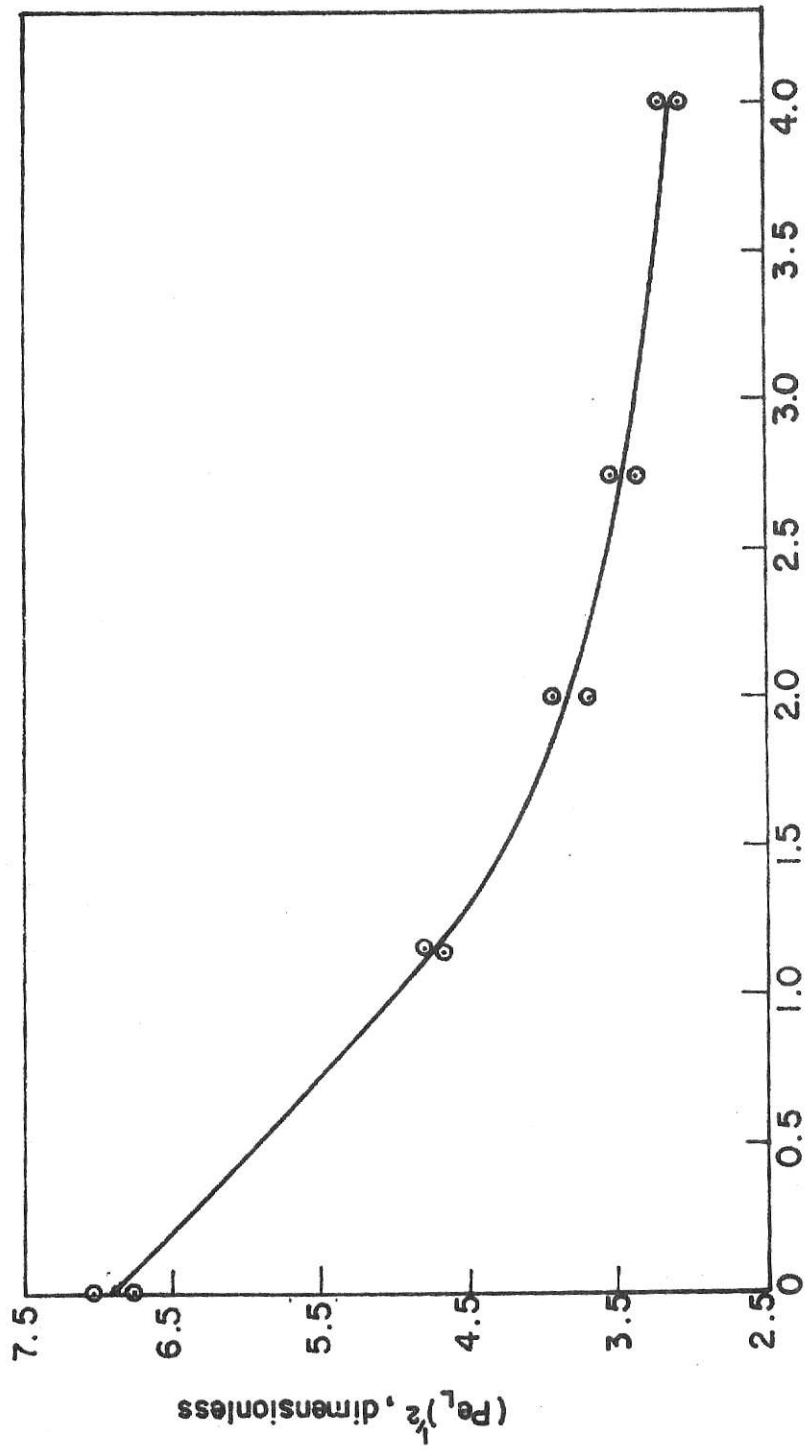

Fig.12. Axial liquid phase Peclet number for 0.1875" glass spheres for $14.3 \leq G' \leq 43.0$, $lb_m/hr-ft^2$.

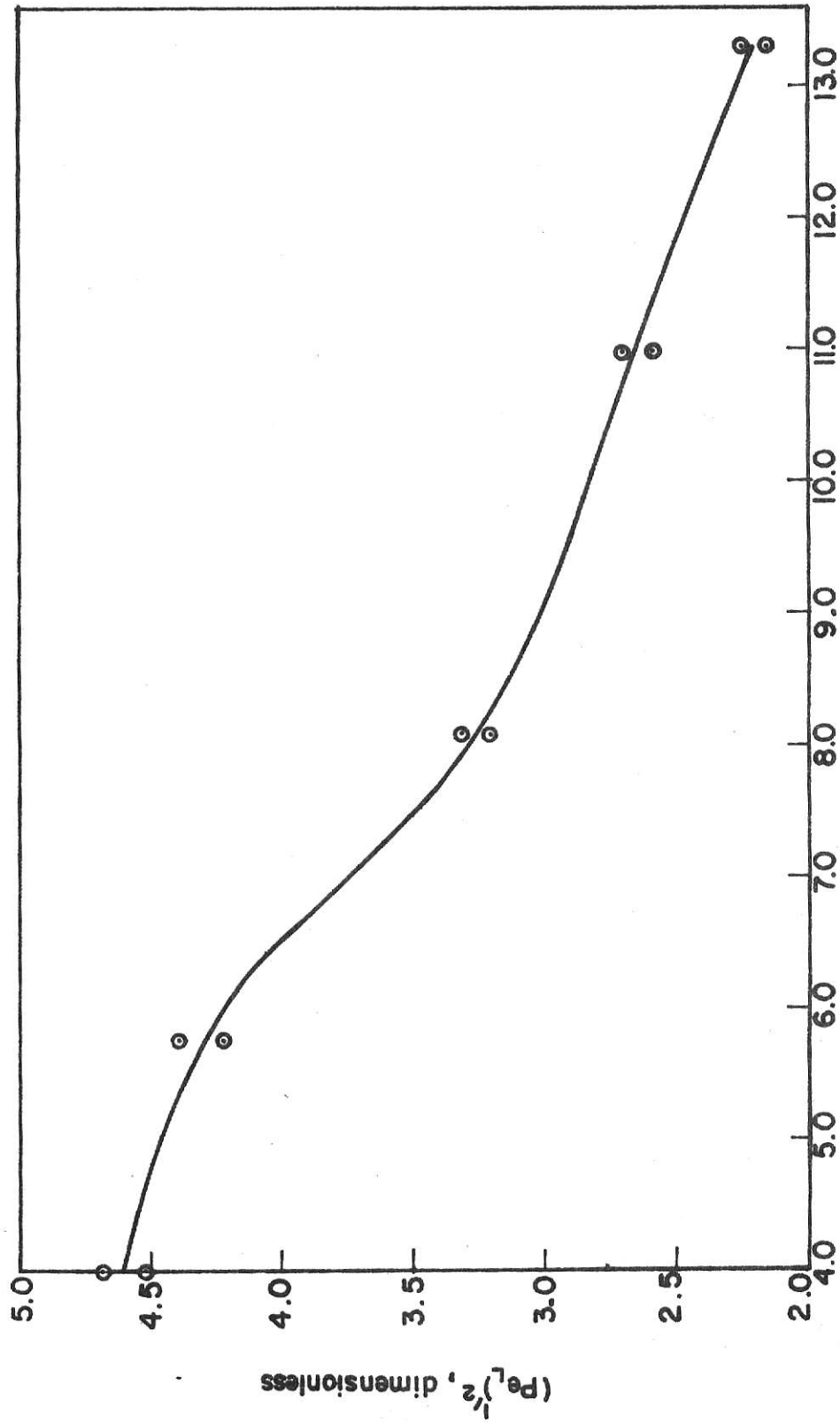

Fig.13. Axial liquid phase Peclet number for plain bubble column for $14.3 \leq G' \leq 43.0, lb_m/hr-ft^2$.

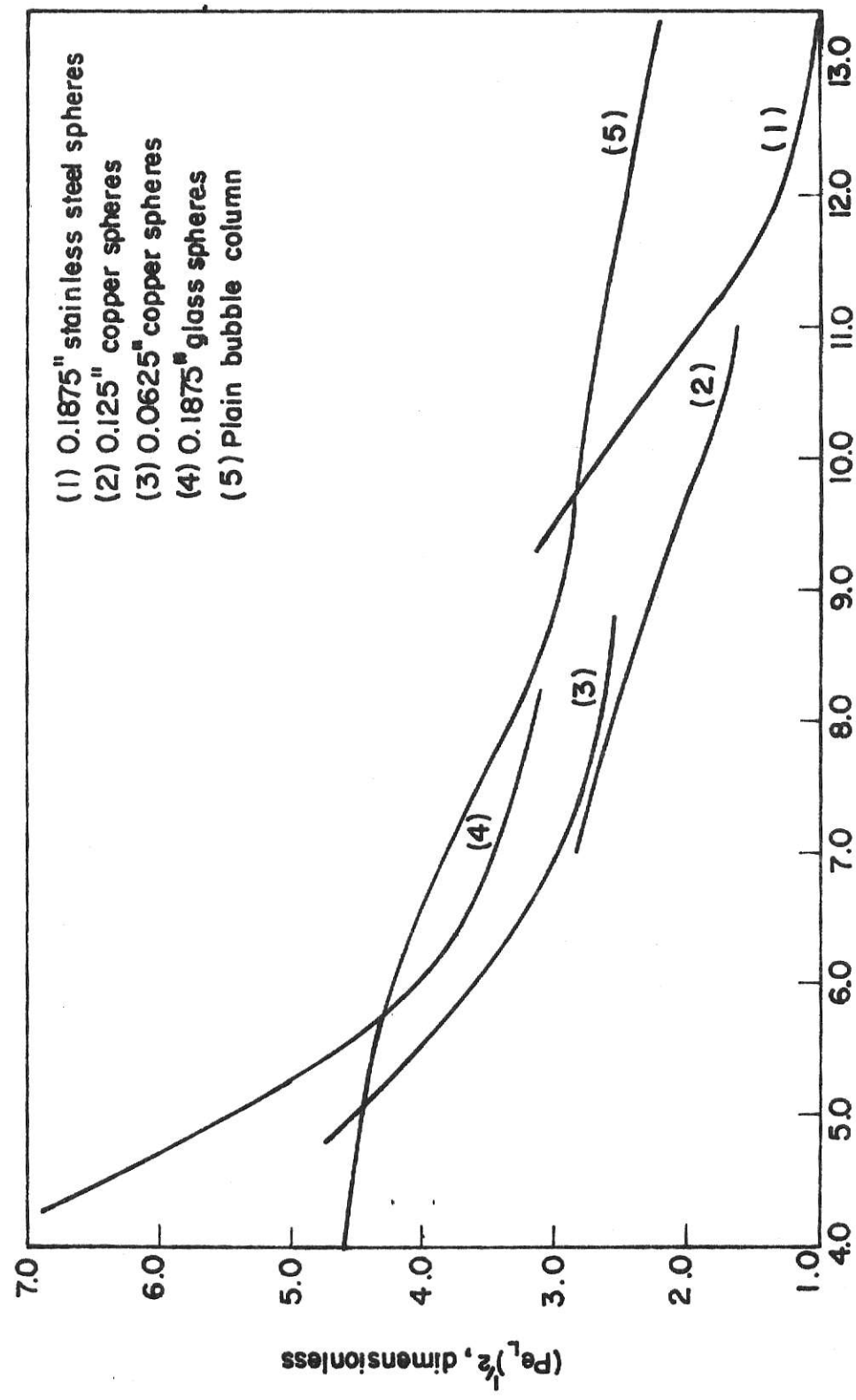

Fig.14. Comparison of axial liquid phase Peclet numbers for $14.3 \leq G' \leq 43.0$, $lb_m/hr\text{-}ft^2$.

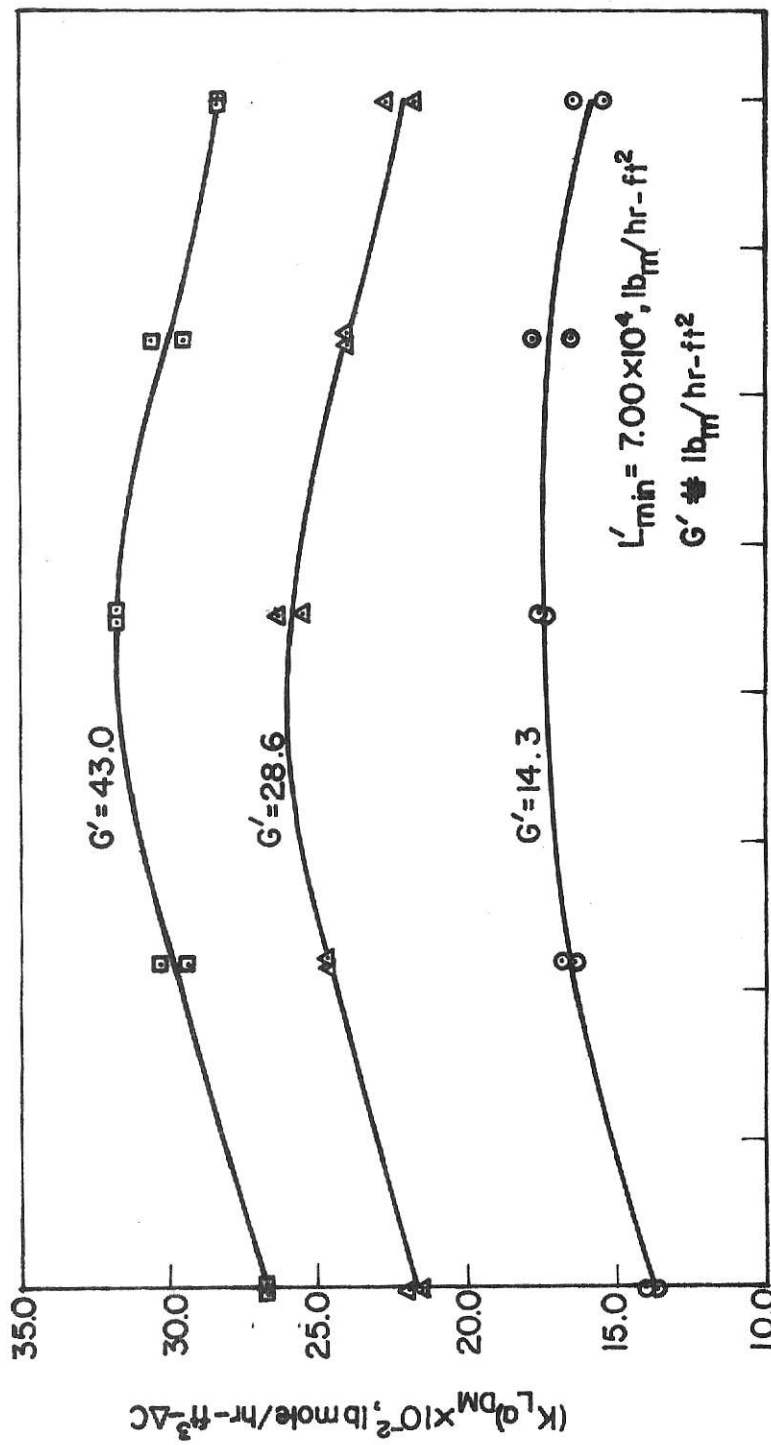

Fig.15. Fluidized bed mass transfer coefficient for 0.125" copper spheres based on the dispersion model.

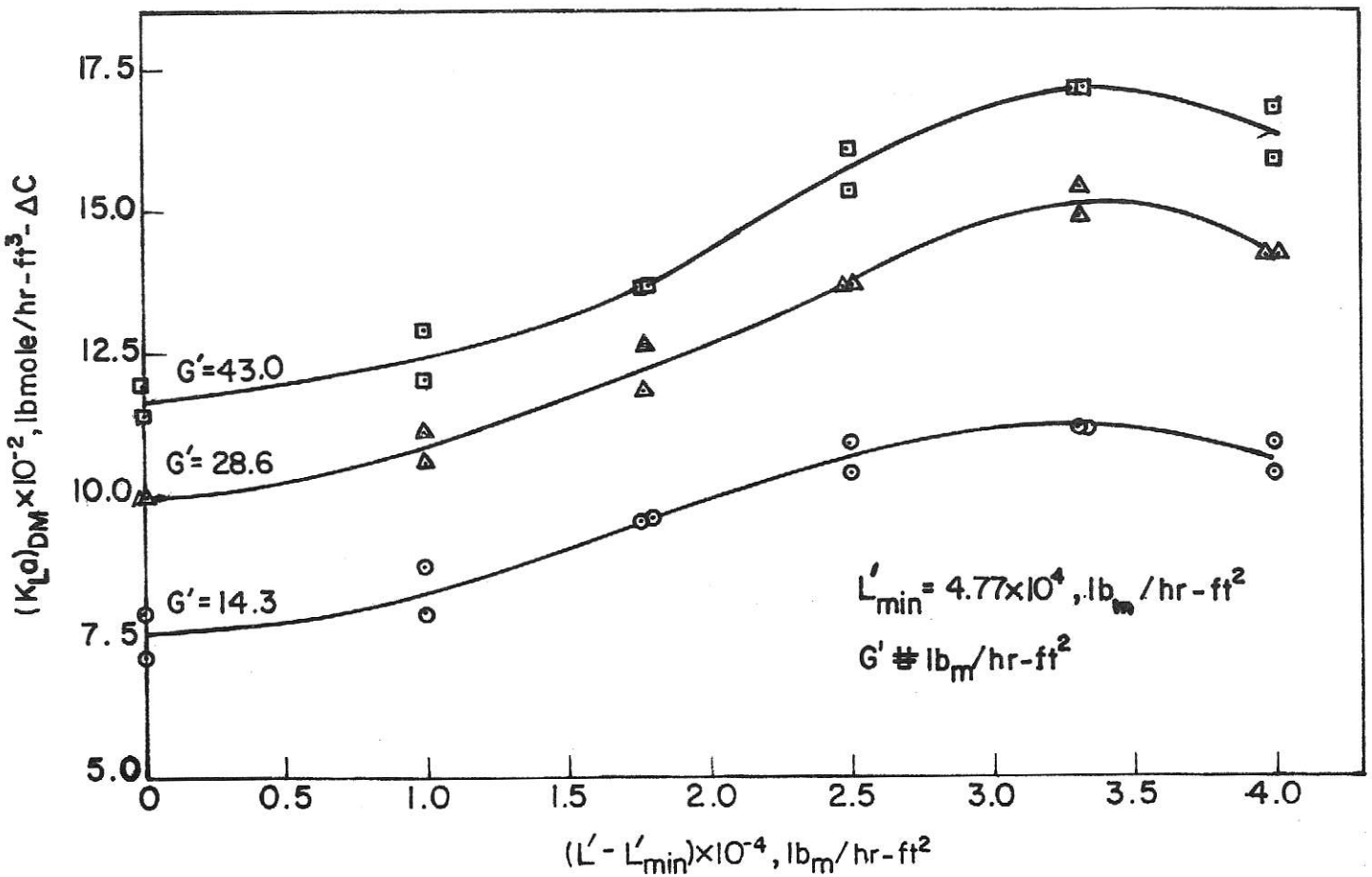

Fig. 16. Fluidized bed mass tranfer coefficient for 0.0625" copper spheres based on the dispersion model.

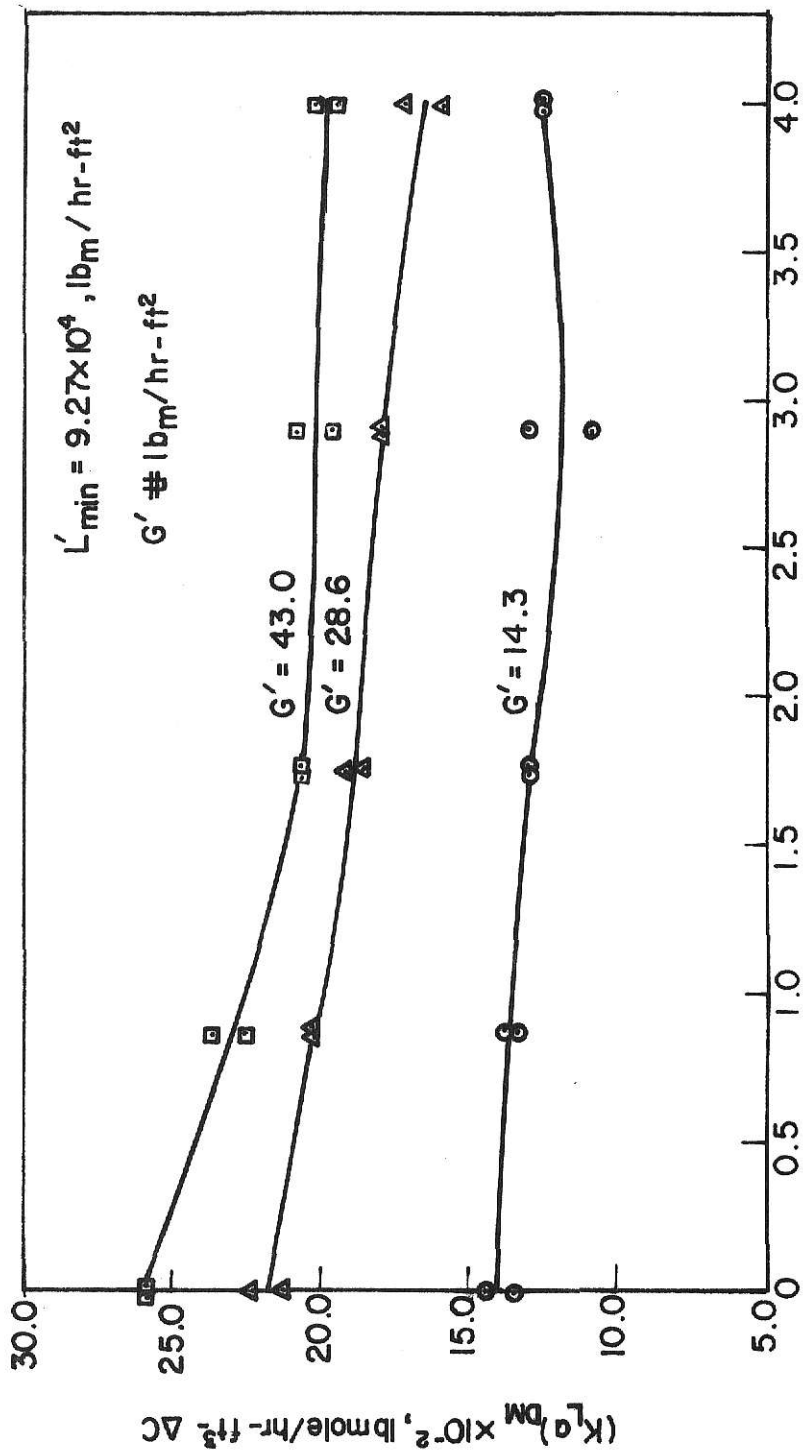

Fig. 17. Fluidized bed mass transfer coefficient for 0.1875" stainless steel spheres based on the dispersion model.

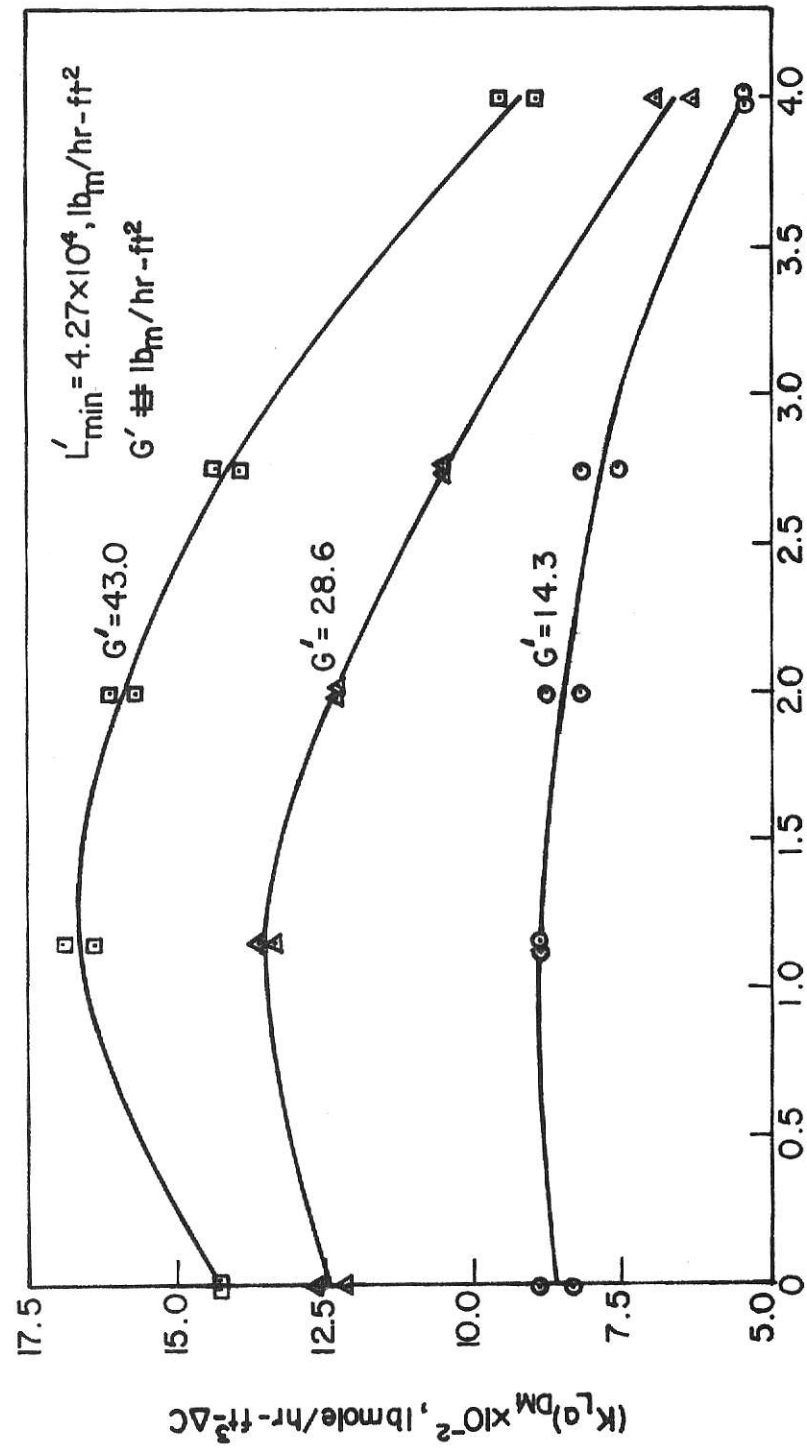

Fig. 18. Fluidized bed mass transfer coefficient for 0.1875" glass spheres based on the dispersion model.

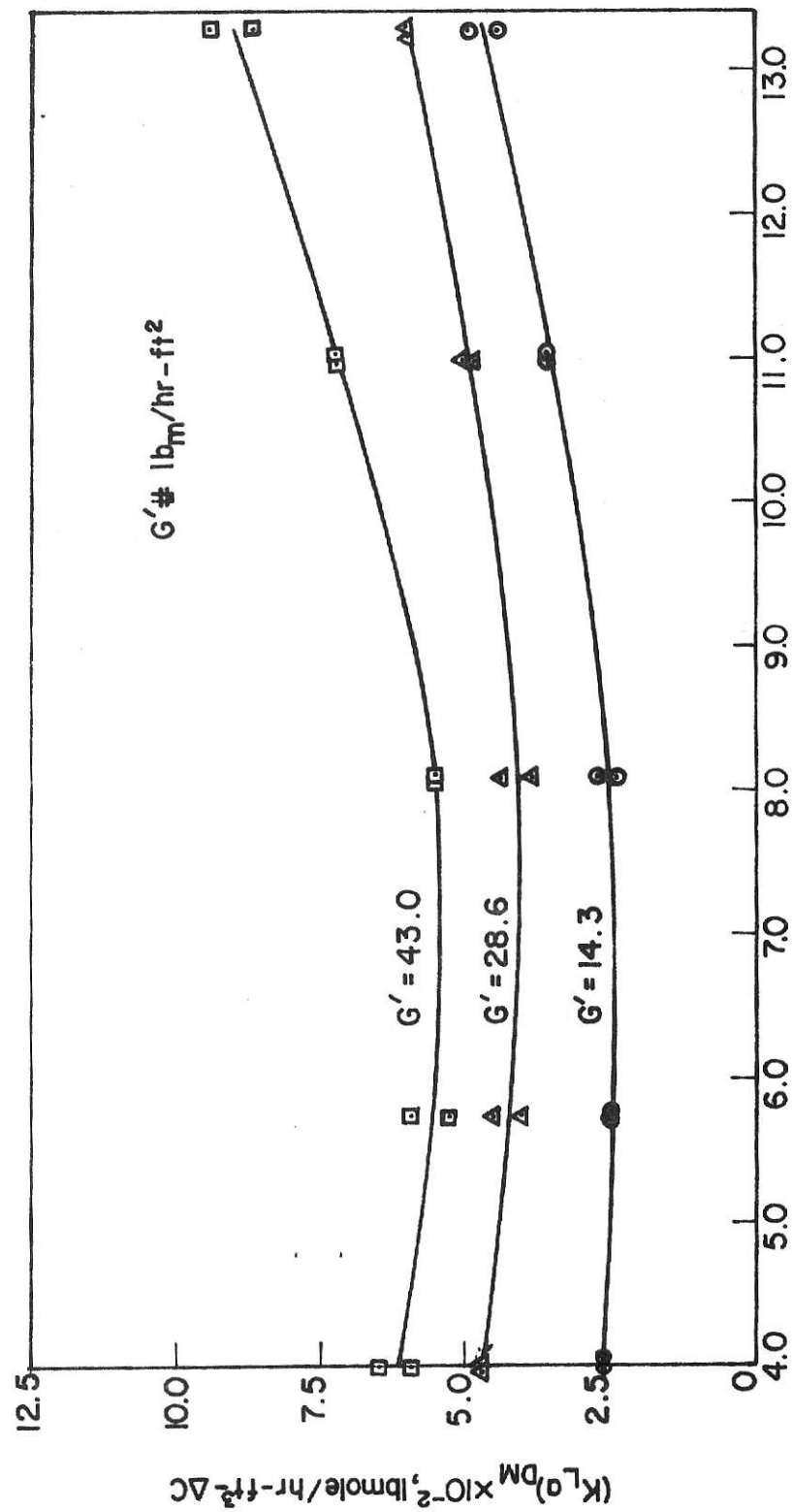

Fig.19. Mass transfer coefficient for plain bubble column based on the dispersion model.

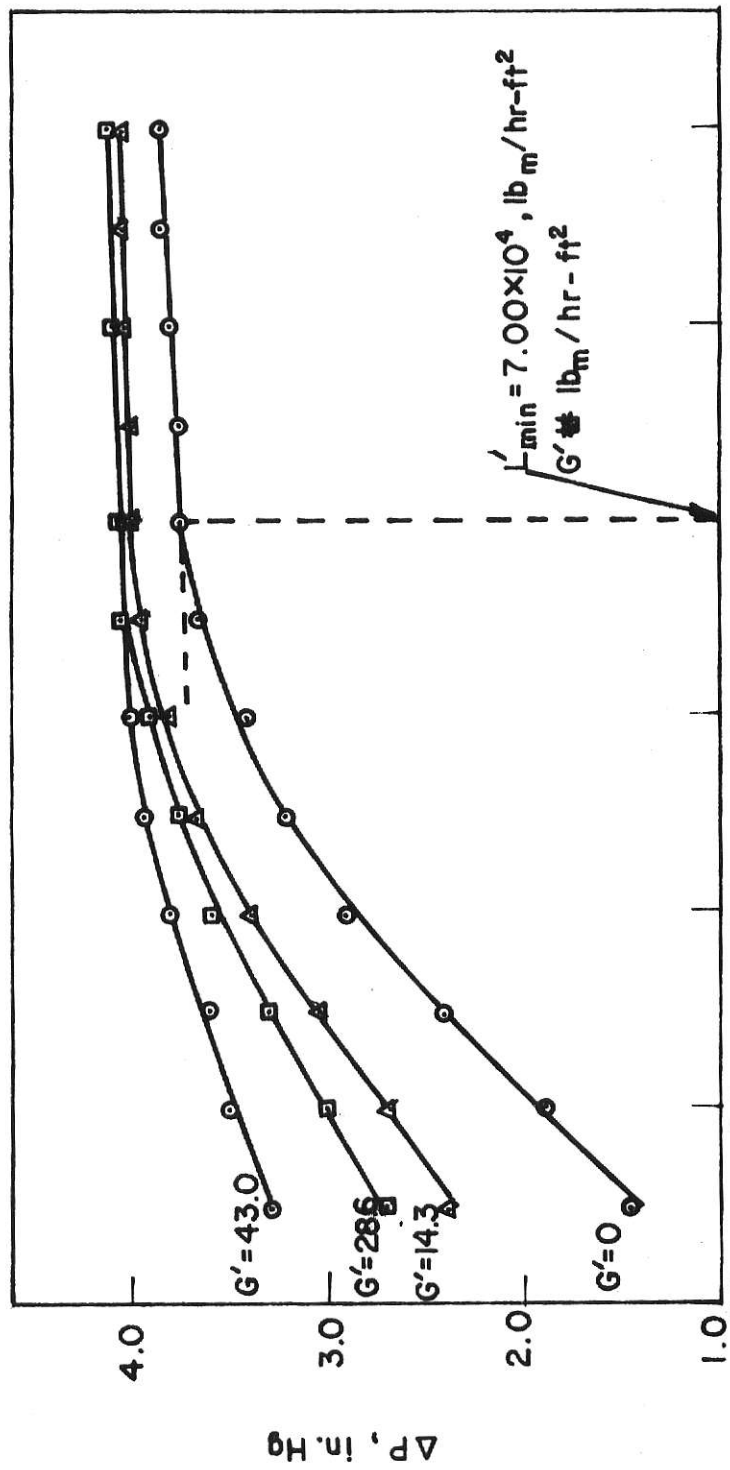

Fig.20. Fluidized bed pressure drop for 0.125" copper spheres.

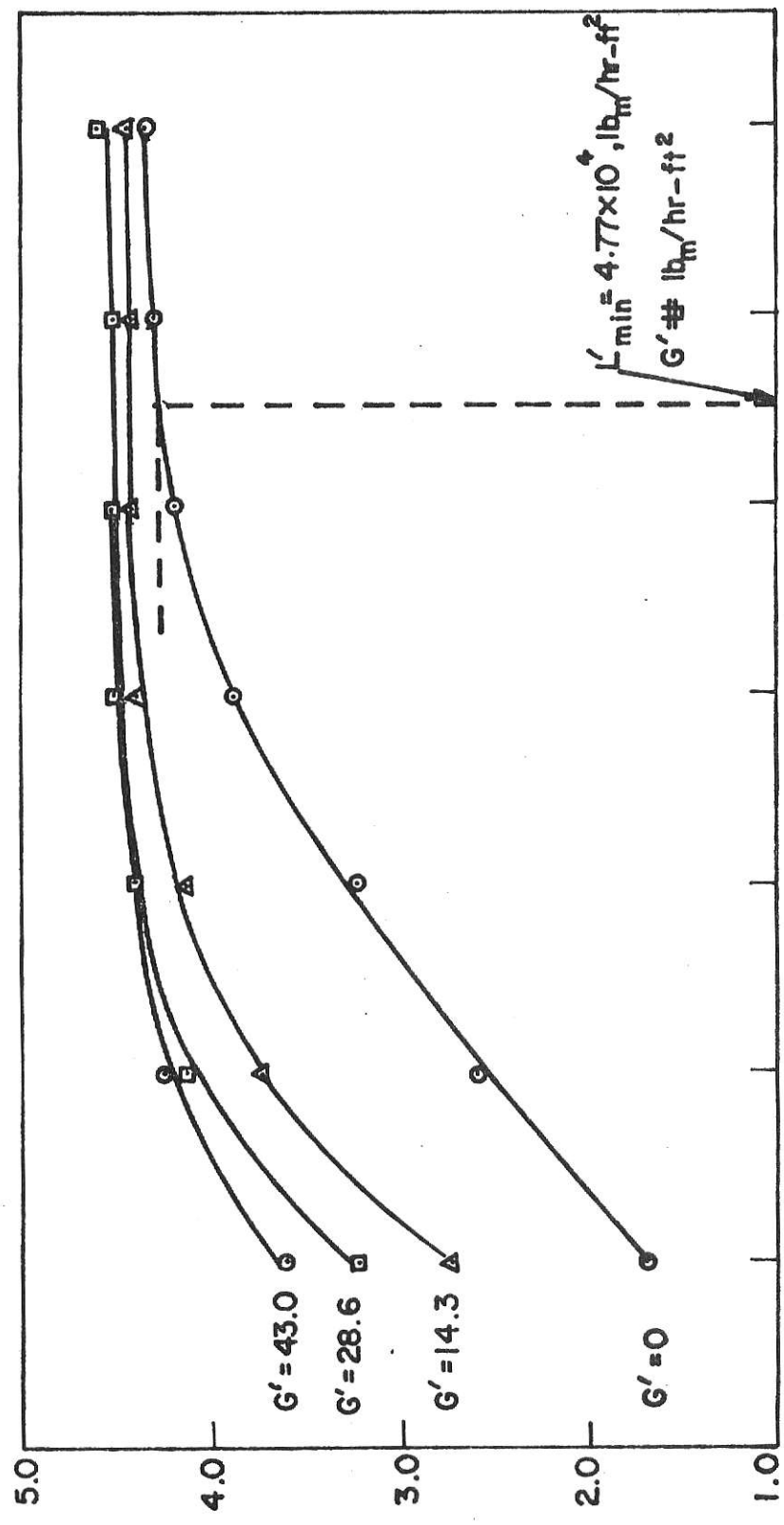

Fig.21. Fluidized bed pressure drop for 0.0625" copper spheres.

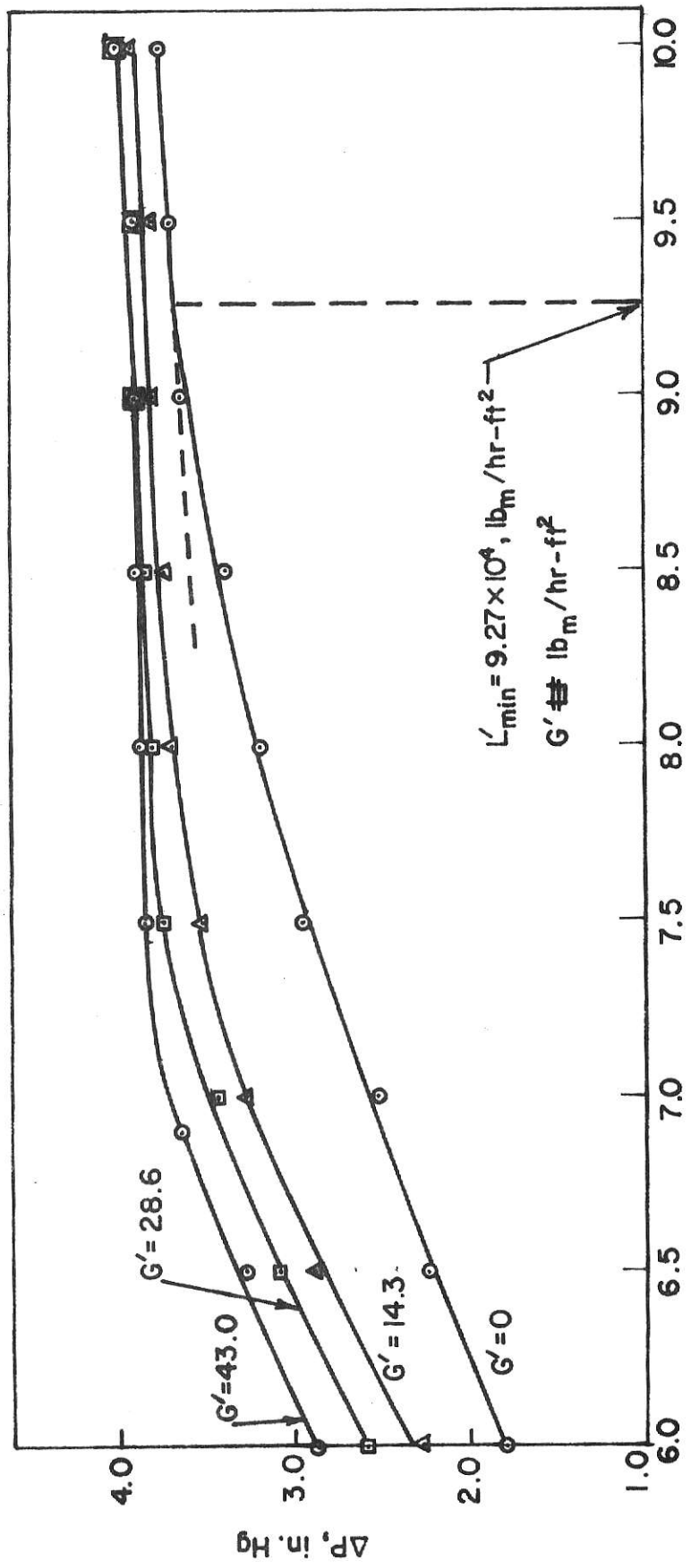

Fig.22. Fluidized bed pressure drop for 0.1875" stainless steel spheres.

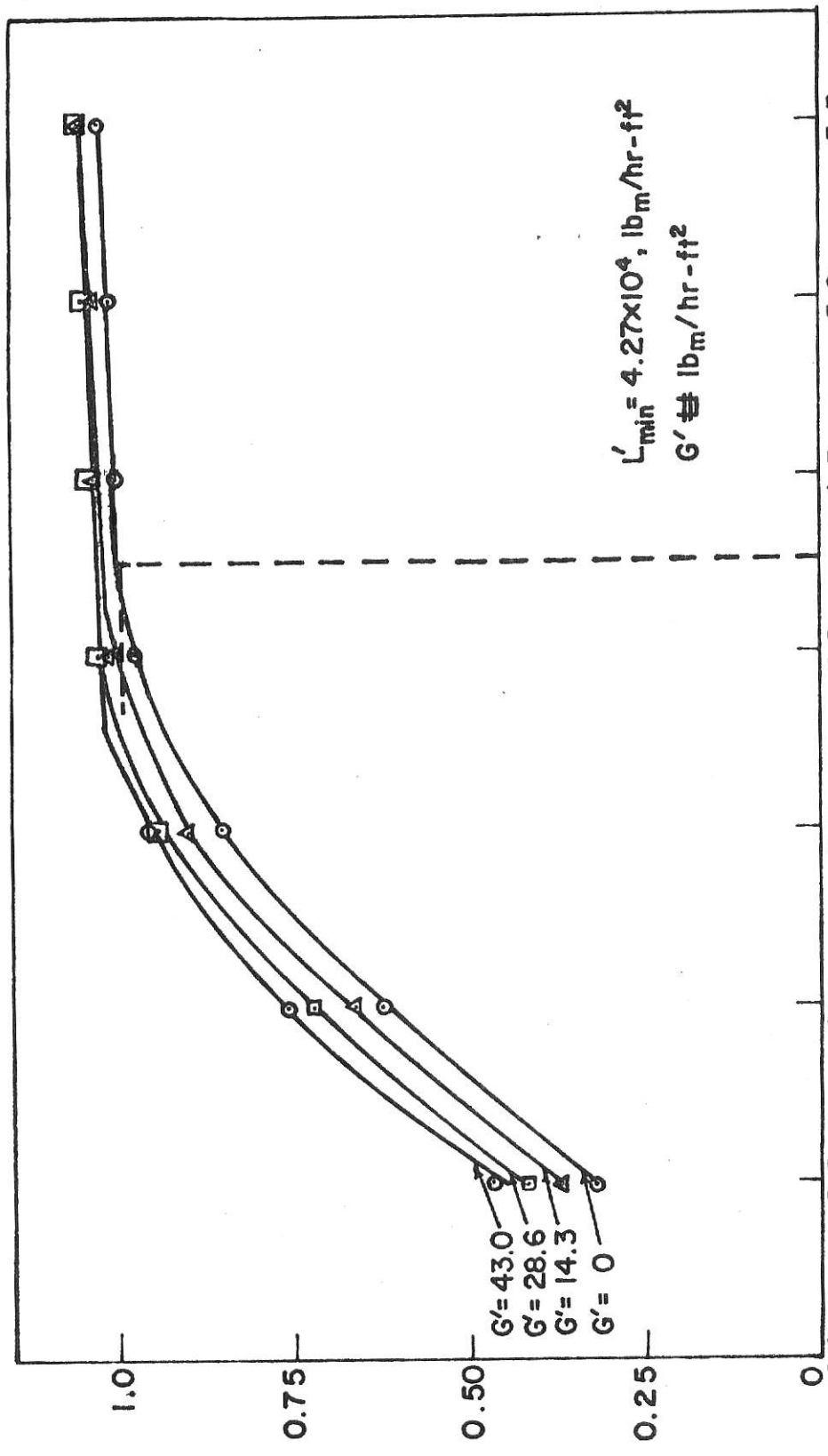

Fig.23. Fluidized bed pressure drop for 0.1875" glass spheres.

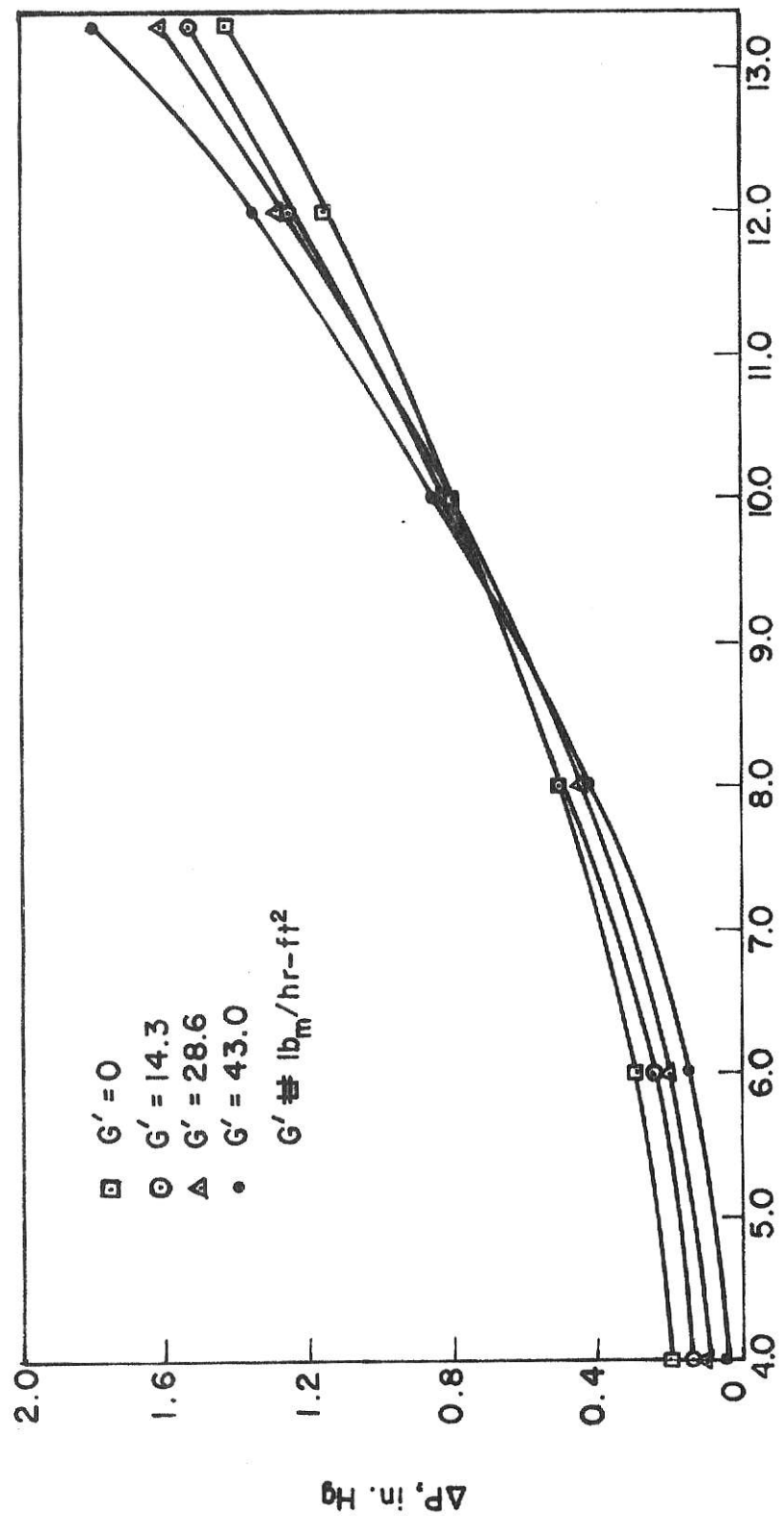

Fig. 24. Pressure drop for plain bubble column.

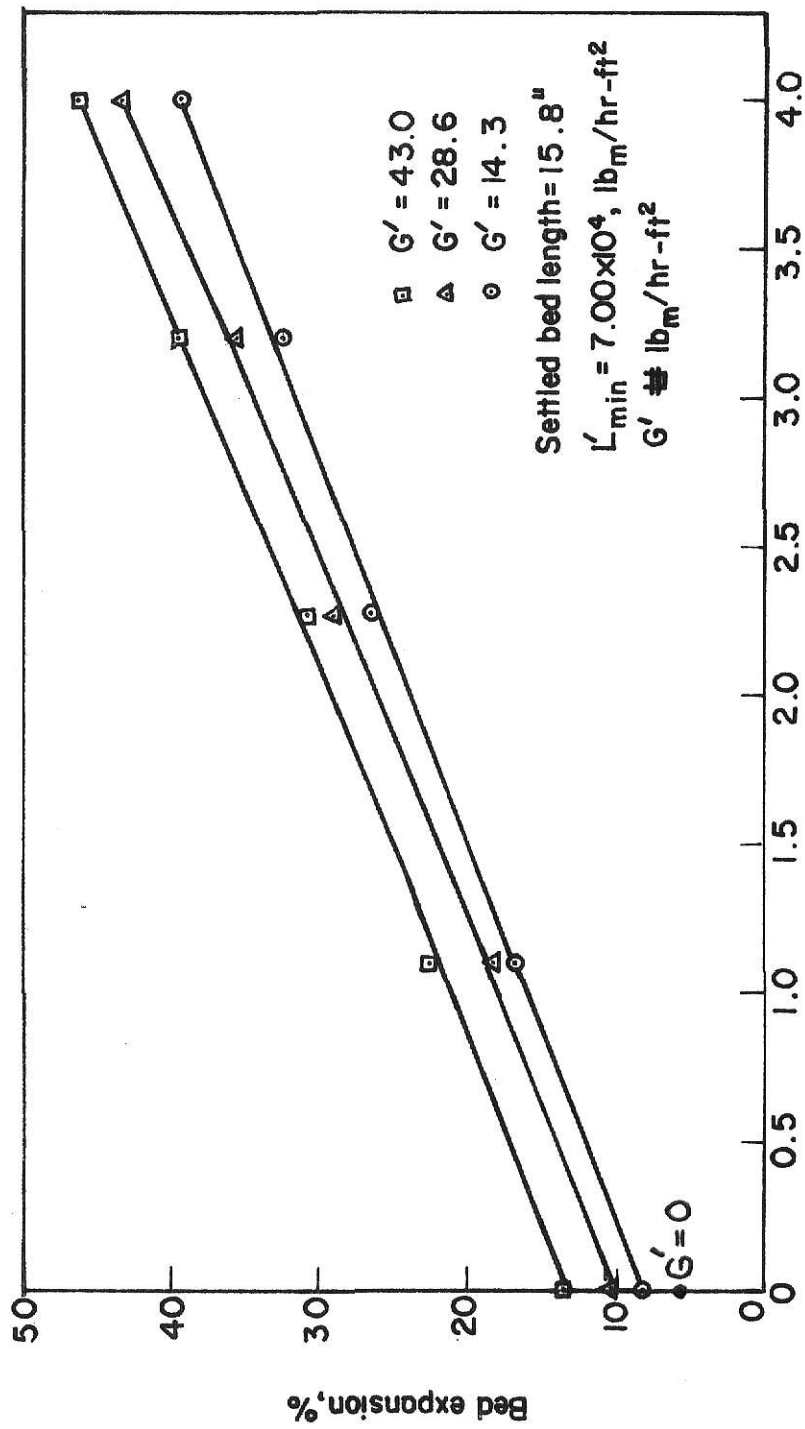

Fig.25. Fluidized bed expansion characteristics for 0.125" copper spheres.

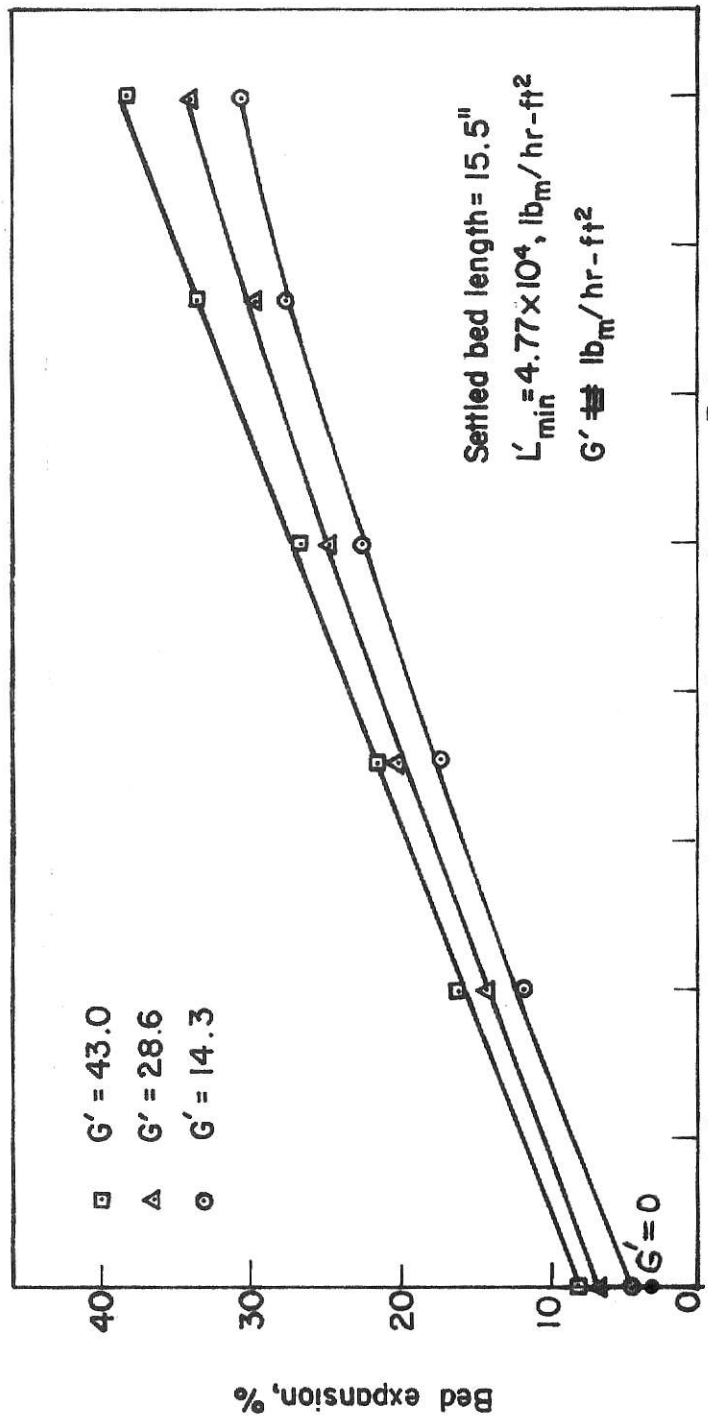

Fig. 26. Fluidized bed expansion characteristics for 0.0625" copper spheres.

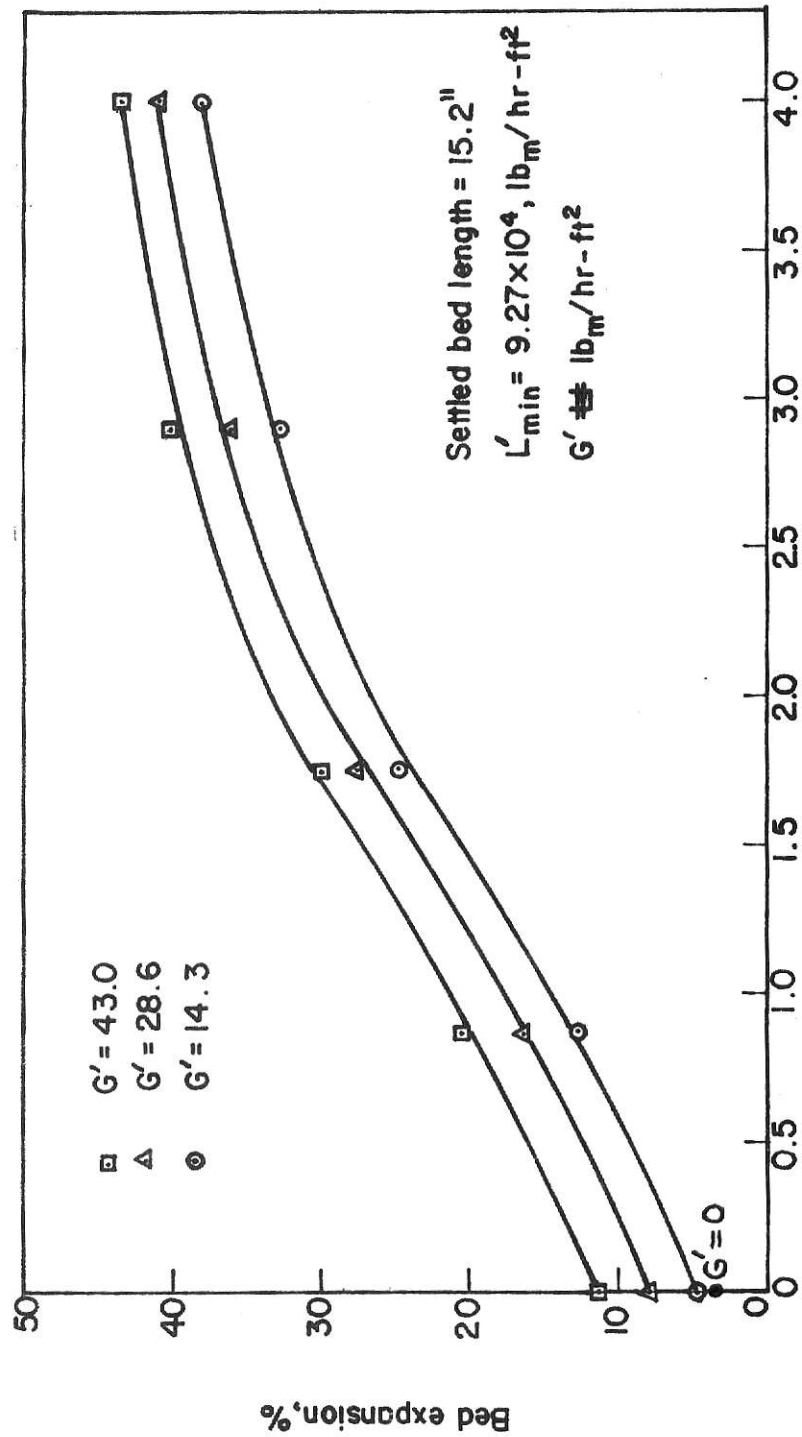

Fig. 27. Fluidized bed expansion characteristics for 0.1875" stainless steel spheres.

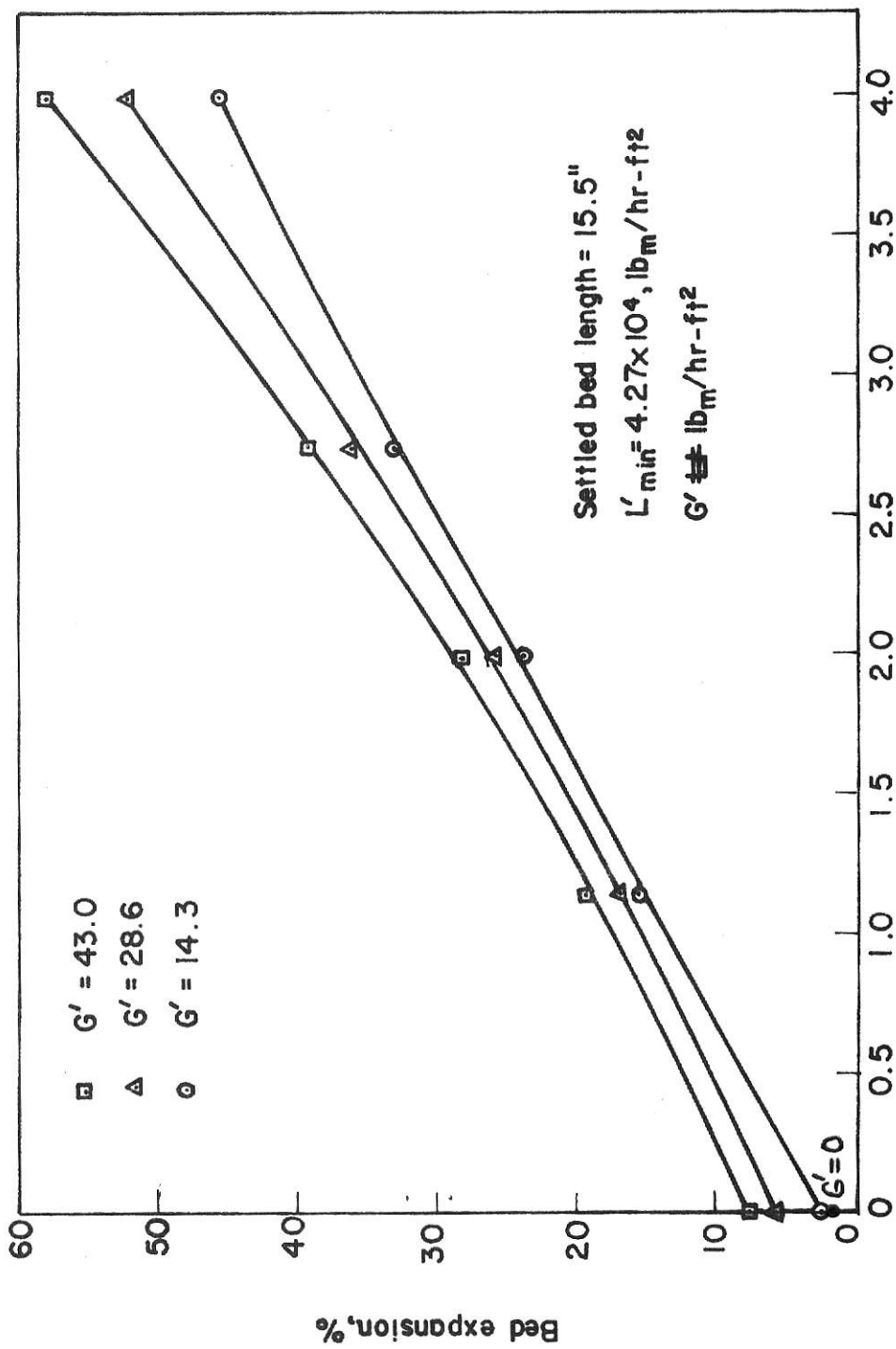

Fig.28. Fluidized bed expansion characteristics for 0.1875" glass spheres.

B. Mass Transfer and Pressure Drop Performance of the Systems Studied, and Comparison of the Models Used.

In order to compare the mass transfer performance of the various fluidized beds with the plain bubble column, Figure 29 through Figure 34 have been prepared. Figure 29 through Figure 31 are based on the plug flow model, and Figure 32 through Figure 34 are based on the dispersion model. We see that overall volumetric mass transfer coefficients ($K_L a$) for all types of fluidized beds are significantly larger than those obtained for the plain bubble column. The largest fluidized bed mass transfer coefficient is obtained for the system of 0.125" copper spheres, and the coefficient is from four to six times larger than that of the plain bubble column at equivalent operating conditions. From Figure 29 through Figure 34, it is obvious that the mass transfer performance of the fluidized beds investigated is superior to the performance of the plain bubble column.

Our experimental results are contrary to those of Maxon and Johnson [7, 13]. In their work on carbon dioxide absorption in a three phase fluidized bed, they reported that absorption rates were lower than those obtained in an equivalent gas-liquid system with no particles present. They have explained this as being due to a higher rate of bubble coalescence and, consequently, a lower gas-liquid interfacial area in the three phase fluidized bed. Maxon and Johnson used both 0.22 mm. sand particles and 0.50-0.80 mm. glass particles as the fluidized bed material. We used much larger particles, varying from 1.6 to 4.8 mm., and different type particles. Therefore, experimental results for absorption in three phase fluidized beds would appear to be valid only for the particular type of fluidized bed material employed. Maxon and Johnson have also pointed this out.

Our experimental results are in agreement with those of Levich [7, 12].

He has reported that for the air-water system with 6.0 mm. glass particles as the fluidized bed material, bubble breakup occurred to the extent of increasing the gas-liquid interfacial area significantly. From these results, Levich has suggested that beds of larger particles may be of practical value because of the improved gas absorption which, presumably, may be obtained. Our experimental results are in agreement with this. It does appear that three phase fluidized beds do have practical value.

Referring to the experimental results reported by Maxon and Johnson [7, 13] and Levich [7, 12], it might be worthwhile to briefly speculate on the causes of the phenomena they observed. Given particles of equal density, small particles are lifted much more easily by the fluidizing media than are large particles. Thus, in a three phase fluidized bed an ascending gas bubble would lift a small particle much easier than a large particle. For large particles then, an ascending gas bubble could meet with considerable resistance and be squeezed between particles, causing bubble breakup and a resultant increase in gas-liquid interfacial area. In contrast, small particles may be pushed aside quite easily by an ascending gas bubble. In this case, there would be negligible bubble breakup and the particles would only serve to occupy volume at the expense of the gas and liquid holdups, with the resultant decrease in gas-liquid interfacial area.

We see from Figure 29 through Figure 34 that there are significant differences in mass transfer performance between the different types of fluidized beds. The best mass transfer performance was obtained from the system of 0.125" copper spheres, and visual observations lend credence to this result. It was observed that the fluidized bed of 0.125" copper spheres was very effective in breaking up large gas bubbles into many

smaller ones. The large gas-liquid interfacial area produced undoubtedly accounts for the large values of ($K_L a$) obtained for the 0.125" copper spheres. The second best mass transfer performance was obtained from the system of 0.1875" stainless steel spheres. Here again, it was observed that the fluidized bed was very effective in breaking up large gas bubbles into many smaller ones. However, it was also observed that a considerable amount of "slugging" [8, 9] occurred in the system of 0.1875" stainless steel spheres. Slugs of liquid containing very few dispersed gas bubbles ascended the column in a periodic fashion. This "slugging" phenomena reduces the overall gas-liquid interfacial area, resulting in smaller values of ($K_L a$). This phenomena was almost entirely absent for the system of 0.125" copper spheres.

We see from Figure 29 through Figure 34 that the mass transfer performance for the system of 0.0625" copper spheres and that for the system of 0.1875" glass spheres are relatively poor compared to the two systems previously discussed. However, their performance is still superior to the equivalent plain bubble column. For these two systems, it was observed that they were both fairly ineffective in breaking up large gas bubbles into many smaller ones. It was also observed that a considerable amount of "slugging" occurred in the system of 0.1875" glass spheres, but was almost entirely absent in the system of 0.0625" copper spheres.

With respect to the differences in mass transfer performance between the different types of fluidized beds, several conclusions can be drawn. First, for particles of equal density, increasing the particle size increases the mass transfer performance of the fluidized bed. Second, for particles of equal size, increasing the particle density increases the mass transfer

performance of the fluidized bed. Third, as particle size increases, fluidized bed "slugging" increases. It must be pointed out here that the above generalizations apply only to the range of fluidized bed properties investigated.

To compare the mass transfer coefficients determined from the plug flow model and the dispersion model, Figure 35 through Figure 39 have been prepared. We see that for all types of fluidized beds as well as the plain bubble column, the values of $(K_L a)_{DM}$ are larger than the values of $(K_L a)_{PF}$ at equivalent operating conditions. Liquid dispersion in the systems lowers the concentration driving force (C^*-C) causing the mass transfer. Since (C^*-C) is smaller for the dispersion model than for the plug flow model, $(K_L a)_{DM}$ must be larger than $(K_L a)_{PF}$ for the same experimentally measured value of Γ_e. The difference between the experimentally determined values of $(K_L a)_{PF}$ and $(K_L a)_{DM}$ depends both on the value Pe_L and the value of Γ_e.[1] This causes the difference between $(K_L a)_{PF}$ and $(K_L a)_{DM}$ to be a function of L', G', and the type of system, as is apparent from Figure 35 through Figure 39. Since it was determined experimentally that liquid dispersion existed in our experimental systems ($Pe_L \neq \infty$), the mass transfer coefficient based on the dispersion model $(K_L a)_{DM}$ is a better approximation to the true mass transfer coefficient than $(K_L a)_{PF}$. Therefore, all following discussion will deal exclusively with $(K_L a)_{DM}$.

Up to this point, all discussion has been in terms of mass transfer performance. For completeness, we must discuss the relationship between mass transfer performance and pressure drop for the various systems investigated. In order to do this, Figure 40 through Figure 42 have been prepared.

[1] See Theoretical Section, Figure 2a through Figure 2c.

As indicated in Figure 40, $(K_L a)^*$ is a ratio of the fluidized bed mass transfer coefficient to the plain bubble column mass transfer coefficient, at equivalent experimental operating conditions. $(K_L a)^*$ has been determined from the dispersion model mass transfer coefficients, Figure 15 through Figure 19. As indicated in Figure 40, $(\Delta P)^*$ is a ratio of the fluidized bed pressure drop to the plain bubble column pressure drop, at equivalent experimental operating conditions, and at the same length and cross sectional area. Thus, the experimental data from Figure 20 through Figure 28 have been used to determine $(\Delta P)^*$ for equivalent lengths.

In Figure 40 through Figure 42, the ratio $[(K_L a)^*/(\Delta P)^*]$ is presented as a function of $(L'-L'_{min})$ and G'. $[(K_L a)^*/(\Delta P)^*]$ is a measure of mass transfer performance as related to pressure drop for the fluidized beds as compared to the plain bubble column. Ideally, we would like this ratio to be large, preferably greater than 1.0. We see that in general, the ratio $[(K_L a)^*/(\Delta P)^*]$ increases with increasing liquid rate at a constant gas rate, and appears to level off at the upper end of the experimental liquid range, approaching 1.0 for several of the systems. We also see that the ratio $[(K_L a)^*/(\Delta P)^*]$ changes somewhat with gas rate at a constant liquid rate, but the behavior is erratic and no generalization can be made.

From Figure 40 through Figure 42, we see that in general the two systems of 0.125" copper spheres and 0.1875" stainless steel spheres yield the best mass transfer to pressure drop performance as compared to the plain bubble column. Relative to these two systems, the performance of the system of 0.1875" glass spheres is intermediate and that of the 0.0625" copper spheres is poor.

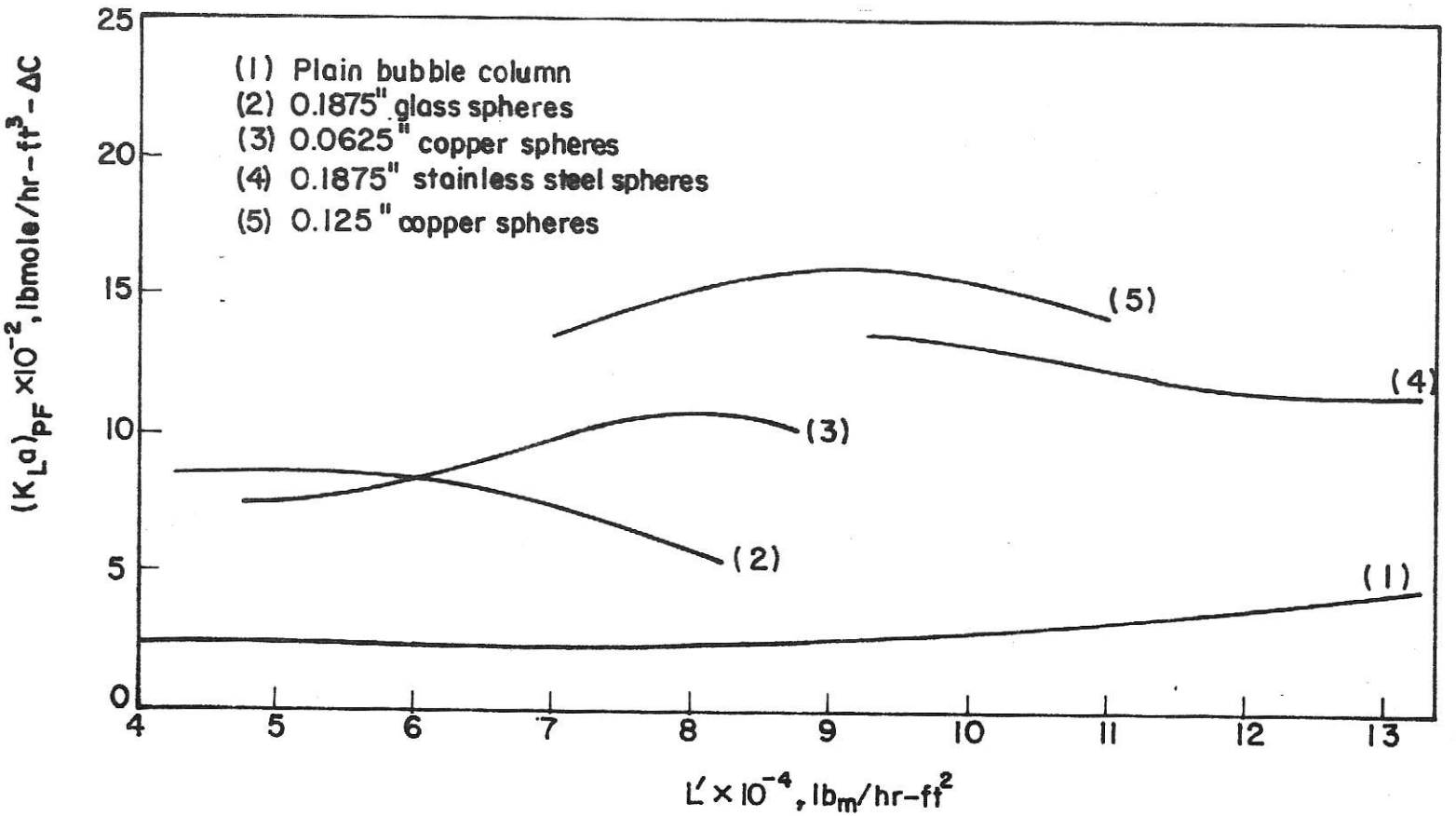

Fig.29. Comparison of mass transfer coefficients for $G' = 14.3$, lb$_m$/hr-ft^2 based on the plug flow model.

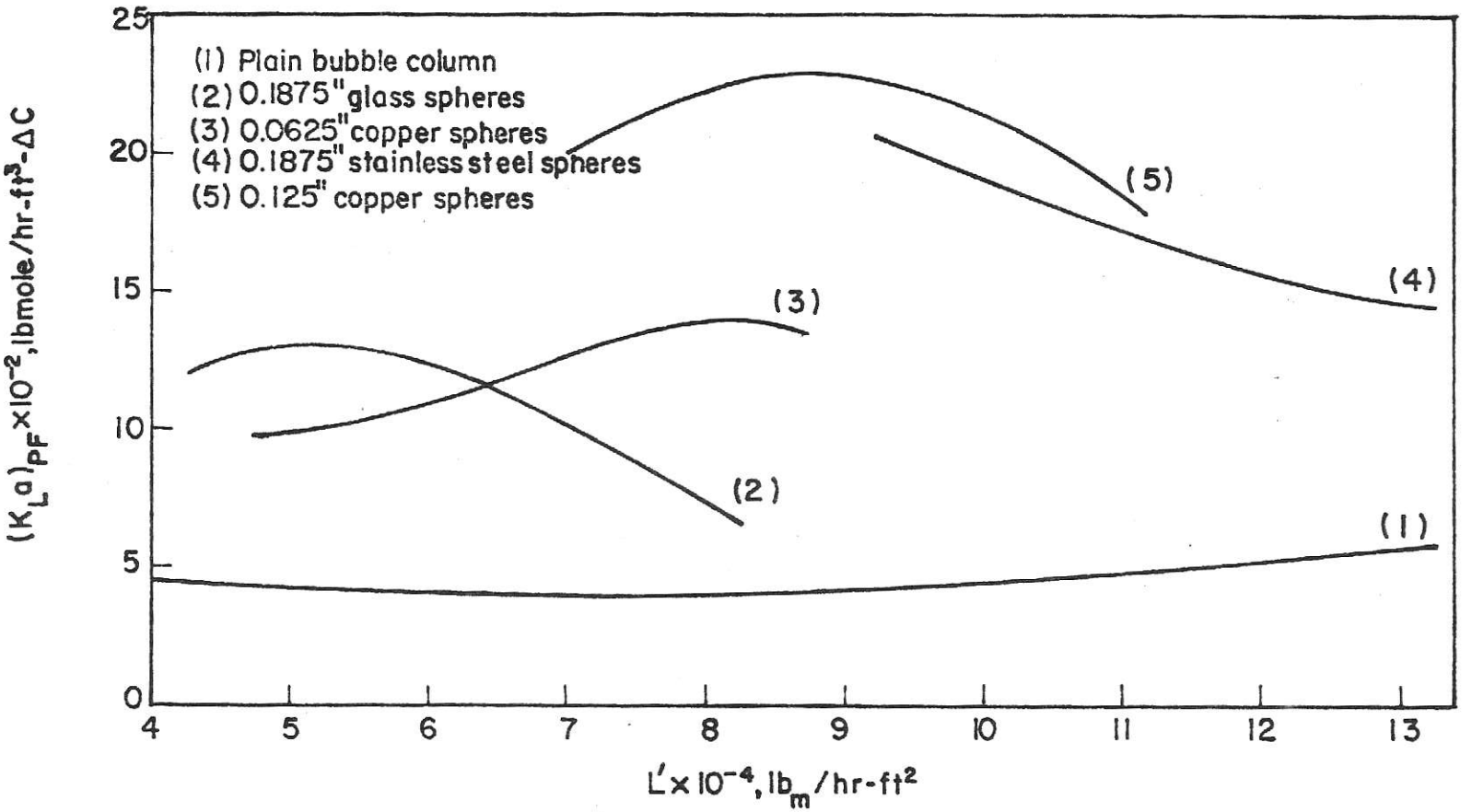

Fig. 30. Comparison of mass transfer coefficients for $G' = 28.6$, lb$_m$/hr-ft^2 based on the plug flow model.

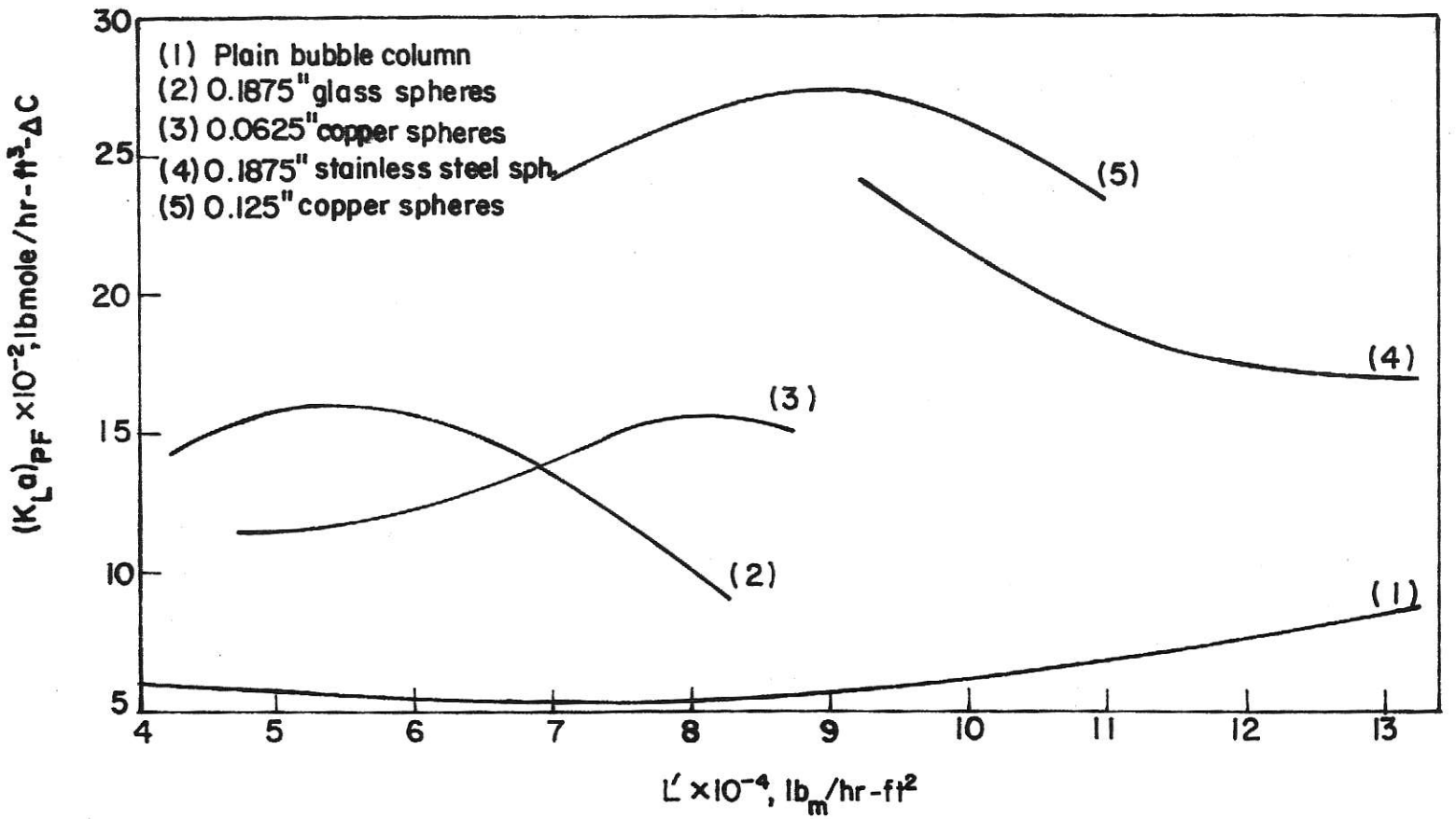

Fig. 31. Comparison of mass transfer coefficients for $G' = 43.0$, $lb_m/hr\text{-}ft^2$ based on the plug flow model.

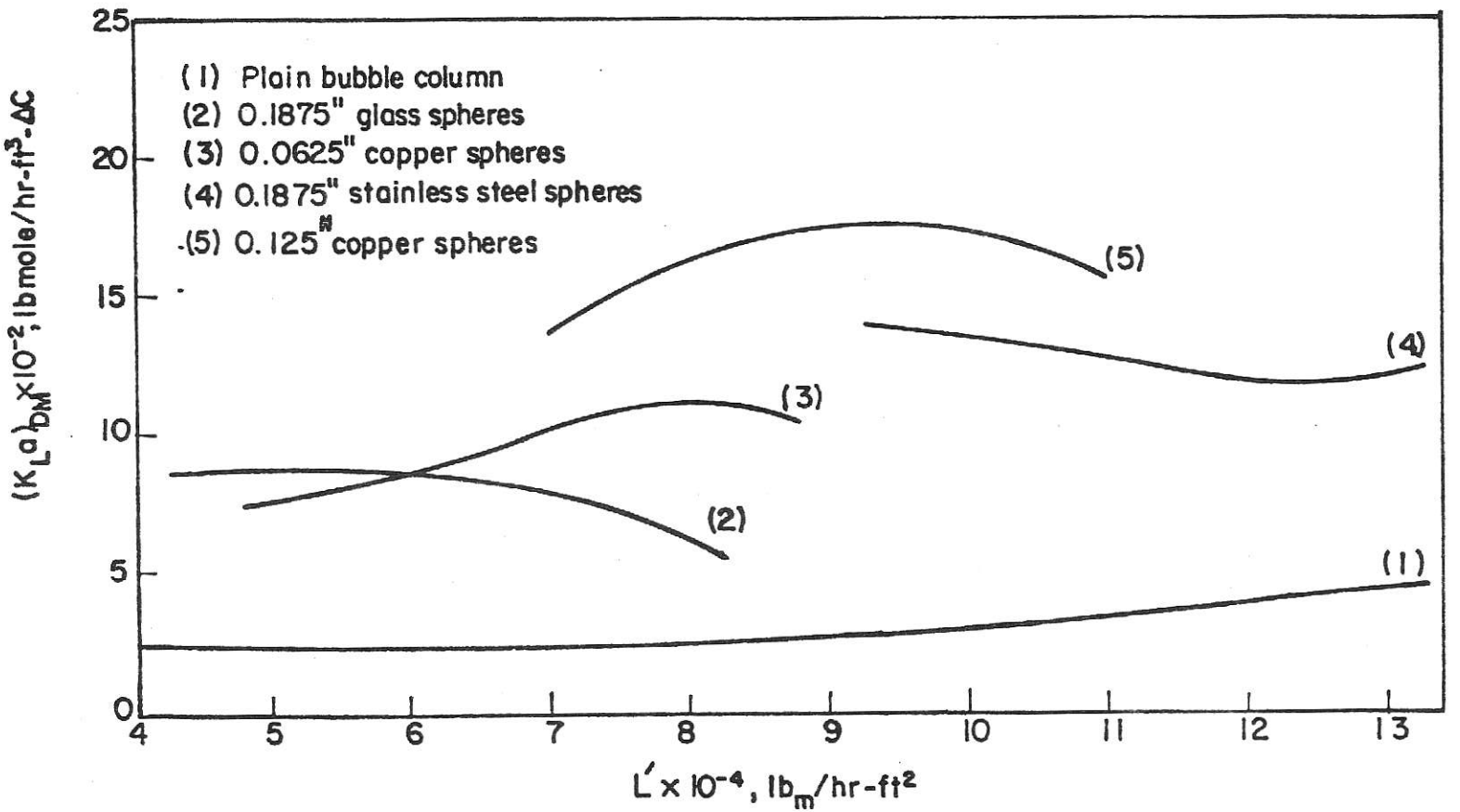

Fig.32. Comparison of mass transfer coefficients for $G' = 14.3$, lb$_m$/hr-ft^2 based on the dispersion model.

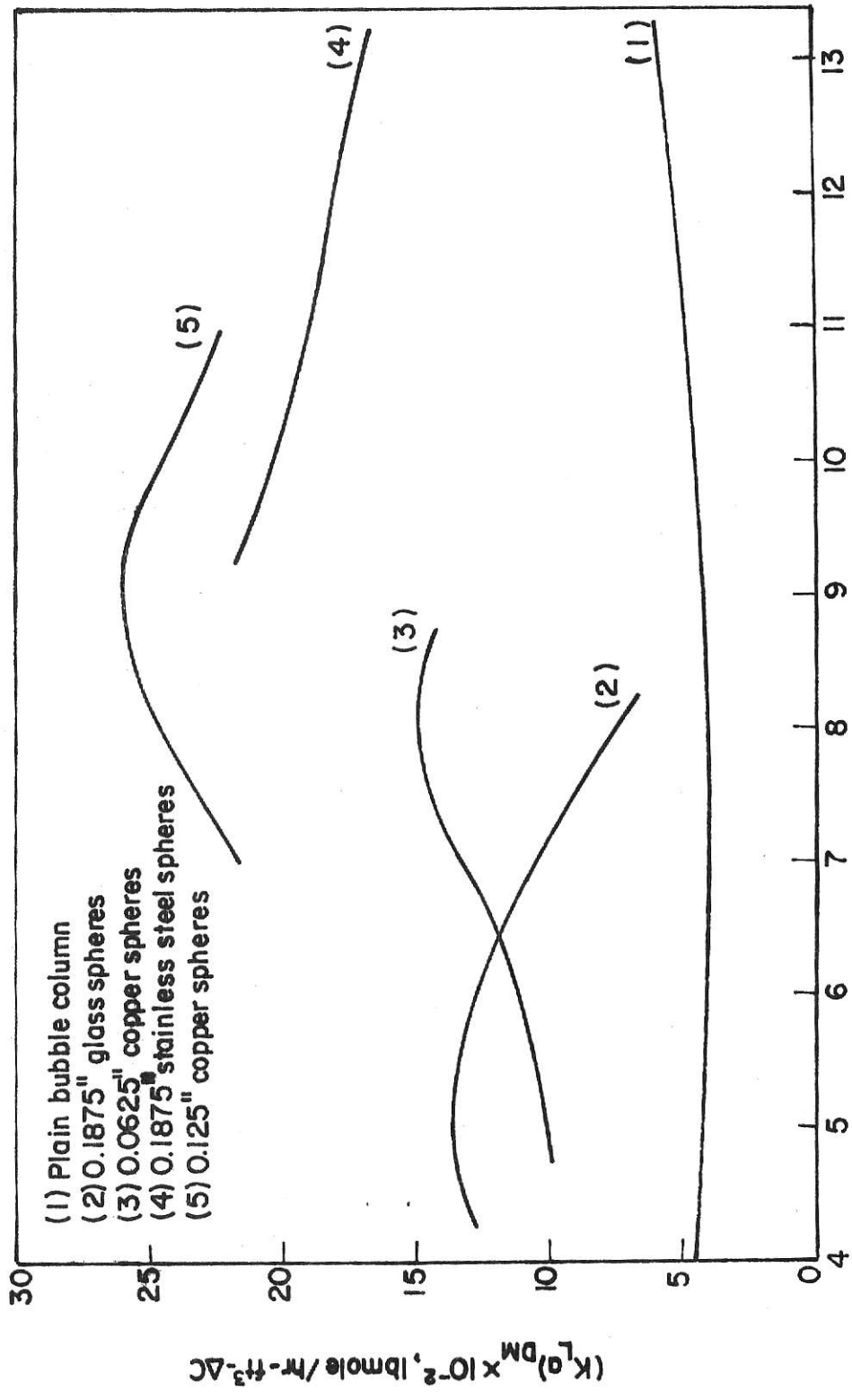

Fig.33. Comparison of mass transfer coefficients for $G' = 28.6$, lb_m/hr-ft^2 based on the dispersion model.

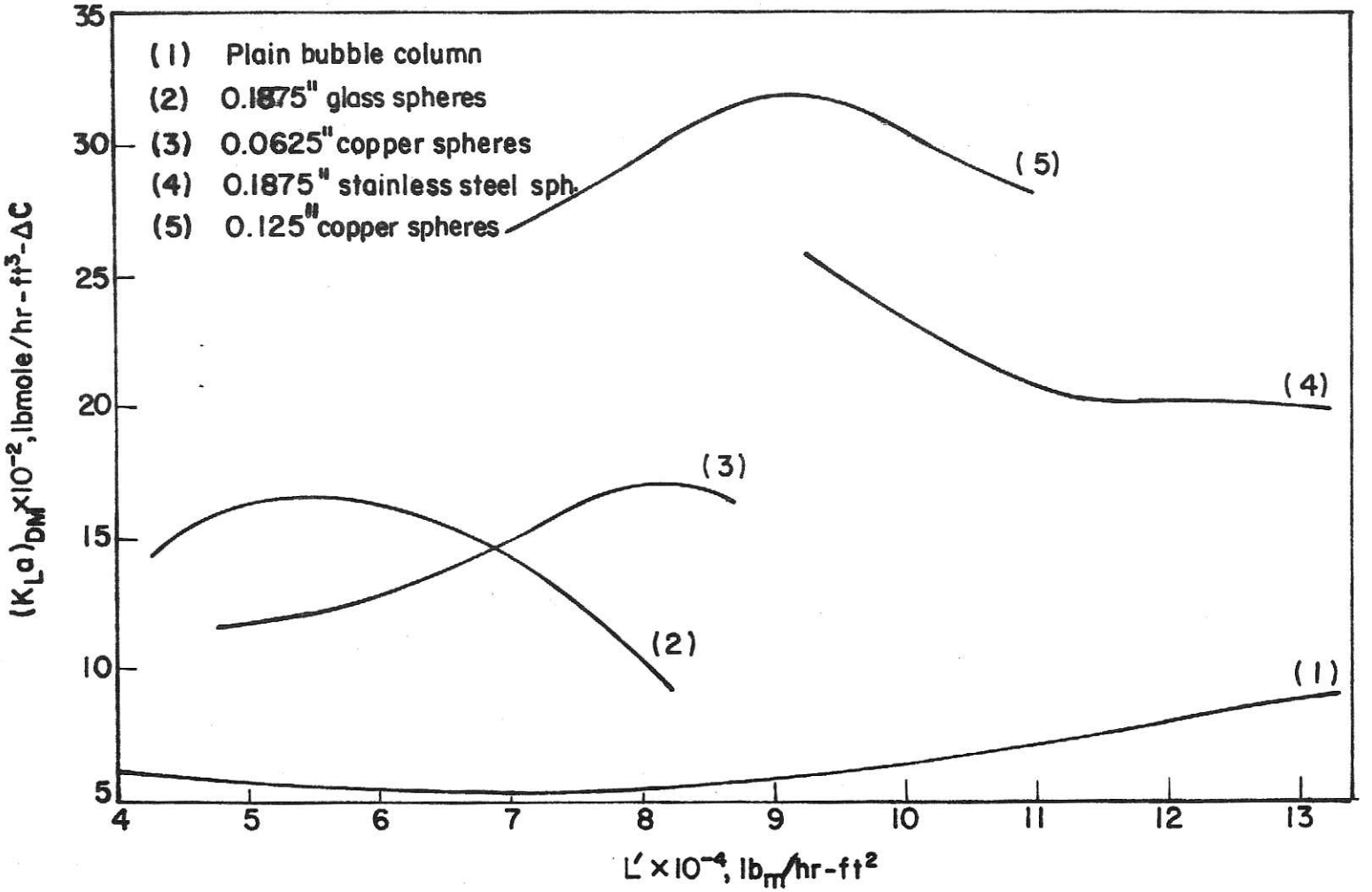

Fig.34. Comparison of mass transfer coefficients for $G' = 43.0$, lb$_m$/hr-ft^2 based on the dispersion model.

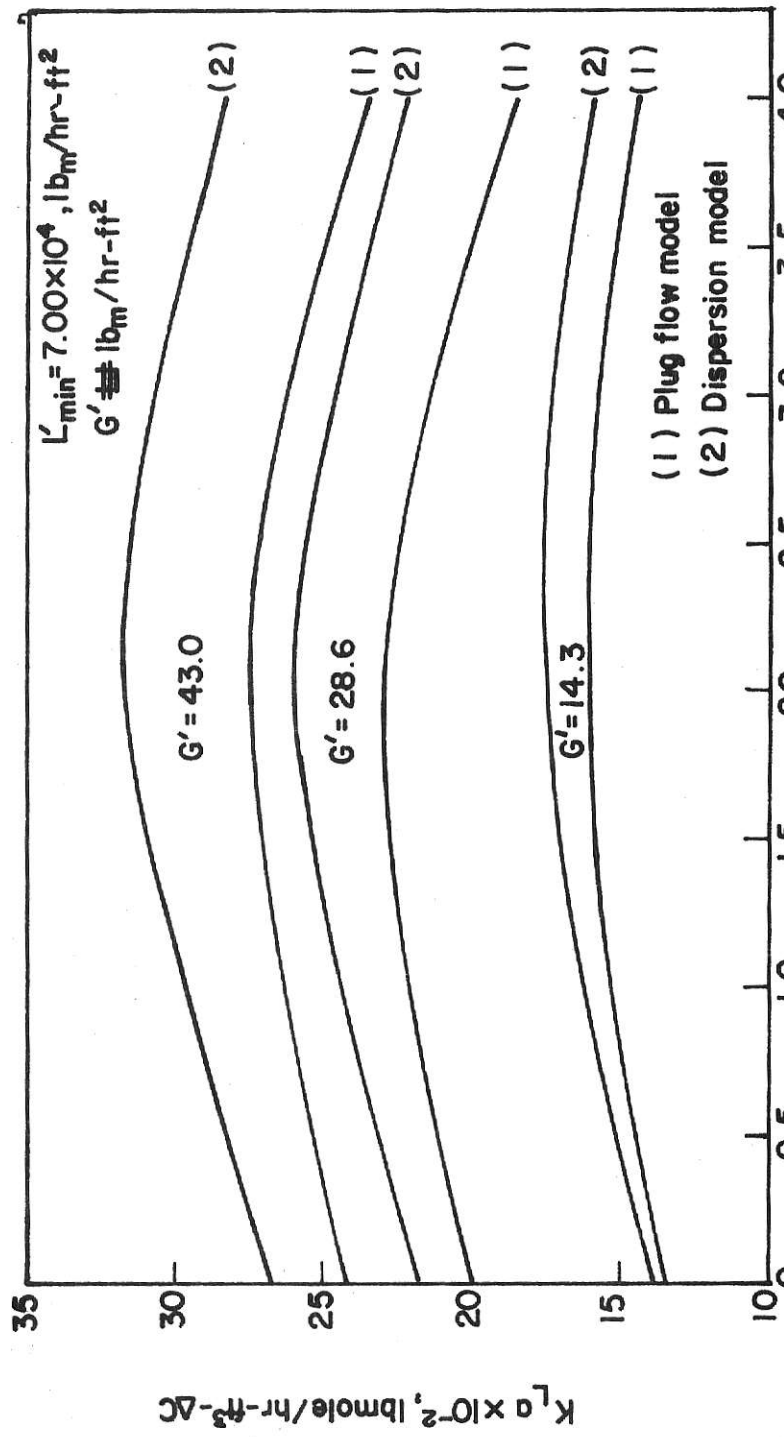

Fig. 35. Comparison of mass transfer coefficients between the plug flow model and dispersion model for 0.125" copper spheres.

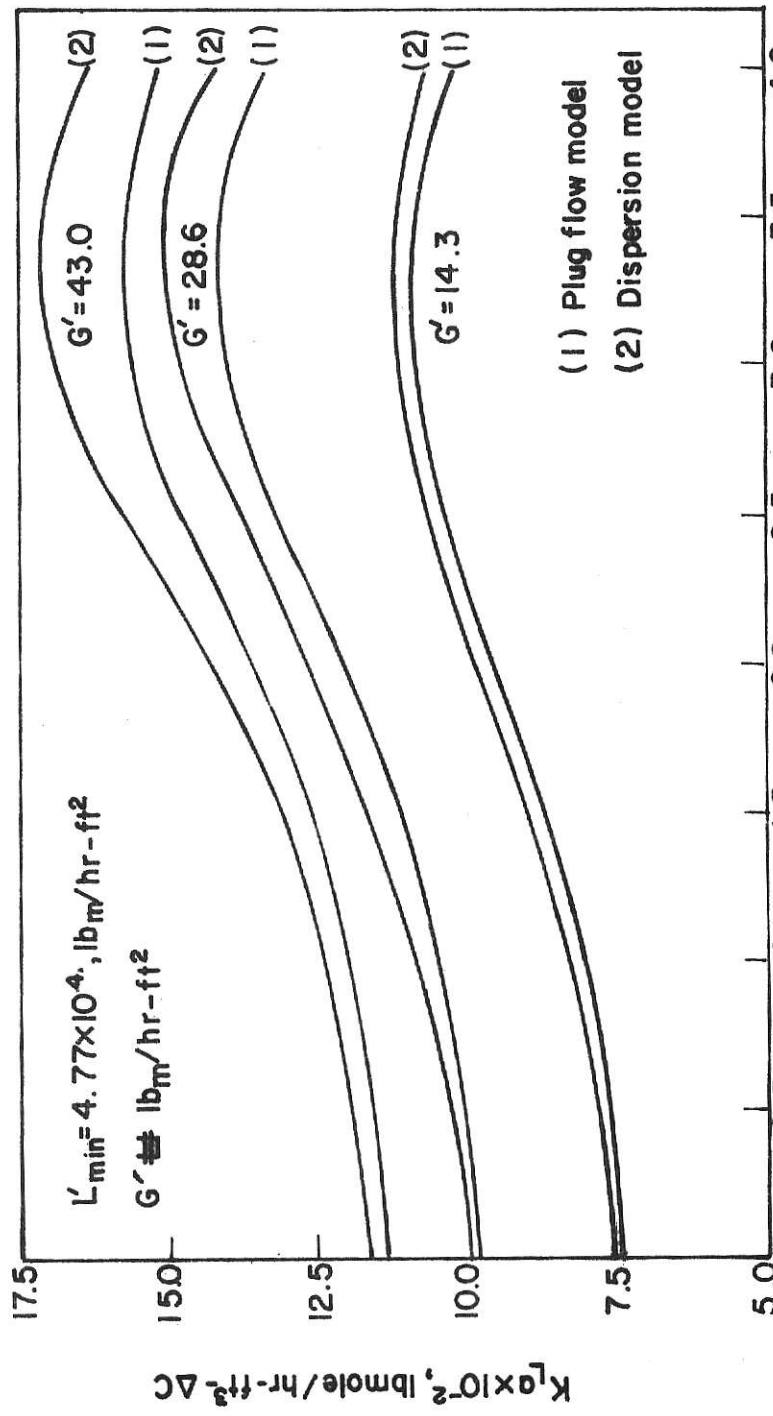

Fig.36. Comparison of mass transfer coefficients between the plug flow model and dispersion model for 0.0625" copper spheres.

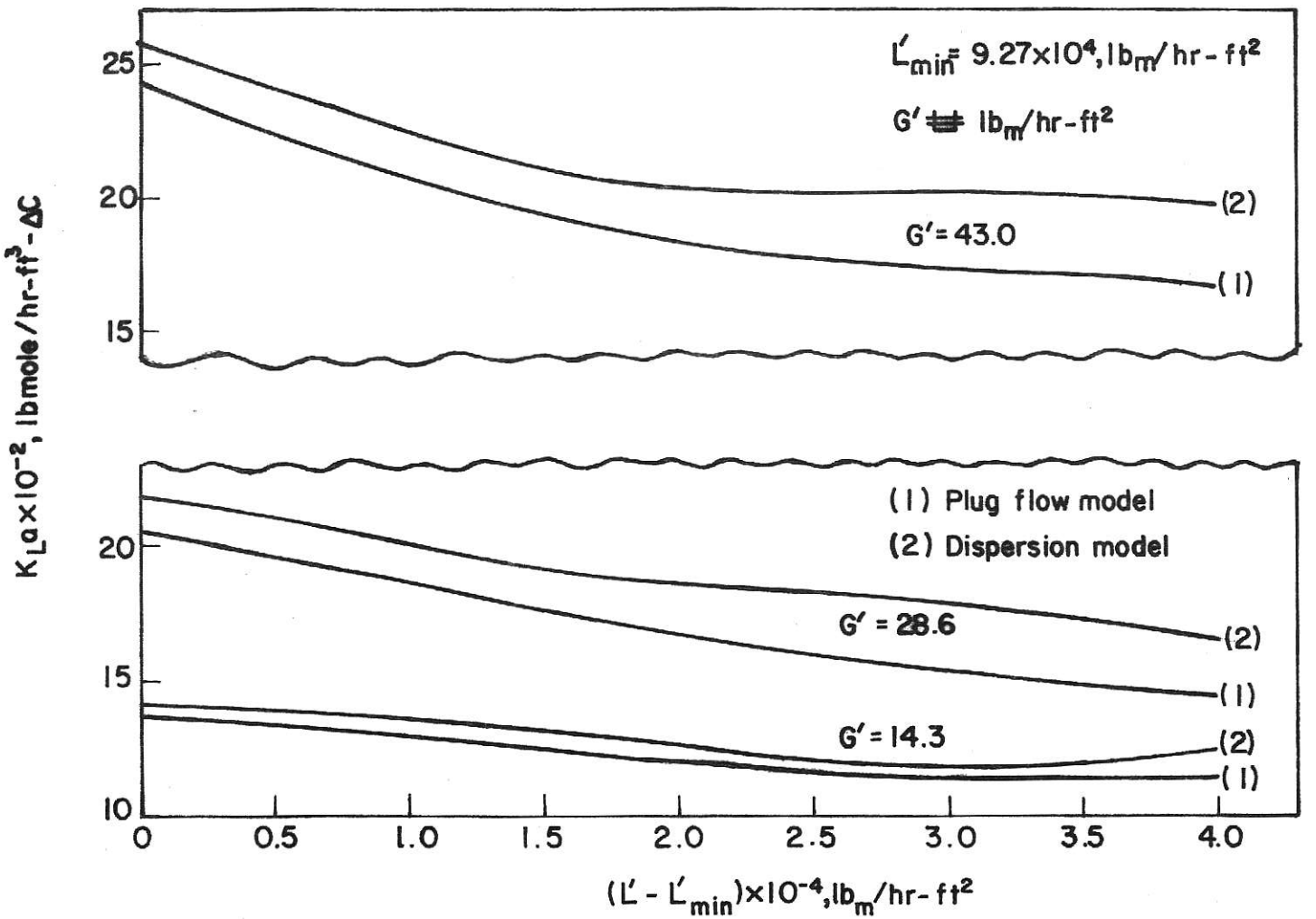

Fig.37. Comparison of mass transfer coefficients between the plug flow model and dispersion model for 0.1875" stainless steel spheres.

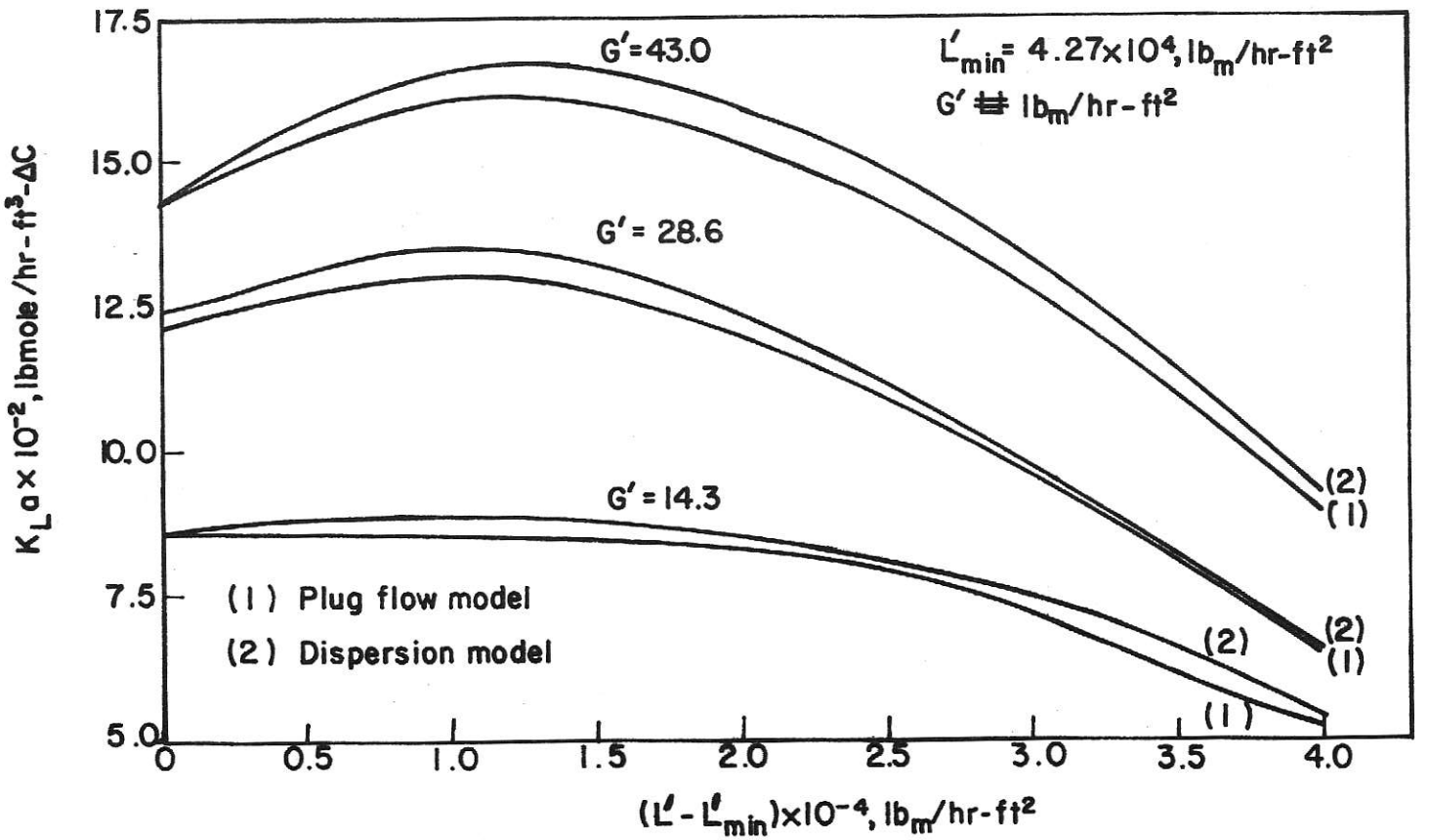

Fig. 38. Comparison of mass transfer coefficients between the plug flow model and dispersion model for 0.1875" glass spheres.

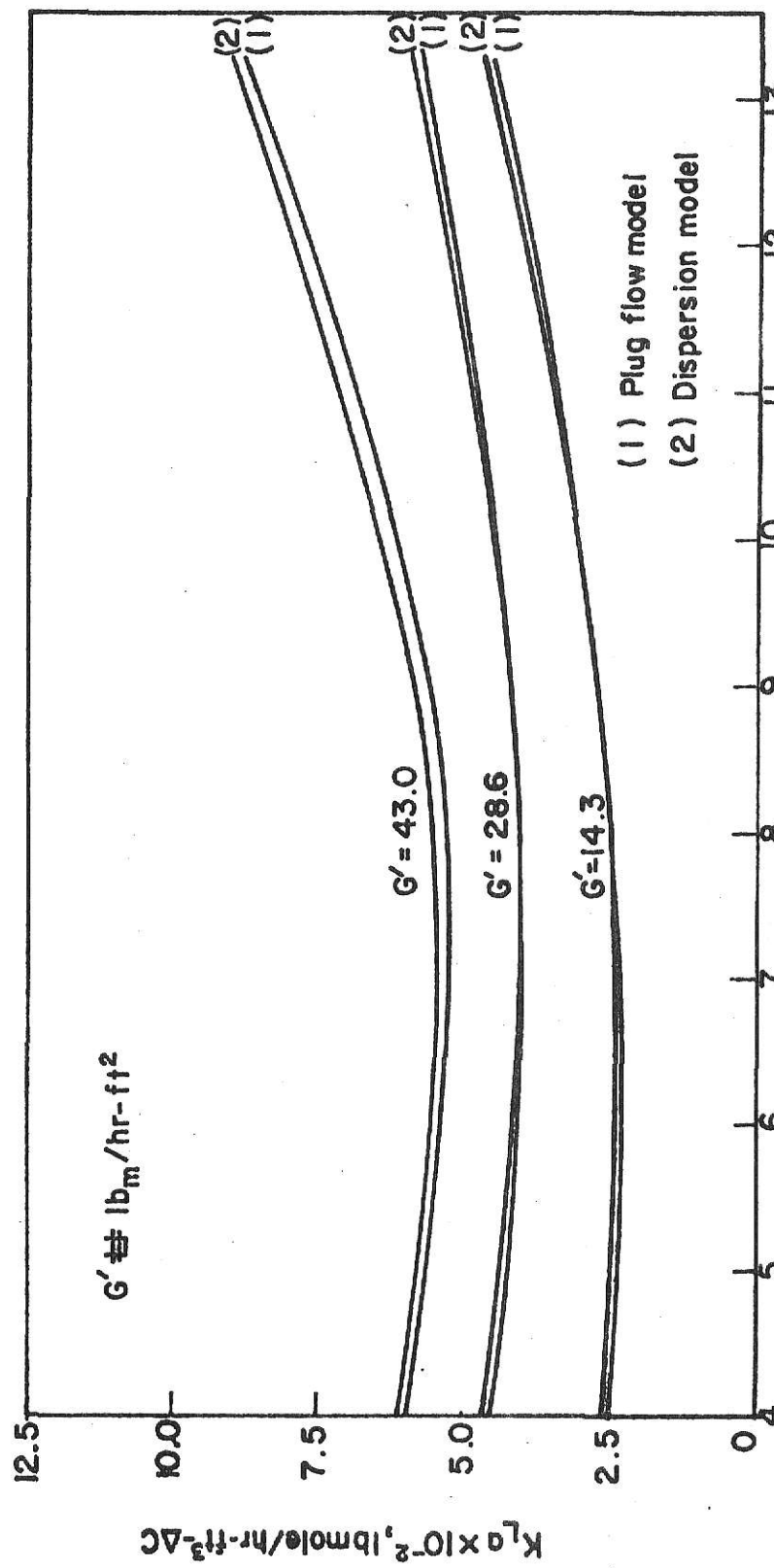

Fig. 39. Comparison of mass transfer coefficients between the plug flow model and dispersion model for the plain bubble column.

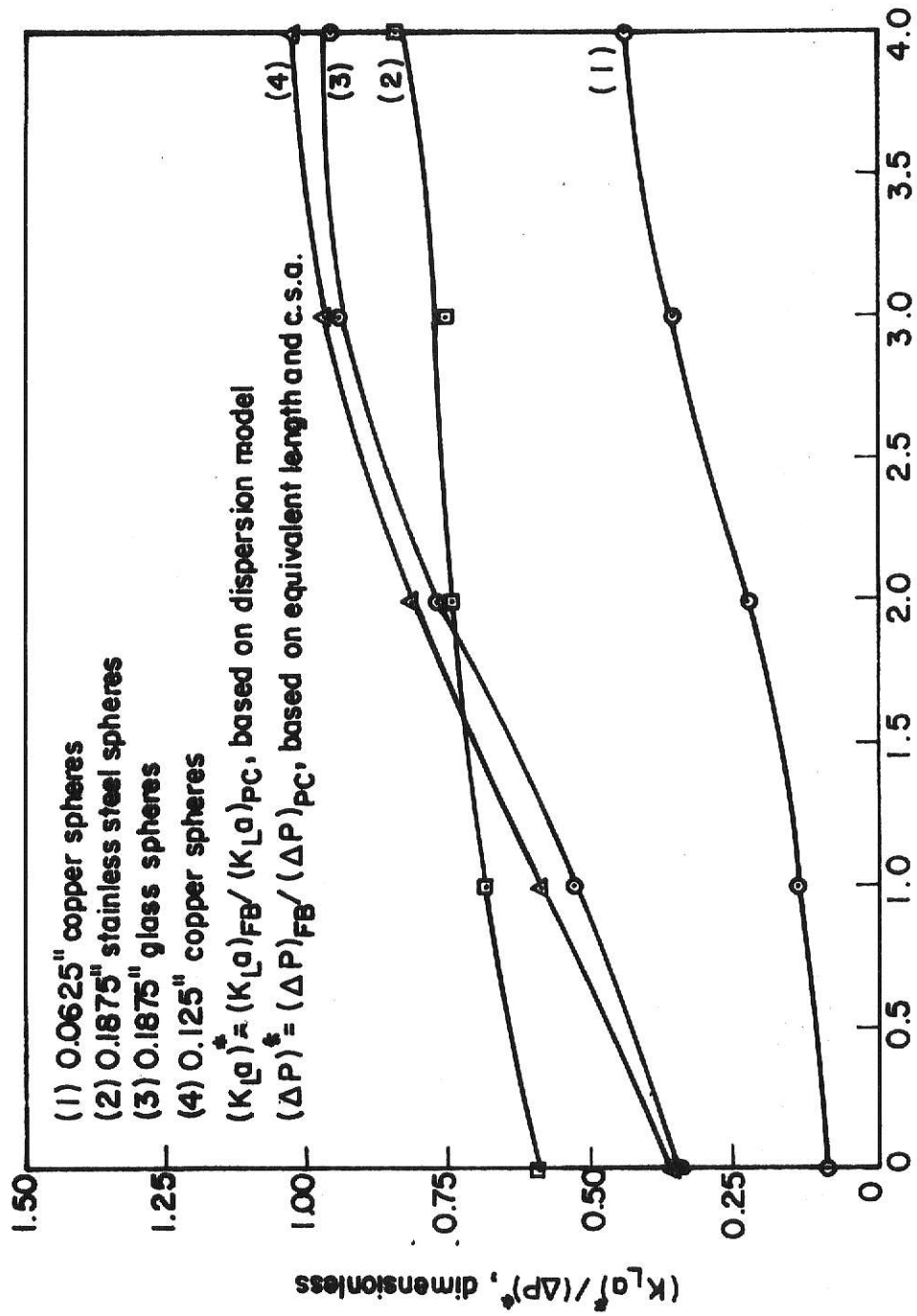

Fig.40. Comparison of mass transfer and pressure drop between fluidized beds and plain bubble column for $G' = 14.3, lb_m/hr\text{-}ft^2$.

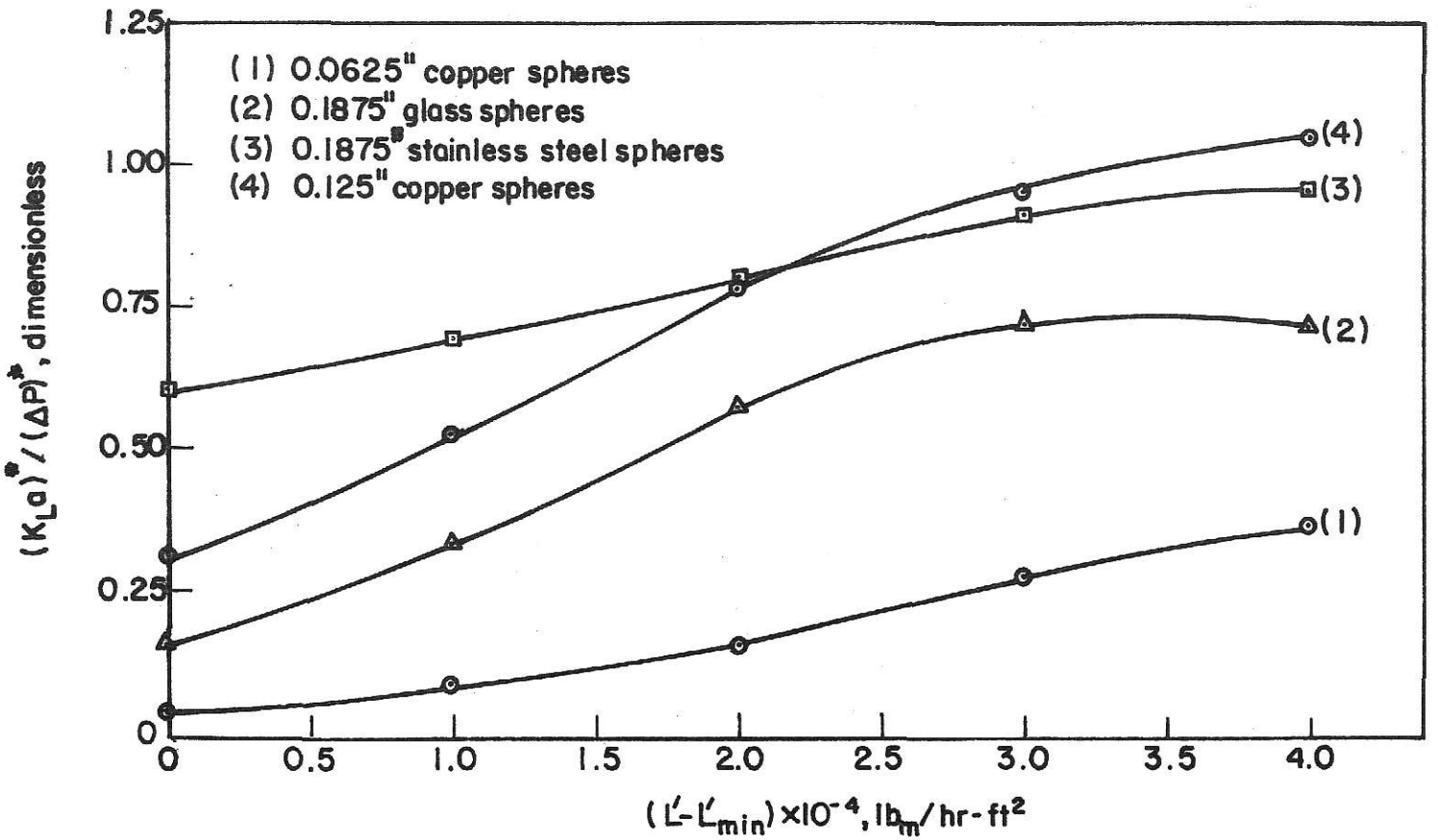

Fig. 41. Comparison of mass transfer and pressure drop between fluidized beds and plain bubble column for $G' = 28.6, lb_m/hr-ft^2$.

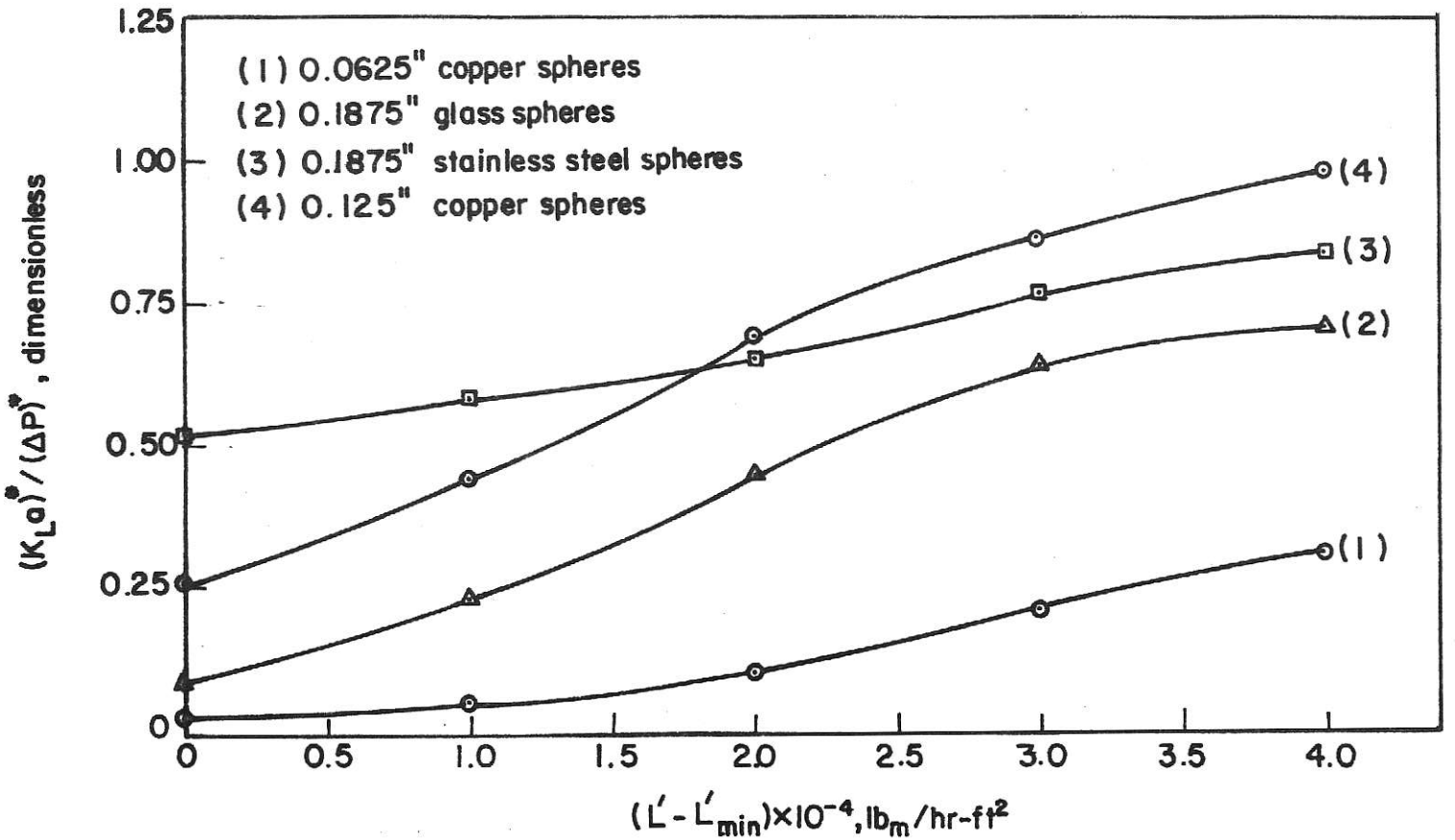

Fig.42. Comparison of mass transfer and pressure drop between fluidized beds and plain bubble column for $G'=43.0, lb_m/hr\text{-}ft^2$.

C. Empirical Correlations Derived from Experimental Data.

In order to apply the results obtained to the design of large scale three phase fluidized beds for the absorption of oxygen in water, it is necessary to develop generalized correlations for predicting design parameters as a function of fluidized bed properties and operating conditions. To this end, the following correlations have been developed.

The experimental results from Figure 20 through Figure 23 have been used to develop the correlation shown in Figure 43. The particle Reynolds number at the fluidization onset point (Re_{min}) is defined as $D_p\rho_p L'_{min}/\mu_m\rho_m$. A least-squares fit of the experimental data yields the following empirical correlation shown in Figure 43 [6].

$$(Re_{min})^{\frac{1}{2}} = (7.75)(D_p\rho_p) + 6.82$$
$$2.53 \leq D_p\rho_p \leq 7.82 \qquad (11)$$

Empirical correlations for predicting the fluidization onset point are available in the literature [9]. These correlations generally apply to a very wide range of particle properties and operating conditions. The correlation shown in Figure 43 applies only to our experimental systems.

For a given set of fluidized bed particle properties and liquid properties, the correlation in Figure 43 may be used to estimate the minimum required fluidization onset velocity (L'_{min}). As previously discussed, (L'_{min}) is the minimum required liquid mass velocity for fluidization at zero gas rate, $G' = 0$. Attempts were made to develop a correlation similar to Figure 43 for $G' > 0$, however, this was not successful. Since the actual value of L' required for fluidization will be smaller than (L'_{min}) when $G' > 0$, the

use of the correlation in Figure 43 for design calculations will always insure an adequate liquid rate for fluidization.

The experimental results from Figure 9 through Figure 12 have been used to develop the correlation shown in Figure 44. The particle Reynolds number (Re) is defined as $D_p \rho_p L'/\mu_m \rho_m$. A least-squares fit of the experimental data yields the following empirical relationship shown in Figure 44.

$$\begin{aligned} &\ln(Pe_L^{1/2}) = 2.154 - (0.0176)(L'/L'_{min})Re^{1/2} \\ &26.2 \leq (L'/L'_{min})Re^{1/2} \leq 116.0 \\ &14.3 \leq G' \leq 43.0 \end{aligned} \tag{12}$$

For a given set of fluidized bed particle properties and operating conditions, the correlation in Figure 44 may be used to estimate the value of Pe_L for the fluidized bed. Thus, the liquid dispersion characteristics of the particular fluidized bed may be predicted from the correlation in Figure 44.

The experimental results from Figure 9 through Figure 12 and Figure 15 through Figure 18 have been used to develop the correlations shown in Figure 45 through Figure 47. $(K_L a)_c$ is defined as $(K_L a)_{DM}/(K_L a)_{base}$ in these figures and is based on dispersion model mass transfer coefficients, $(K_L a)_{DM}$. Least-squares fits of the experimental data yield the following empirical relationships shown in Figure 45 through Figure 47.

For Figure 45

$$\begin{aligned} &[(K_L a)_c/Pe_L]^{1/4} = (8.12\text{x}10^{-3})(L'/L'_{min})Re^{1/2} + 0.242 \\ &26.2 \leq (L'/L'_{min})Re^{1/2} \leq 116.0 \\ &G' = 14.3 \end{aligned} \tag{13}$$

For Figure 46

$$[(K_L a)_c/Pe_L]^{1/4} = (8.91\times10^{-3})(L'/L'_{min})Re^{1/2} + 0.252$$

$$26.2 \leq (L'/L'_{min})Re^{1/2} \leq 116.0 \qquad (14)$$

$$G' = 28.6$$

For Figure 47

$$[(K_L a)_c/Pe_L]^{1/4} = (9.40\times10^{-3})(L'/L'_{min})Re^{1/2} + 0.259$$

$$26.2 \leq (L'/L'_{min})Re^{1/2} \leq 116.0 \qquad (15)$$

$$G' = 43.0$$

The results of Figure 45 through Figure 47 are combined into Figure 48 for ease of comparison. The results from Figure 45 through Figure 47 have been used to develop the correlation shown in Figure 49 for the experimental range of gas rates. $(G')_c$ is defined as G'/G'_{base}.

A least-squares fit of the experimental data yields the following empirical relationship shown in Figure 49.

$$[(K_L a)_c/Pe_L]^{1/4}/[(G')_c]^{1/8} = (9.00\times10^{-3})(L'/L'_{min})Re^{1/2} + 0.189$$

$$26.2 \leq (L'/L'_{min})Re^{1/2} \leq 116.0 \qquad (16)$$

$$14.3 \leq G' \leq 43.0$$

For a given set of fluidized bed particle properties and operating conditions, the correlations shown in Figure 48 or Figure 49 may be used to estimate the value of $[(K_L a)_c/Pe_L]$. Knowing the value of Pe_L from Figure 44 determines

the value of $(K_L a)_c$. Thus, the dispersion model mass transfer coefficient $(K_L a)_{DM}$ for the fluidized bed may be determined from Figure 48 or Figure 49.

The experimental results from Figure 40 through Figure 42 have been used to develop the correlation shown in Figure 50. In Figure 50, we see from the scatter of data that there is no discernible dependence of the ordinate on gas rate. Therefore, the correlation is presented for the experimental gas rate range, $14.3 \leq G' \leq 43.0$, and is assumed to be applicable anywhere within this range. A least-squares fit of the experimental data yields the following empirical relationship shown in Figure 50.

$$\{[(K_L a)^*]^{1/2}[(\Delta P)^*]^{1/4}\}/\{[\rho_p/\rho_m]^{1/2}\} = 2.10 - (0.0122)(L'/L'_{min})Re^{1/2}$$

$$26.2 \leq (L'/L'_{min})Re^{1/2} \leq 116.0 \qquad (17)$$

$$14.3 \leq G' \leq 43.0$$

For a given set of fluidized bed particle properties and operating conditions, the correlation shown in Figure 50 may be used to estimate the value of $[(K_L a)^*]^{1/2}[(\Delta P)^*]^{1/4}$. $(K_L a)^*$ may be determined from the correlations in Figure 48 or Figure 49 for the fluidized bed, along with the experimental data for the plain bubble column, Figure 19. Knowing the value of $(K_L a)^*$ determines the value of $(\Delta P)^*$. Thus, the correlation shown in Figure 50 may be used to compare mass transfer and pressure drop performance between a fluidized bed and a plain bubble column.

In order to determine how well the linear relationships shown in Figure 43 through Figure 50 fit the experimental data, it is desirable to make some statistical analyses. As defined by Draper [6], we have used two statistical measures, σ^2_{yx} and R^2. σ^2_{yx} is the variance of the experimental data points

about the least-squares line. For a perfect fit of the data points, σ^2_{yx} will be zero, therefore a small value of σ^2_{yx} close to zero is desirable. R^2 is the percentage of the total variation about the mean value of the ordinate which is explained by the least-squares line. For a perfect fit of the data points, R^2 will be 100%, therefore a large value of R^2 close to 100% is desirable. The following values of σ^2_{yx} and R^2 have been determined for the correlations shown in Figure 43 through Figure 50.

For Figure 43

$$\sigma^2_{yx} = 0.0100$$
$$R^2 = 99.8\%$$

For Figure 44

$$\sigma^2_{yx} = 0.0158$$
$$R^2 = 92.3\%$$

For Figure 45

$$\sigma^2_{yx} = 0.00700$$
$$R^2 = 84.8\%$$

For Figure 46

$$\sigma^2_{yx} = 0.00813$$
$$R^2 = 85.7\%$$

For Figure 47

$$\sigma^2_{yx} = 0.00838$$
$$R^2 = 86.5\%$$

For Figure 49

$$\sigma^2_{yx} = 0.00702$$
$$R^2 = 84.7\%$$

For Figure 50

$$\sigma^2_{yx} = 0.0312$$
$$R^2 = 73.5\%$$

The foregoing values of σ^2_{yx} and R^2 indicate that the linear relationships shown in Figure 43 through Figure 49 are reasonably good fits of the experimental data. The correlation in Figure 50 is only fair. Considering the complexity of a three phase fluidized bed, considerable scatter of experimental data is not unexpected.

The variables of importance in the development of the correlations shown in Figure 43 through Figure 50 were known from the literature [3, 9, 18]. From this starting point, the correlations have been developed empirically. The correlations shown in Figure 43 through Figure 50 are applicable over a fairly large range of fluidized bed particle properties and operating conditions. The range of particle size investigated was between 0.0625" to 0.1875", and the range of particle density investigated was between 0.0938 lb_m/in^3 to 0.322 lb_m/in^3. The range of liquid mass velocity was between 4.27×10^4 to 13.27×10^4 $lb_m/hr\text{-}ft^2$, and the range of gas mass velocity was between 14.3 to 43.0 $lb_m/hr\text{-}ft^2$.

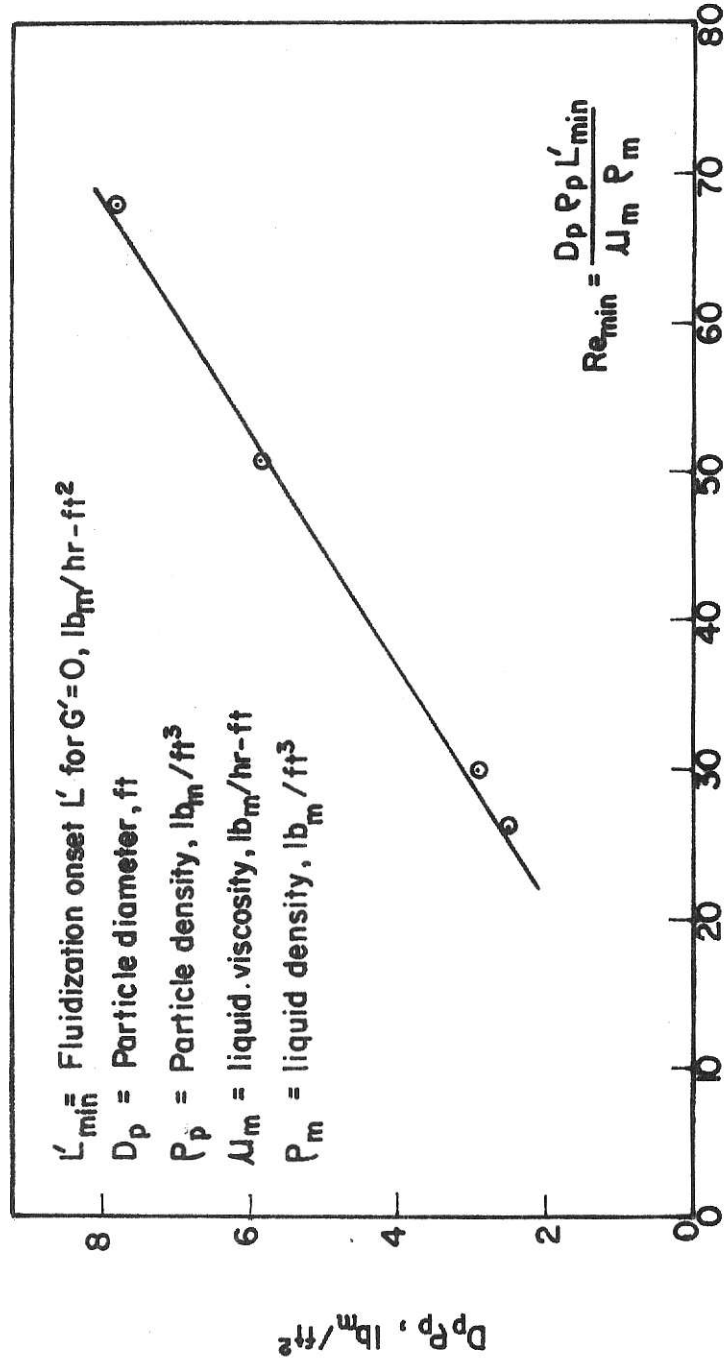

Fig. 43. Dependence of L'_{min} on particle properties.

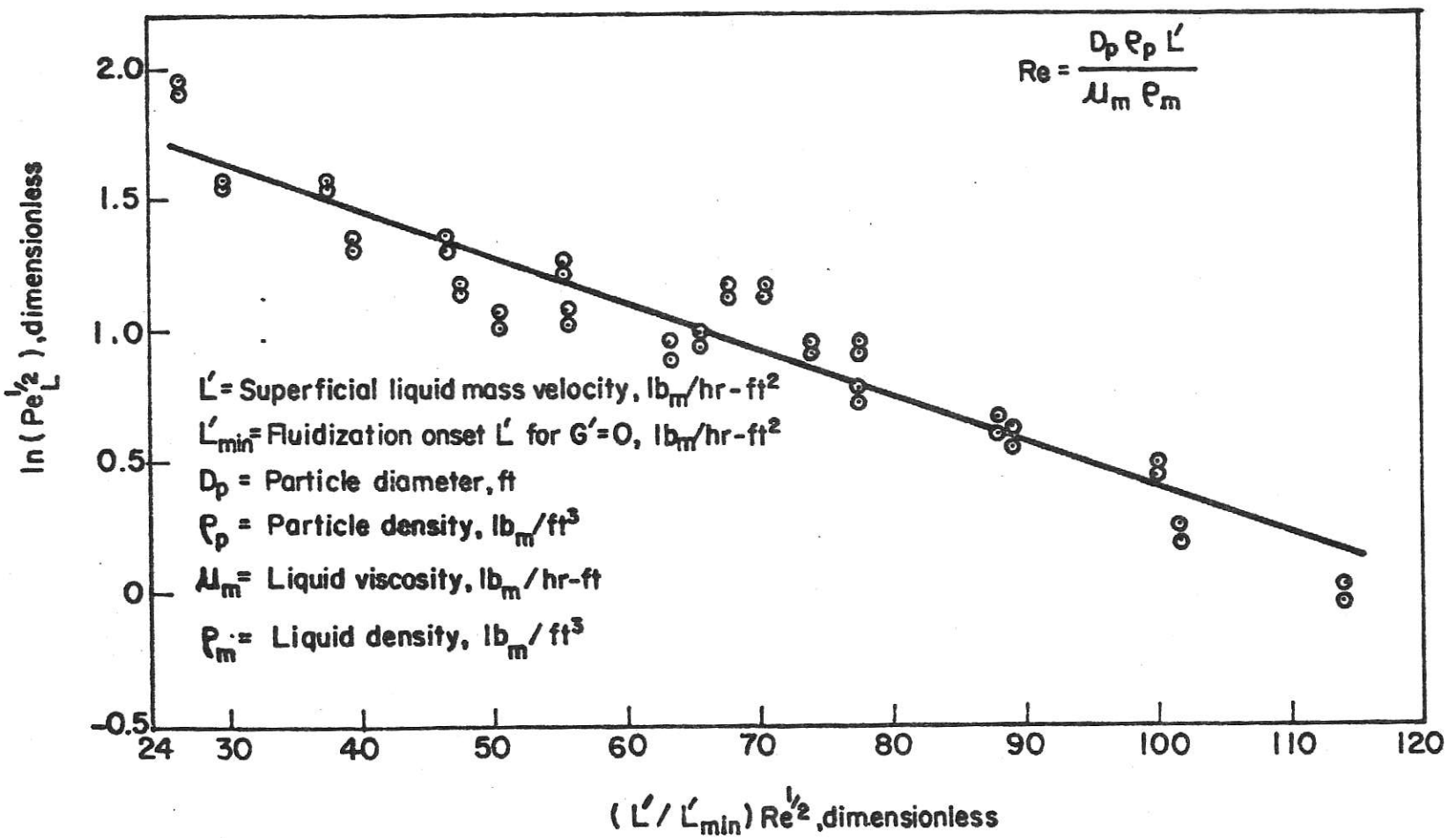

Fig.44. Axial liquid phase Peclet number correlation for $14.3 \leq G' \leq 43.0$, $lb_m/hr-ft^2$.

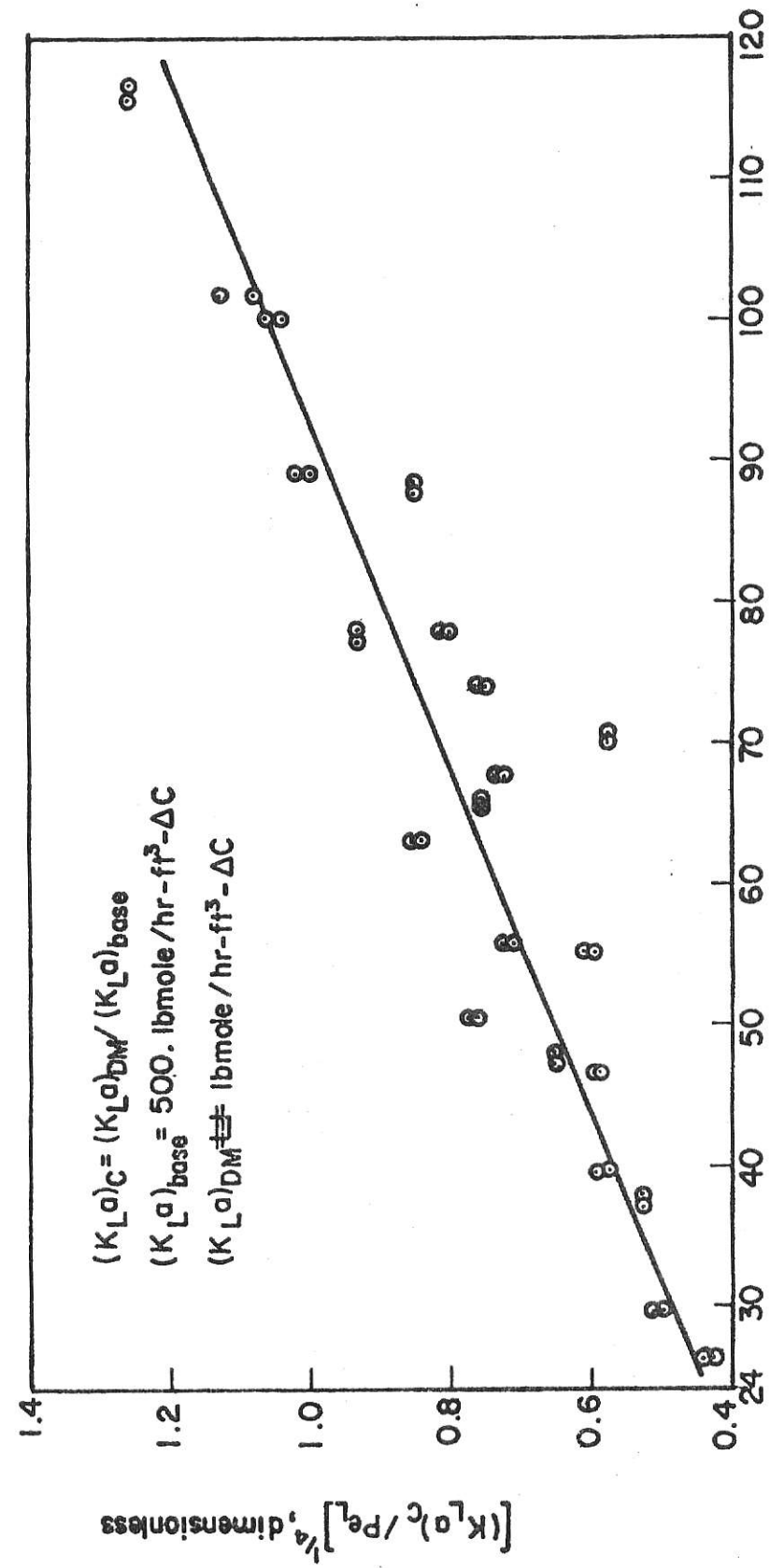

Fig.45. Fluidized bed mass transfer coefficient correlation for $G' = 14.3, lb_m/hr\text{-}ft^2$.

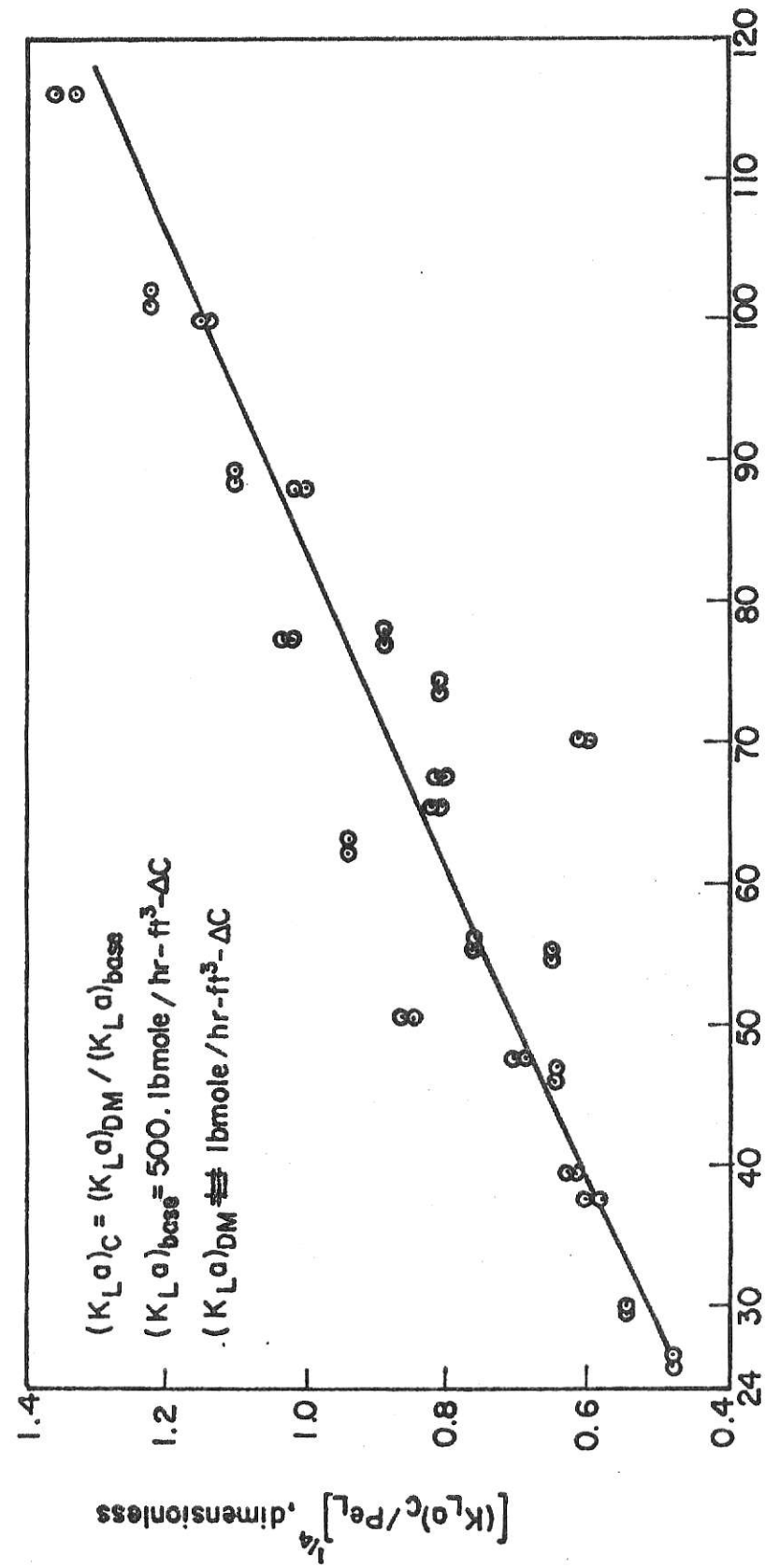

Fig. 46. Fluidized bed mass transfer coefficient correlation for $G' = 28.6, lb_m/hr\text{-}ft^2$.

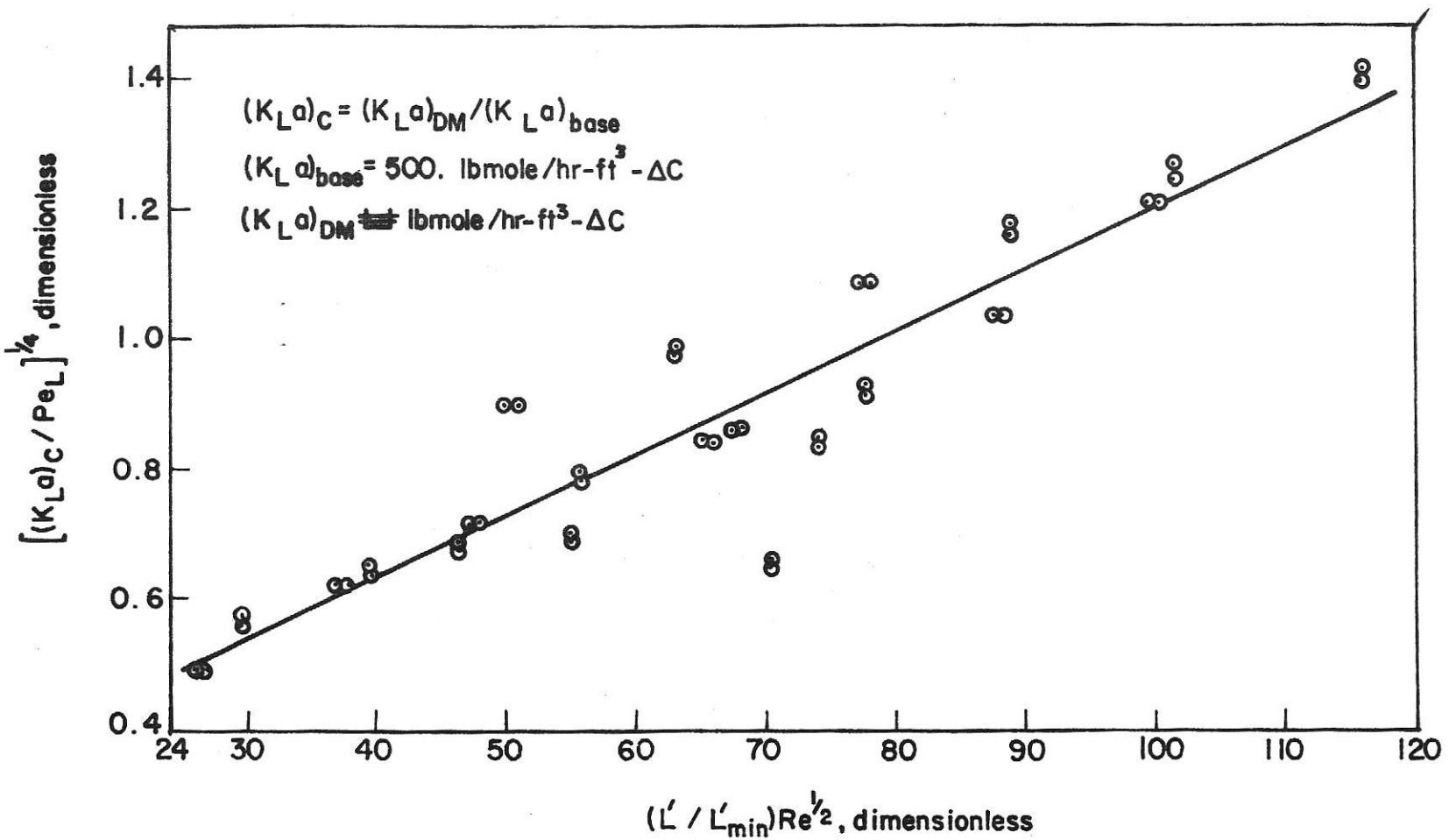

Fig. 47. Fluidized bed mass transfer coefficient correlation for G'=43.0, lb_m/hr-ft^2.

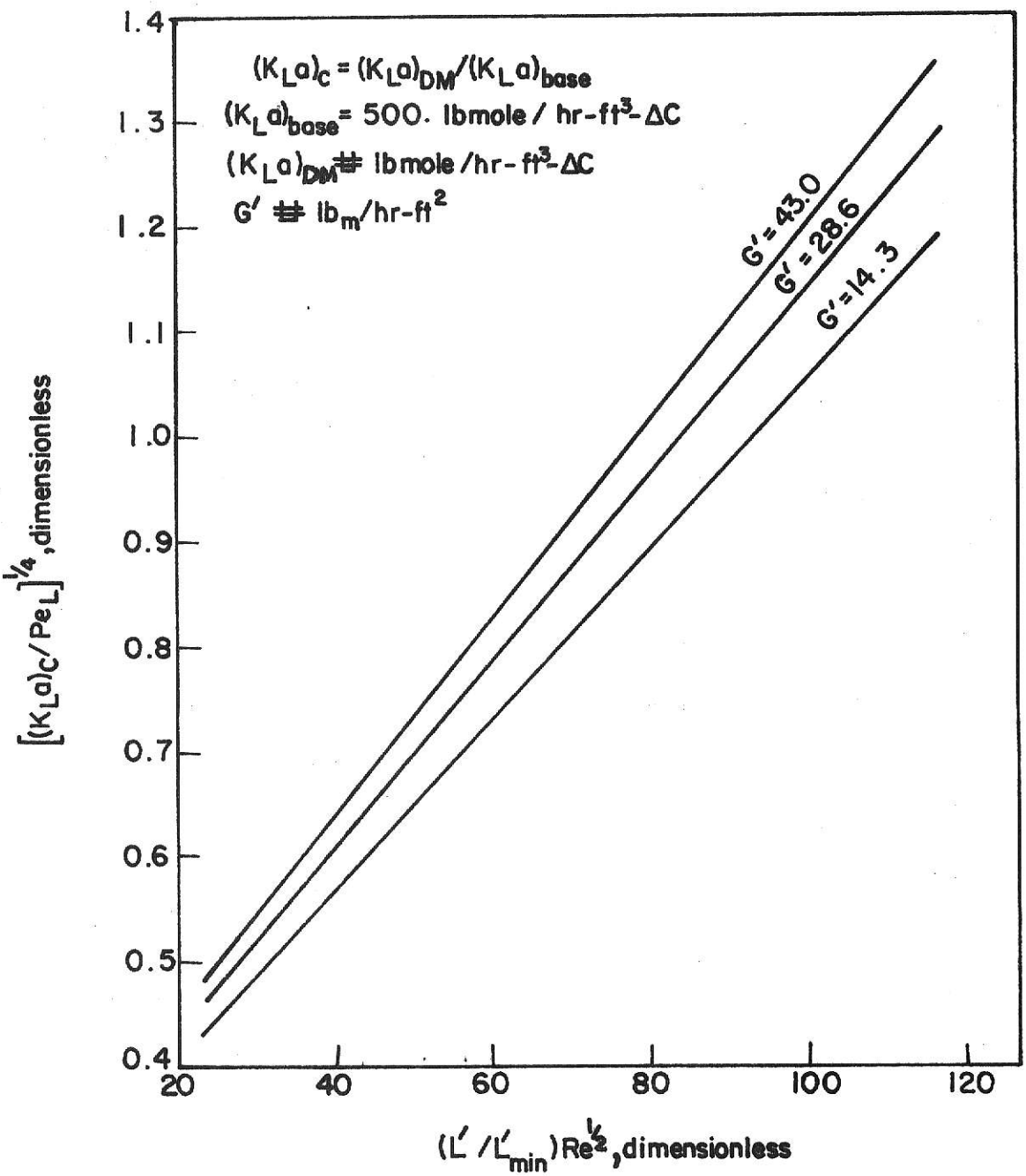

Fig.48. Comparison of fluidized bed mass transfer correlations at different gas rates.

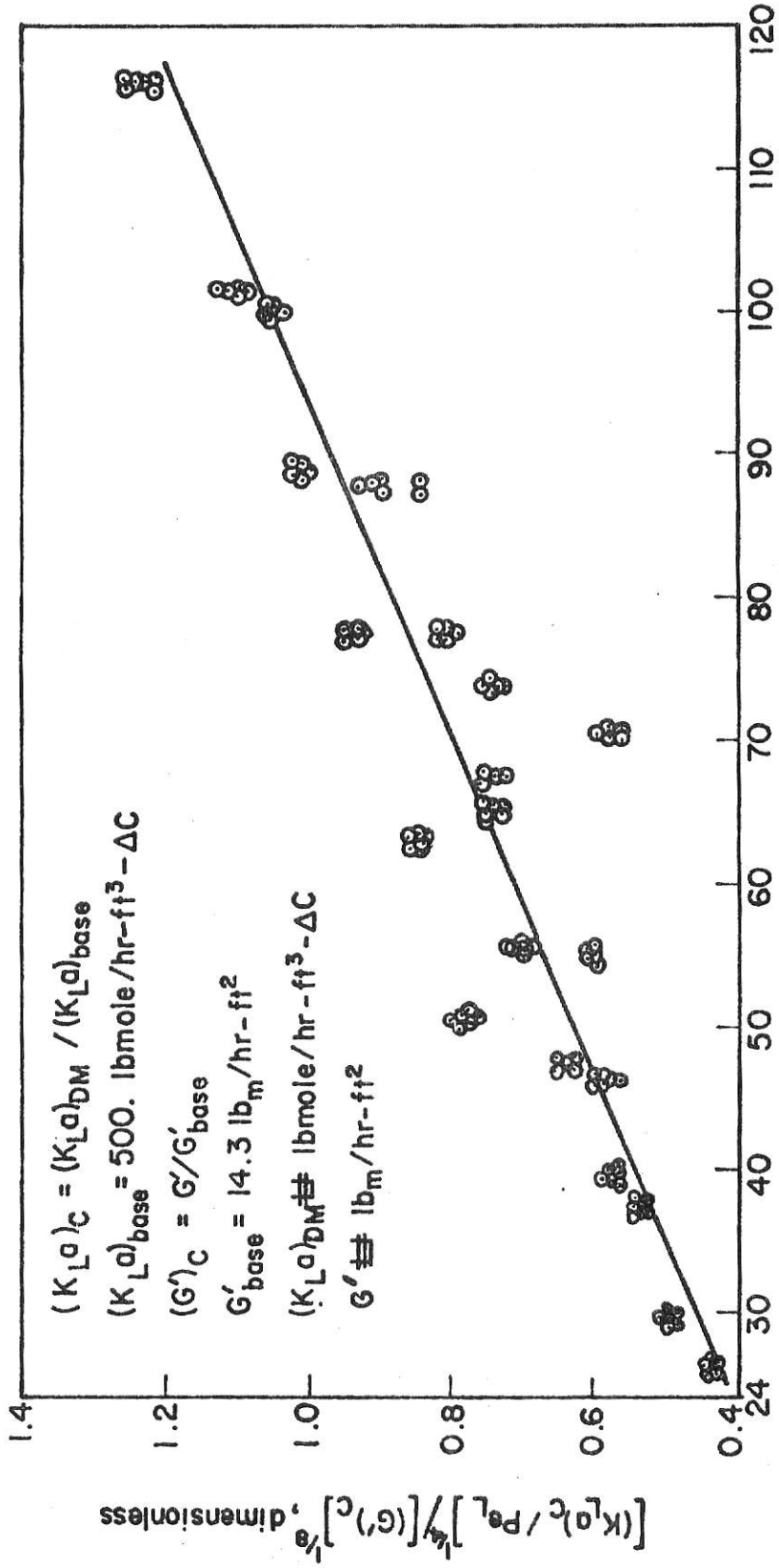

Fig.49. Fluidized bed mass transfer correlation for $14.3 \leqq G' \leqq 43.0$, lb$_m$/hr-ft^2.

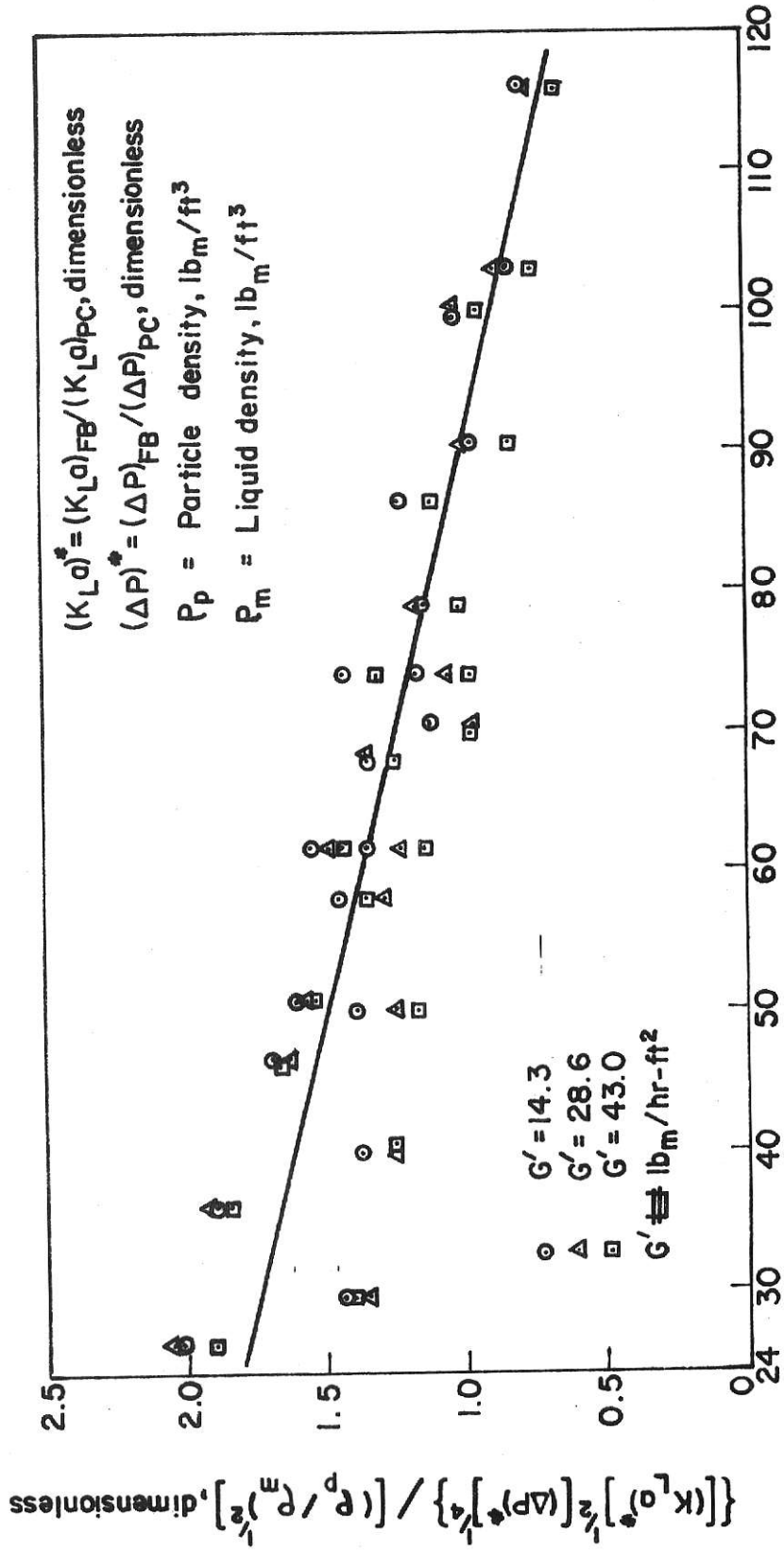

Fig.50. Correlation for comparison of mass transfer and pressure drop between fluidized beds and plain bubble column for $14.3 \leq G' \leq 43.0$, $lb_m/hr\text{-}ft^2$.

D. Application of Results.

This work has shown that the mass transfer performance of three phase fluidized beds can be considerably better than that of the conventional bubble column. It has also been shown that the type of fluidized bed material employed has a significant effect upon mass transfer performance. This work indicates that large particles of high density material produce the best mass transfer performance.

The experimental results obtained for the O_2-H_2O system have direct application in the field of sewage treatment. The use of the three phase fluidized bed for oxygen absorption in waste water could prove to be a considerable improvement over the conventional gas bubbling technique. Also, in the production of protein from hydrocarbons, the three phase fluidized bed is applicable to the problem of oxygen absorption by the liquid phase hydrocarbon.

The results of this work suggest that the three phase fluidized bed might be used to enhance the mass transfer performance of many two phase systems. This includes liquid-liquid systems as well as gas-liquid systems. Any operation which contacts a continuous and dispersed phase would be a possible area for application of the three phase fluidized bed.

Application of the experimental results obtained in this work can only be strictly applied over the range of fluidized beds and operating conditions investigated. Also, problems related to scaleup from laboratory equipment to industrial size equipment would probably be encountered. However, it is felt that reasonable estimates can be made for the design of large scale three phase fluidized beds from the results of this research work. A design example follows.

E. Design Example.

Suppose that we are given the following information

1. O_2-H_2O system.
2. Required liquid processing rate = 100.GPM.
3. Liquid temperature = 20.°C.
4. 3/32" brass spheres are available for the fluidized bed material.
5. A gas rate of 15. lb_m/hr is available.

With the above information given, let us pose the following design problems

1. Design a three phase fluidized bed absorption system based on the dispersion model, for which $\Gamma_e = 0.10$.
2. Design a conventional bubble column absorption system at the same operating conditions determined in Problem 1 based on the dispersion model, for which $\Gamma_e = 0.10$.
3. Make a comparison of the two designs determined in Problem 1 and Problem 2.

Solution to Problem 1

$$D_p = 3/32" = 7.82\text{x}10^{-3} \text{ ft}$$

$$\rho_p = 0.316 \text{ lb}_m/\text{in}^3 = 5.46\text{x}10^2 \text{ lb}_m/\text{ft}^3$$

$$\mu_{m_{20°C}} = 1.005 \text{ cp.} = 2.43 \text{ lb}_m/\text{hr-ft}$$

$$\rho_{m_{20°C}} = 0.998 \text{ gm/cm}^3 = 62.3 \text{ lb}_m/\text{ft}^3$$

$$D_p\rho_p = (7.82\text{x}10^{-3} \text{ ft})(5.46\text{x}10^2 \text{ lb}_m/\text{ft}^3) = 4.27 \text{ lb}_m/\text{ft}^2$$

From Figure 43 for $D_p\rho_p = 4.27\ lb_m/ft^2$

$$[Re_{min}]^{1/2} = 39.0$$

$$Re_{min} = (39.)^2 = 1520.$$

$$L'_{min} = \frac{(Re_{min})\mu_m\rho_m}{D_p\rho_p}$$

$$L'_{min} = \frac{(1520.)(2.43\ lb_m/hr\text{-}ft)(62.3\ lb_m/ft^3)}{(4.27\ lb_m/ft^2)} = 5.39x10^4\ lb_m/hr\text{-}ft^2$$

For the correlations developed in Figure 44 through Figure 50, $1 \leq [L'/L'_{min}] < 2$. Therefore, assume that we operate at a value of L' such that

$$[L'/L'_{min}] = 1.5$$

Thus

$$L' = (1.5)(5.39x10^4\ lb_m/hr\text{-}ft^2) = 8.10x10^4\ lb_m/hr\text{-}ft^2$$

Required liquid processing rate = 100 GPM = $4.99x10^4\ lb_m/hr$

Therefore

$$\text{Required column cross sectional area} = \frac{4.99x10^4\ lb_m/hr}{8.10x10^4\ lb_m/hr\text{-}ft^2} = 0.616\ ft^2$$

$$\text{Required column diameter} = \sqrt{\frac{(4)(0.616\ ft^2)}{\pi}} = 0.886\ ft = 10.63"$$

Thus

$$G' = \frac{15.0\ lb_m/hr}{0.616\ ft^2} = 24.4\ lb_m/hr\text{-}ft^2$$

From Figure 44

$$Re = \frac{D_p \rho_p L'}{\mu_m \rho_m} = \frac{(4.27\ lb_m/ft^2)(8.10 \times 10^4\ lb_m/hr\text{-}ft^2)}{(2.43\ lb_m/hr\text{-}ft)(62.3\ lb_m/ft^3)} = 2280.$$

$$[L'/L'_{min}]Re^{1/2} = (1.5)(2280.)^{1/2} = 71.6$$

From Figure 44 for $[L'/L'_{min}]Re^{1/2} = 71.6$ and $14.3 \leq G' \leq 43.0$

$$\ln[Pe_L^{1/2}] = 0.90$$

$$Pe_L = [e^{0.90}]^2 = 6.05$$

From Figure 48 for $[L'/L'_{min}]Re^{1/2} = 71.6$ and $G' = 24.4\ lb_m/hr\text{-}ft^2$

$$[(K_L a)_c/Pe_L]^{1/4} = 0.871$$

$$(K_L a)_c = (0.871)^4(Pe_L) = (0.575)(6.05) = 3.48$$

$$(K_L a)_{DM} = (K_L a)_c (K_L a)_{base} = (3.48)(500.\ lbmole/hr\text{-}ft^3\text{-}\Delta C)$$

$$= 1740.\ lbmole/hr\text{-}ft^3\text{-}\Delta C$$

From Figure 2c for $\Gamma_e = 0.10$ and $Pe_L = 6.05$

$$\beta = 1.746$$

Therefore

$$\sqrt{1 + \frac{4(R)_{DM}}{Pe_L}} = 1.746 \ ; \ (R)_{DM} = [\frac{Pe_L}{4}][(1.746)^2 - 1]$$

$$(R)_{DM} = [\frac{6.05}{4}][3.049-1] = 3.10$$

$$Z = \frac{(R)_{DM}\ L'}{(K_L a)_{DM}\ M_m}$$

$$= \frac{(3.10)(8.10\text{x}10^4\ \text{lb}_m\text{H}_2\text{O/hr-ft}^2)}{(1740.\ \text{lbmole O}_2\text{/hr-ft}^3 - \frac{\text{lbmole O}_2}{\text{lbmole H}_2\text{O}})(18.0\ \text{lb}_m\text{H}_2\text{O/lbmole H}_2\text{O})}$$

$$= 8.02\ \text{ft}$$

Therefore

Required column height = 8.02 ft

Solution to Problem 2

The operating conditions are to be the same as determined in Problem 1. Therefore

$$L' = 8.10\text{x}10^4\ \text{lb}_m\text{/hr-ft}^2$$

$$G' = 24.4\ \text{lb}_m\text{/hr-ft}^2$$

Required column diameter = 10.63"

From Figure 13 for $L' = 8.10\text{x}10^4$ and $14.3 \leq G' \leq 43.0$

$$[Pe_L]^{\frac{1}{2}} = 3.25\ ;\ Pe_L = (3.25)^2 = 10.57$$

From Figure 19 for $L' = 8.10\text{x}10^4$ and $G' = 24.4$

$$(K_L a)_{DM} = 363.\ \text{lbmole/hr-ft}^3 - \Delta C$$

From Figure 2c for $\Gamma_e = 0.10$ and $Pe_L = 10.57$

$$\beta = 1.454$$

Therefore

$$\sqrt{1 + \frac{4(R)_{DM}}{Pe_L}} = 1.454 \; ; \; (R)_{DM} = [\frac{Pe_L}{4}][(1.454)^2-1]$$

$$(R)_{DM} = [\frac{10.57}{4}][2.120-1] = 2.96$$

$$Z = \frac{(R)_{DM} L'}{(K_L a)_{DM} M_m}$$

$$= \frac{(2.96)(8.10 \times 10^4 \text{ lb}_m H_2O/\text{hr-ft}^2)}{(363. \text{ lbmole}O_2/\text{hr-ft}^3 - \frac{\text{lbmole}O_2}{\text{lbmole}H_2O})(18.0 \text{ lb}_m H_2O/\text{lbmole}H_2O)}$$

$$= 36.7 \text{ ft}$$

Therefore

Required column height = 36.7 ft

Solution to Problem 3

In order to make a thorough comparison of the two designs we must estimate the relative pressure drop for the two designs.

For the proposed design in Problem 1

$$[L'/L'_{min}] \; Re^{1/2} = 71.6$$

From Figure 50 for $[L'/L'_{min}] \; Re^{1/2} = 71.6$ and $14.3 \leq G' \leq 43.0$

$$\{[(K_L a)^*]^{1/2} [(\Delta P)^*]^{1/4}\}/\{[\rho_p/\rho_m]^{1/2}\} = 1.23$$

$$(K_L a)^* = (K_L a)_{FB}/(K_L a)_{PC} = \frac{1740.\ \text{lbmole/hr-ft}^3-\Delta C}{363.\ \text{lbmole/hr-ft}^3-\Delta C} = 4.79$$

$$[(K_L a)^*]^{1/2} = (4.79)^{1/2} = 2.19$$

$$[\rho_p/\rho_m]^{1/2} = \left[\frac{546.\ \text{lb}_m/\text{ft}^3}{62.3\ \text{lb}_m/\text{ft}^3}\right]^{1/2} = (8.77)^{1/2} = 2.96$$

Therefore

$$[(\Delta P)^*]^{1/4} = \frac{(1.23)(2.96)}{(2.19)} = 1.66$$

$$(\Delta P)^* = (1.66)^4 = 7.59$$

Thus, $(\Delta P)_{FB}/(\Delta P)_{PC} = 7.59$, when the fluidized bed and plain bubble column are of the same length and cross sectional area. Comparison of pressure drop based on column heights determined in Problem 1 and Problem 2 then gives

$$\Delta P_{(1)}/\Delta P_{(2)} = [7.59]\left[\frac{8.02\ \text{ft}}{36.7\ \text{ft}}\right] = 1.66$$

Thus, for the given operating conditions and the desired results, the design criteria are

1. Three phase fluidized bed of 3/32" brass spheres

   Required column diameter = 10.63"

   Required column height = 8.02 ft

2. Plain bubble column

   Required column diameter = 10.63"

   Required column height = 36.7 ft

3. Comparison of the two designs

$$Z_{(1)}/Z_{(2)} = [\frac{8.02 \text{ ft}}{36.7 \text{ ft}}] = 0.219$$

$$\Delta P_{(1)}/\Delta P_{(2)} = [7.59][\frac{8.02 \text{ ft}}{36.7 \text{ ft}}] = 1.66$$

CONCLUSIONS

For the types of three phase fluidized beds investigated in this work, the mass transfer performance of the three phase fluidized beds was found to be superior to that of the conventional bubble column. As seen from the design example, this superior mass transfer performance allows the three phase fluidized bed to be much shorter than the conventional bubble column for equivalent absorption requirements. The pressure drop, and consequently, the power requirements for the three phase fluidized bed are greater than for the conventional bubble column. Also, the conventional bubble column does not require a particle bed. In most cases, these two disadvantages are of minor concern compared to the much improved mass transfer performance provided by the three phase fluidized bed.

The empirical correlations developed in this work allow a three phase fluidized bed absorption system to be designed based on the dispersion model, which is a much more realistic model than either the plug flow or perfectly mixed models. Thus, the system design obtained from our empirical correlations should be reasonably reliable.

ACKNOWLEDGEMENT

The author wishes to express his sincere appreciation to Dr. Liang-tseng Fan for his constant support and advice during the process of this work, and to both the National Science Foundation and the Dow Chemical Company for their financial support.

REFERENCES

1. Agnew, J. B., Rev. Pure and Appl. Chem., 19, 208 (1969).

2. Burghart, A., and T. Zaleski, Chem. Eng. Sci., 23, 575-577 (1968).

3. Chen, B. H., and W. J. Douglas, Canadian Journal of Chem. Eng., 47, 113-117 (1969).

4. Dakshinamurty, P., V. Subrahmanyam, and J. N. Rao, Ind. Eng. Chem. Process Des. Develop., 10, 322-327 (1971).

5. Danckwerts, P. V., Chem. Eng. Sci., 2, 9-11 (1953).

6. Draper, N. R., and H. Smith, "Applied Regression Analysis," p. 7-16, John Wiley and Sons, New York (1968).

7. Drew, T. B., G. R. Cokelet, J. W. Hoopes, and T. Vermeulen, "Advances in Chemical Engineering," Vol. 7, p. 124-126, Academic Press, New York (1968).

8. Kadlec, R. H., Ph. D. thesis, Dept. Chem. Eng., University of Michigan, Ann Arbor (1962).

9. Leva, M., "Fluidization," p. 15-111, McGraw-Hill, New York (1959).

10. Levenspiel, O., "Chemical Reaction Engineering," p. 242-281, John Wiley and Sons, New York (1962).

11. Levenspiel, O., and W. K. Smith, Chem. Eng. Sci., 6, 189 (1957).

12. Levich, V. G., "Physiochemical Hydrodynamics," Prentice-Hall, New Jersey (1962).

13. Maxon, W. D., and M. J. Johnson, Ind. Eng. Chem., 45, 2554 (1953).

14. Ostergaard, K., Chem. Eng. Sci., 20, 165-167 (1965).

15. Ostergaard, K., and P. I. Theisen, Chem. Eng. Sci., 21, 413-417 (1966).

16. Perry, J. H., "Chemical Engineers Handbook," 4th ed., p. 14-6, McGraw-Hill, New York (1963).

17. Stewart, P. S., and J. F. Davidson, Chem. Eng. Sci., 19, 319-322 (1964).

18. Treyball, R., "Mass Transfer Operations," p. 227-240, McGraw-Hill, New York (1955).

NOMENCLATURE

A = fluidized bed cross sectional area, ft^2

C = liquid phase O_2 concentration, lbmole O_2/lbmole H_2O

C^* = liquid phase O_2 concentration at the gas-liquid interface, lbmole O_2/lbmole H_2O

$\bar{C}$ = $C^* - C$, lbmole O_2/lbmole H_2O

C_o = bulk liquid phase tracer concentration at t = 0 based on the liquid holdup, gm/ml

$C(t)$ = exit liquid phase tracer concentration as a function of time, gm/ml

D = apparent axial liquid phase dispersion coefficient, ft^2/hr

D_m = axial liquid phase dispersion coefficient, ft^2/hr

D_p = particle diameter, ft or in.

D_t = column diameter, ft

E_f = energy for fluidization, lb_f.ft/hr

E_{fT} = total energy for fluidization, lb_f.ft/hr

$E(\theta)$ = exit age distribution for an impulse input of tracer, dimensionless

G' = superficial gas mass velocity based on A, $lb_m/hr\text{-}ft^2$

$(G')_c$ = G'/G'_{base}, dimensionless

G'_{base} = smallest experimental gas rate, $lb_m/hr\text{-}ft^2$

G_f = superficial fluid mass velocity, $lb_m/hr\text{-}ft^2$

G_{mf} = minimum fluidization velocity required, $lb_m/hr\text{-}ft^2$

H = Henry's law equilibrium constant, atm./mole fraction

k = proportionality constant, $hr/lb_f\text{-}ft$

$K_L a$ = overall volumetric mass transfer coefficient based on a unit volume of fluidized bed, lbmole/hr-ft^3-ΔC

$(K_L a)'$ = overall volumetric mass transfer coefficient based on a unit volume of liquid, lbmole/hr-ft^3-ΔC

$(K_L a)_c$ = $(K_L a)_{DM}/(K_L a)_{base}$, dimensionless

$(K_L a)_{base}$ = 500. lbmole/hr-ft^3-ΔC

$(K_L a)^*$ = $(K_L a)_{FB}/(K_L a)_{PC}$, dimensionless

L' = superficial liquid mass velocity based on A, lb_m/hr-ft^2

L'_{min} = fluidization onset L' for $G' = 0$, lb_m/hr-ft^2

M_m = liquid molecular weight, lb_m/lbmole

P_{atm} = atmospheric pressure, atm.

$\bar{P}$ = average fluidized bed operating pressure, atm.

$\bar{P}_{O_2}$ = oxygen partial pressure, atm.

Pe_L = $L'Z/\rho_m D$, dimensionless axial liquid phase Peclet number

ΔP = pressure drop, in.Hg or lb_f/ft^2

$(\Delta P)^*$ = $(\Delta P)_{FB}/(\Delta P)_{PC}$, dimensionless

R = $(K_L a)M_m Z/L'$, dimensionless absorption number

R' = $(K_L a)'\varepsilon_m M_m Z/L'$, dimensionless absorption number

R^2 = percentage of the total variation about the mean value of the ordinate which is explained by the least-squares line, %

Re = $D_p \rho_p L'/\mu_m \rho_m$, dimensionless particle Reynolds number

Re_{min} = $D_p \rho_p L'_{min}/\mu_m \rho_m$, dimensionless particle Reynolds number at the fluidization onset point

t = time, sec

T_L = liquid temperature, °C

u = liquid velocity, ft/hr

W = weight of the particle bed, lb_f

x = fluidized bed length, ft

z = x/Z, dimensionless

Z = total fluidized bed length, ft

Z_s = settled particle bed length, ft

Greek Letters

α = D_e/D, dimensionless

β = $\sqrt{1 + 4R/Pe_L}$, dimensionless

β' = $\sqrt{1 + 4R'/Pe_L}$, dimensionless

ε_g = volume fraction occupied by gas, dimensionless

ε_m = volume fraction occupied by liquid, dimensionless

ε_p = volume fraction occupied by particles, dimensionless

ρ_F = fluid density, lb_m/ft^3

ρ_g = gas density, lb_m/ft^3

ρ_m = liquid density, lb_m/ft^3

ρ_p = particle density, lb_m/ft^3

σ^2 = variance of the C(t) distribution, dimensionless

σ^2_{yx} = variance of experimental data points about the least-squares line, dimensionless

θ = t/τ, dimensionless time

τ = mean liquid residence time based on the liquid holdup, sec

Γ = $\bar{C}/\bar{C}_i$, dimensionless

μ = fluid viscosity, cp.

μ_m = liquid viscosity, $lb_m/hr\text{-}ft$

Additional subscripts

DM - pertains to the dispersion model

PF - pertains to the plug flow model

FB - pertains to the three phase fluidized bed

PC - pertains to the plain bubble column

i - pertains to inlet conditions

e - pertains to exit conditions

(1) - pertains to a hypothetical three phase fluidized bed design

(2) - pertains to a hypothetical plain bubble column design

APPENDIX

I. Derivation of the Model Equations with the Overall Volumetric Mass Transfer Coefficient Based on a Unit Volume of Fluidized Bed.

The assumptions made in the development of the model equations are

1. Steady state operation prevails.
2. The O_2-H_2O solution is very dilute. Therefore, $L'_{in} = L'_{out} = L'$.
3. The principal resistance to mass transfer resides in the liquid phase.
4. The gas-liquid interface is in equilibrium. The interface is at the temperature of the liquid and the prevailing system pressure.
5. All mass transfer takes place in the fluidized bed.
6. The rate of dispersion in the radial direction is infinite, and the dispersion coefficient in the axial direction is finite and constant.
7. Wall effects have a negligible influence on the performance of the fluidized bed.

Referring to Figure 51, a liquid phase oxygen balance on the differential section Δx of the three phase fluidized bed yields

$$\text{output} = \text{input} + \text{production} \tag{A-1}$$

$$\text{output} = \left[\frac{L'CA}{M_m}\right]_{out} - \left[\frac{\rho_m}{M_m} D_m \varepsilon_m A \frac{dC}{dx}\right]_{out} , \text{ lbmoles } O_2/\text{hr} \tag{A-2}$$

$$\text{input} = \left[\frac{L'CA}{M_m}\right]_{in} - \left[\frac{\rho_m}{M_m} D_m \varepsilon_m A \frac{dC}{dx}\right]_{in} , \text{ lbmoles } O_2/\text{hr} \tag{A-3}$$

$$\text{production} = (K_L a)\, A\Delta x\, (C^* - C) , \text{ lbmoles } O_2/\text{hr} \tag{A-4}$$

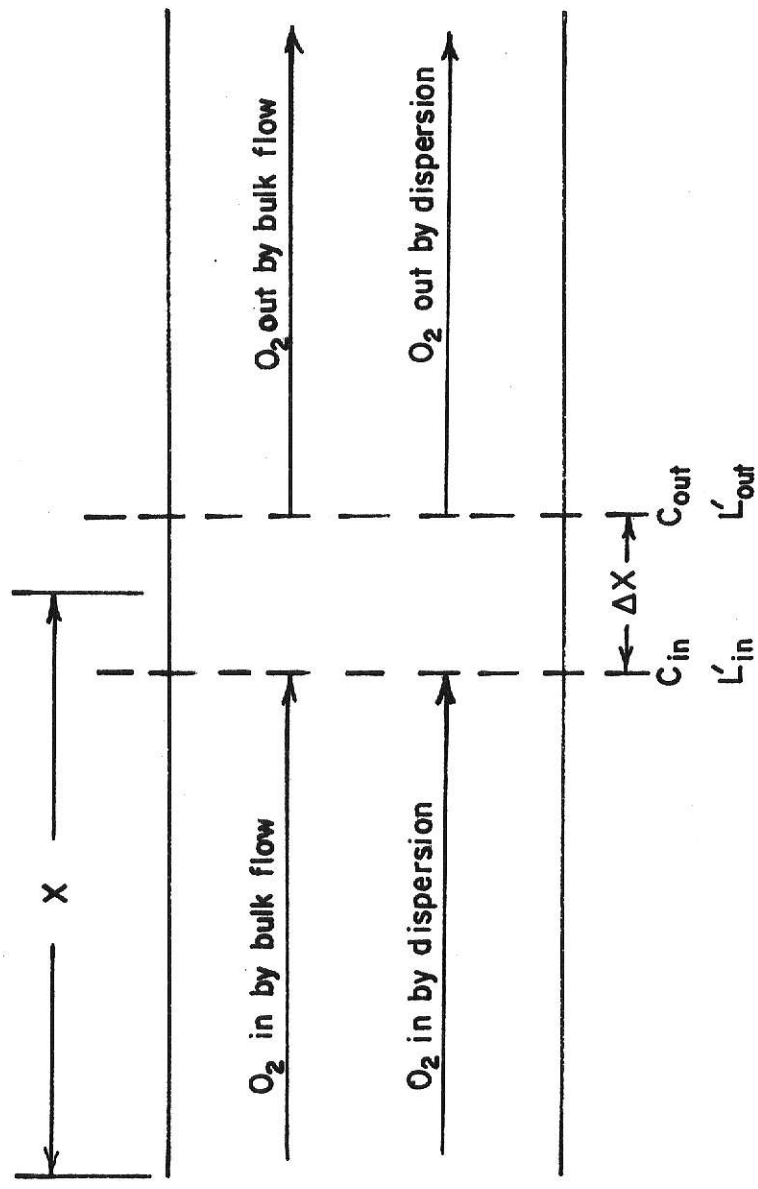

Fig.51. Schematic of three phase fluidized bed differential section.

where

ρ_m = liquid density, lb_m/ft^3

M_m = liquid molecular weight, $lb_m/lbmole$

D_m = axial liquid phase dispersion coefficient, ft^2/hr

ε_m = volume fraction occupied by liquid, dimensionless $(\frac{ft^3 H_2O}{ft^3})$

C = liquid phase O_2 concentration, lbmole O_2/lbmole H_2O

C^* = liquid phase O_2 concentration at the gas-liquid interface, lbmole O_2/lbmole H_2O

x = fluidized bed length, ft

A = fluidized bed cross sectional area, ft^2

L' = superficial liquid mass velocity based on A, $lb_m/hr\text{-}ft^2$

K_La = overall volumetric mass transfer coefficient based on a unit volume of fluidized bed, $lbmole/hr\text{-}ft^3\text{-}\Delta C$

We now define an apparent axial liquid phase dispersion coefficient such that, $D = D_m \varepsilon_m$. Using this definition, and substitution of Equation (A-2) through Equation (A-4) into Equation (A-1) yields

$$\left[\frac{L'CA}{M_m}\right]_{out} - \left[\frac{\rho_m}{M_m} DA \frac{dC}{dx}\right]_{out} = \left[\frac{L'CA}{M_m}\right]_{in} - \left[\frac{\rho_m}{M_m} DA \frac{dC}{dx}\right]_{in} + (K_La)\, A\Delta x\, (C^*-C) \qquad (A\text{-}5)$$

where

D = apparent axial liquid phase dispersion coefficient, ft^2/hr

Division of Equation (A-5) by A followed by rearrangement yields

$$\frac{L'}{M_m}(C_{out}-C_{in}) - \left[\frac{\rho_m}{M_m} D\right]\left[\left(\frac{dC}{dx}\right)_{out} - \left(\frac{dC}{dx}\right)_{in}\right] - (K_La)\, \Delta x\, (C^*-C) = 0 \qquad (A\text{-}6)$$

Division of Equation (A-6) by Δx and taking the limit as Δx approaches zero yields

$$\left[\frac{\rho_m}{M_m} D\right] \frac{d^2C}{dx^2} - \left[\frac{L'}{M_m}\right] \frac{dC}{dx} + (K_L a)(C^*-C) = 0 \qquad \text{(A-7)}$$

According to Danckwerts [5], the boundary conditions are

$$C = C_i + \left[\frac{\rho_m D}{L'}\right] \frac{dC}{dx} \quad \text{at} \quad x = 0^+ \qquad \text{(A-8)}$$

$$\frac{dC}{dx} = 0 \quad \text{at} \quad x = Z^- \qquad \text{(A-9)}$$

where

C_i = liquid phase O_2 concentration at x = 0, lbmole O_2/lbmole H_2O

Z = total fluidized bed length, ft

Let

$$\bar{C} = C^* - C \text{ , lbmole } O_2\text{/lbmole } H_2O \qquad \text{(A-10)}$$

$$\bar{C}_i = C^* - C_i \text{, lbmole } O_2\text{/lbmole } H_2O \qquad \text{(A-11)}$$

$$\bar{C}_e = C^* - C_e \text{, lbmole } O_2\text{/lbmole } H_2O \qquad \text{(A-12)}$$

$$\Gamma = \bar{C} \ / \ \bar{C}_i \text{, dimensionless} \qquad \text{(A-13)}$$

$$\Gamma_e = \bar{C}_e \ / \ \bar{C}_i \text{, dimensionless} \qquad \text{(A-14)}$$

$$z = x \ / \ Z \text{ , dimensionless} \qquad \text{(A-15)}$$

where

C_e = liquid phase O_2 concentration at x = Z, lbmole O_2/lbmole H_2O

Thus

$$\frac{dC}{dx} = - \frac{d\bar{C}}{dx} = - \left[\frac{\bar{C}_i}{Z}\right] \frac{d\Gamma}{dz} \qquad \text{(A-16)}$$

$$\frac{d^2C}{dx^2} = -\frac{d}{dx}\left(\frac{d\bar{C}}{dx}\right) = -\left[\frac{\bar{C}_i}{Z^2}\right]\frac{d^2\Gamma}{dz^2} \tag{A-17}$$

Substitution of Equation (A-16) and Equation (A-17) into Equation (A-7) followed by simplification yields

$$\left[\frac{\rho_m D}{L'Z}\right]\frac{d^2\Gamma}{dz^2} - \frac{d\Gamma}{dz} - \left[\frac{(K_L a)M_m Z}{L'}\right]\Gamma = 0 \tag{A-18}$$

Substitution of Equation (A-10), Equation (A-11), Equation (A-15), and Equation (A-16) into Equation (A-8) followed by simplification yields

$$\Gamma = 1 + \left[\frac{\rho_m D}{L'Z}\right]\frac{d\Gamma}{dz} \quad \text{at} \quad z = 0^+ \tag{A-19}$$

Substitution of Equation (A-15) and Equation (A-16) into Equation (A-9) yields

$$-\left[\frac{\bar{C}_i}{Z}\right]\frac{d\Gamma}{dz} = 0 \quad \text{at} \quad z = 1^- \tag{A-20}$$

Let

$$R = \frac{(K_L a)M_m Z}{L'}\text{, dimensionless absorption number} \tag{A-21}$$

$$Pe_L = \frac{L'Z}{\rho_m D}\text{, dimensionless axial liquid phase Peclet number} \tag{A-22}$$

Substitution of Equation (A-21) and Equation (A-22) into Equation (A-18); Equation (A-22) into Equation (A-19), and simplification of Equation (A-20) yields the dimensionless equations [2]

$$[\frac{1}{Pe_L}] \frac{d^2\Gamma}{dz^2} - \frac{d\Gamma}{dz} - R\Gamma = 0 \qquad \text{(A-23)}$$

Boundary conditions

$$\Gamma = 1 + [\frac{1}{Pe_L}] \frac{d\Gamma}{dz} \quad \text{at} \quad z = 0^+ \qquad \text{(A-24)}$$

$$\frac{d\Gamma}{dz} = 0 \quad \text{at} \quad z = 1^- \qquad \text{(A-25)}$$

Case I.1. Plug flow model

If the liquid phase of the fluidized bed is in plug flow, then $D \to 0$ and $Pe_L \to \infty$. For this case, the exit boundary condition (Equation (A-25)) is not required and solution of Equation (A-23) and Equation (A-24) yields

$$\Gamma_e = EXP(-R) \qquad \text{(A-26)}$$

Case I.2. Dispersion model

If the liquid phase of the fluidized bed is not in perfect plug flow, then $D \neq 0$ and $Pe_L \neq \infty$. For this case, solution of Equation (A-23) through Equation (A-25) yields [5, 10]

$$\Gamma_e = \frac{4\beta EXP(Pe_L/2)}{(1+\beta)^2 EXP(\beta Pe_L/2) - (1-\beta)^2 EXP(-\beta Pe_L/2)} \qquad \text{(A-27)}$$

where

$$\beta = \sqrt{1 + 4R/Pe_L} \qquad \text{(A-28)}$$

Case I.3. Perfectly mixed model

If the liquid phase of the three phase fluidized bed is perfectly mixed, a differential oxygen balance is not required and Equation (A-1) becomes

$$\frac{L'C_e A}{M_m} = \frac{L'C_i A}{M_m} + (K_L a)\ AZ\ (C^*-C_e) \tag{A-29}$$

Division of Equation (A-29) by A followed by rearrangement yields

$$\frac{C_e - C_i}{C^* - C_e} = \frac{(K_L a)ZM_m}{L'} \tag{A-30}$$

Substitution of Equation (A-11), Equation (A-12), Equation (A-14) and Equation (A-21) into Equation (A-30) followed by rearrangement yields

$$\Gamma_e = \frac{1}{R + 1} \tag{A-31}$$

II. Derivation of the Model Equations with the Overall Volumetric Mass Transfer Coefficient Based on a Unit Volume of Liquid.

For this basis Equation (A-1), Equation (A-2), and Equation (A-3) are again applicable; however, the production term becomes

$$\text{production} = (K_L a)'(\varepsilon_m)\ A\Delta X\ (C^*-C),\ \text{lbmoles } O_2/\text{hr} \qquad \text{(A-32)}$$

where

ε_m = volume fraction occupied by liquid, dimensionless

$(K_L a)'$ = overall volumetric mass transfer coefficient based on a unit volume of liquid, lbmole/hr-ft^3-ΔC

Proceeding through the derivation as previously shown with the new production term yields

Case II.1. Plug flow model

$$\Gamma_e = \text{EXP}(-R') \qquad \text{(A-33)}$$

Case II.2. Dispersion model

$$\Gamma_e = \frac{4\beta'\text{EXP}(Pe_L/2)}{(1+\beta')^2\text{EXP}(\beta' Pe_L/2) - (1+\beta')^2\text{EXP}(-\beta' Pe_L/2)} \qquad \text{(A-34)}$$

Case II.3. Perfectly mixed model

$$\Gamma_e = \frac{1}{R' + 1} \qquad \text{(A-35)}$$

where

$$R' = \frac{(K_L a)'(\varepsilon_m) M_m Z}{L'}$$

$$\beta' = \sqrt{1 + 4R'/Pe_L}$$

III. Development of the Equations Describing the Tracer Model Employed.

The assumptions made in the development of the tracer model equations are

1. The tracer input is a perfect impulse function.
2. The system is closed. There is no liquid dispersion for $x < 0$ and $x > Z$.[1]
3. The rate of dispersion in the radial direction is infinite and the dispersion coefficient in the axial direction is finite and constant.

For a closed system, the variance of θ is defined as follows [10]

$$\text{var}(\theta) = \int_0^\infty (\theta-1)^2 \, E(\theta) d\theta \qquad \text{(A-36)}$$

where

θ = t/τ, dimensionless time

t = time, sec

τ = mean liquid residence time based on the liquid holdup, sec

$E(\theta)$ = exit age distribution for an impulse input of tracer, dimensionless

Equation (A-36) is equivalent to [10]

$$\sigma^2 = \frac{1}{\tau C_o} \int_0^\infty (t/\tau-1)^2 \, C(t) \, dt \qquad \text{(A-37)}$$

where

σ^2 = var(θ), dimensionless

[1] See Figure 52.

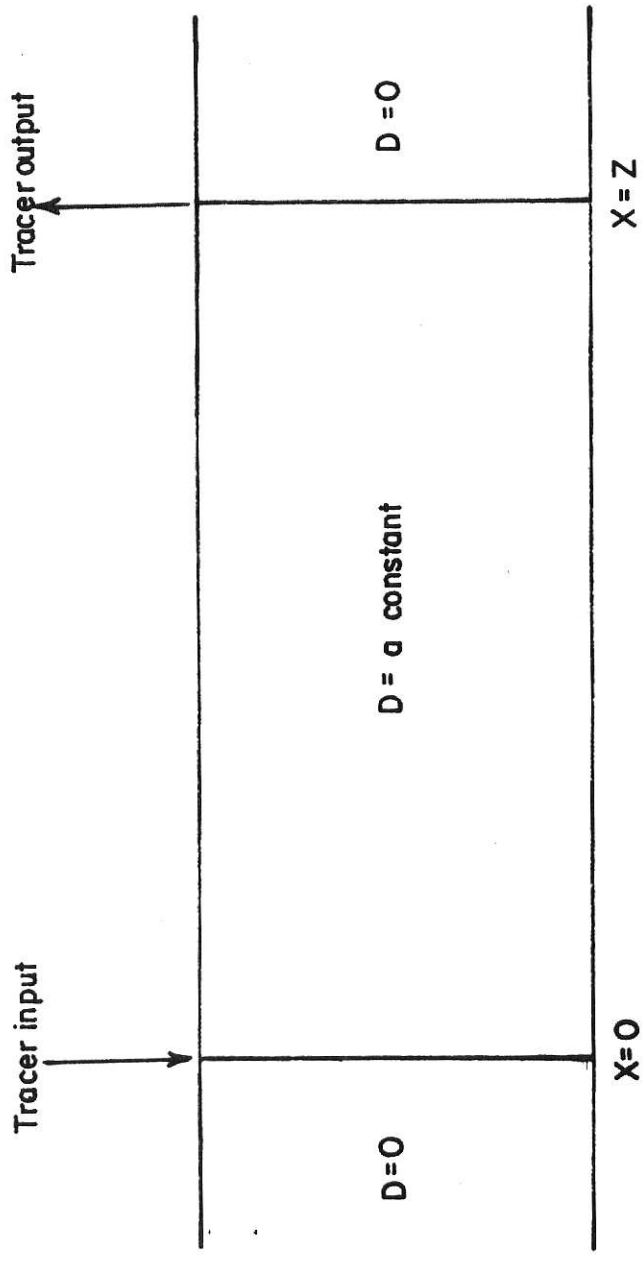

Fig.52. Schematic of tracer studies model.

C_o = bulk liquid phase tracer concentration at $t = 0$ based on the liquid holdup, gm/ml

$C(t)$ = exit liquid phase tracer concentration as a function of time, gm/ml.

For a closed system, σ^2 is given as [10, 11]

$$\sigma^2 = 2(1/Pe_L) - 2(1/Pe_L)^2 \, [1-EXP(-Pe_L)] \qquad (A-38)$$

Therefore

$$\sigma^2 = \frac{1}{\tau C_o} \int_o^\infty (t/\tau-1)^2 \, C(t)dt$$

$$= 2(1/Pe_L) - 2(1/Pe_L)^2 \, [1-EXP(-Pe_L)] \qquad (A-39)$$

Thus, the value of Pe_L is determined experimentally from $C(t)$ versus t curves for an impulse input of tracer.

IV. Sample Calculation of the Plug Flow Model Mass Transfer Coefficient $(K_L a)_{PF}$, Based on a Unit Volume of Fluidized Bed.

Case I.1. Sample Calculation

Fluidized bed

0.125" copper spheres

Operating conditions

$L' = 8.10 \times 10^4$ $lb_m/hr\text{-}ft^2$

$G' = 28.6$ $lb_m/hr\text{-}ft^2$

$Z = 1.56$ ft

$T_L = 18.0°C$

$P_{atm.} = 1.001$ atm.

$\bar{P} = 0.282$ atm.

where

G' = superficial gas mass velocity based on A, $lb_m/hr\text{-}ft^2$

T_L = liquid temperature, °C

$P_{atm.}$ = atmospheric pressure, atm.

$\bar{P}$ = average fluidized bed operating pressure, atm.

Thus

$\bar{p}_{o_2} = 1.001 + 0.282 = 1.283$ atm. (oxygen partial pressure)

For $\bar{p}_{o_2} = 1.283$ atm. and $T_L = 18.0°C$

$H = 3.91 \times 10^4$ atm./mole fraction (Henry's law constant) [16]

$$C^* = \left[\frac{\bar{p}_{o_2}/H}{1 - \bar{p}_{o_2}/H}\right]\left[\frac{Mwt.O_2}{Mwt.\ Soln.}\right] = \left[\frac{0.0000328}{1 - 0.0000328}\right]\left[\frac{32.0}{18.0}\right]$$

$$= 5.83 \times 10^{-5} \ \frac{gm\ O_2}{gm\ H_2O}$$

For $T_L = 18.0°C$; $\rho_{H_2O} = 0.998$ gm/ml

Therefore

$$C^* = (5.83\text{x}10^{-5})(0.998) = 5.82\text{x}10^{-5} \frac{\text{gm } O_2}{\text{ml } H_2O} \cong 58.20 \text{ mg } O_2/\ell \text{ Soln.}$$

The experimentally measured values of C_i and C_e are

$$C_i = 9.93 \text{ mg}/\ell$$

$$C_e = 35.95 \text{ mg}/\ell$$

Therefore

$$\Gamma_e = \left[\frac{58.20 - 35.95}{58.20 - 9.93}\right] = 0.461$$

Note that for the calculation of Γ_e, C ≠ mg/ℓ has been used instead of C ≠ lbmole O_2/lbmole H_2O. The units of C do not affect the value of Γ_e.

From Equation (A-26)

$$\Gamma_e = \text{EXP}[-R] \text{ , } \ln\Gamma_e = -R$$

$$R = \ln[1/\Gamma_e] = \ln[1/0.461] = \ln[2.170] = 0.775$$

From Equation (A-21)

$$R = \frac{(K_L a)M_m Z}{L'} \text{ , } K_L a = \frac{RL'}{M_m Z}$$

$$K_L a = \frac{(0.775)(8.10\text{x}10^4)}{(18.0)(1.56)} = 2235. \text{ lbmole/hr-ft}^3\text{-}\Delta C$$

Therefore

$$(K_L a)_{PF} = 2235. \text{ lbmole/hr-ft}^3\text{-}\Delta C$$

V. Sample Calculation of the Dispersion Model Mass Transfer Coefficient $(K_L a)_{DM}$, Based on a Unit Volume of Fluidized Bed.

Case I.2. Sample Calculation

Fluidized bed

0.125" copper spheres

Operating conditions

$L' = 10.20 \times 10^4$ $lb_m/hr\text{-}ft^2$

$G' = 28.6$ $lb_m/hr\text{-}ft^2$

$Z = 1.78$ ft.

$T_L = 18.0°C$

$P_{atm.} = 1.001$ atm.

$\bar{P} = 0.349$ atm.

For $\bar{p}_{O_2} = 1.350$ atm. and $T_L = 18.0°C$, $C^* \cong 60.95$ mg O_2/ℓ Soln.

The experimentally measured values of C_i and C_e are

$C_i = 9.93$ mg/ℓ

$C_e = 34.55$ mg/ℓ

Therefore

$$\Gamma_e = \left[\frac{60.95 - 34.55}{60.95 - 9.93}\right] = 0.518$$

Column cross sectional area $= 1/4\pi D^2 = 1/4\pi(2.0in)^2 = \pi in^2 = 2.18 \times 10^{-2} ft^2$

Liquid rate $= (10.20 \times 10^4\ lb_m/hr\text{-}ft^2)(2.18 \times 10^{-2} ft^2)(1 ft^3/62.3 lb_m)(1 hr/3600 sec)$

$= 9.90 \times 10^{-3} ft^3/sec$

Total Volume of fluidized bed $= (Z)(C.S.A.) = (1.78\ ft)(2.18 \times 10^{-2} ft^2)$

$= 3.88 \times 10^{-2} ft^3$

Volume occupied by copper spheres = $1.11 \times 10^{-2} ft^3$

Gas holdup = (0.23) V_{TOT} = $(0.23)(3.88 \times 10^{-2} ft^3) = 0.89 \times 10^{-2} ft^3$

Therefore

$$\text{Liquid holdup} = [3.88 \times 10^{-2}] - [1.11 \times 10^{-2}] - [0.89 \times 10^{-2}] = 1.88 \times 10^{-2} ft^3$$

$$\tau = \text{Liquid holdup/Liquid rate} = \frac{1.88 \times 10^{-2} ft^3}{9.90 \times 10^{-3} ft^3/sec} = 1.90 \text{ sec}$$

Concentration of NaCl tracer solution injected = 0.13 gm/ml

Volume of NaCl tracer solution injected = 4.0 ml

Total mass of NaCl injected = (0.13 gm/ml)(4.0 ml) = 0.52 gm.

Therefore

$$C_o = \frac{0.52 \text{ gm}}{1.88 \times 10^{-2} ft^3} = 27.7 \text{ gm/ft}^3 = 9.78 \times 10^{-4} \text{ gm/ml}$$

For $C_o = 9.78 \times 10^{-4}$ gm/ml, the recorder reading is

$$C_o = 37.1 \text{ c.u.}$$

Note that the NaCl tracer concentration in units of recorder reading (c.u.) is used for calculation of σ^2 instead of gm/ml. The units of C_o and C(t) do not affect the value of σ^2.

An experimental C(t) versus t curve is shown in Figure 53 for an impulse input of tracer (C_o=37.1 c.u.). Also, a plot of $[t/\tau-1]^2$ C(t) versus t is shown in Figure 53.

$$\tau C_o = (1.90 \text{ sec})(37.1 \text{ c.u.}) = 70.5 \text{ sec} \cdot \text{c.u.}$$

By graphical integration, the area under the $[t/\tau-1]^2$ C(t) versus t plot is 30.8 sec · c.u.

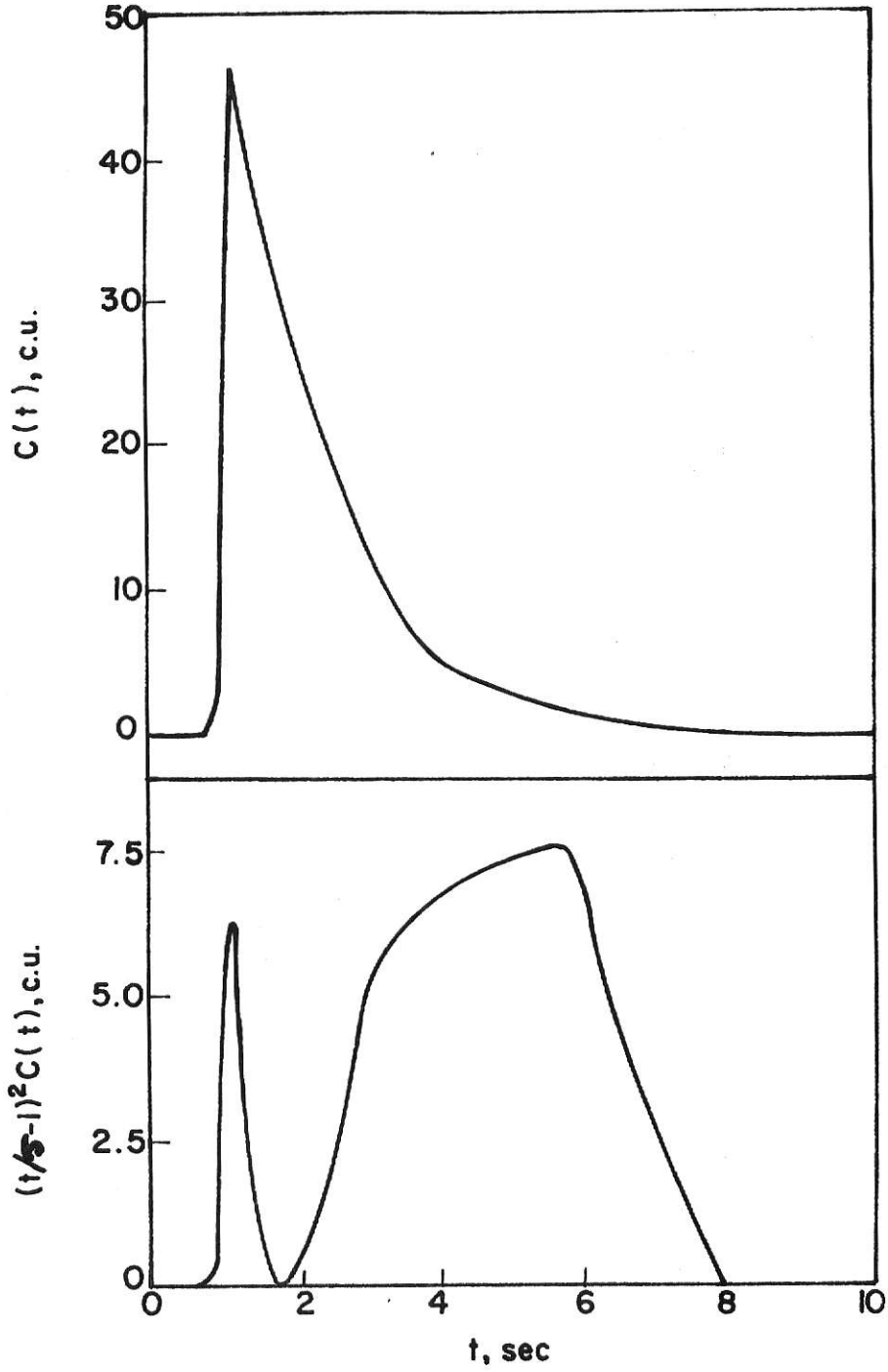

Fig.53. Experimental determination of σ^2.

Therefore

$$\int_0^\infty [t/\tau-1]^2 \, C(t)dt = 30.8 \text{ sec} \cdot \text{c.u.}$$

The tracer experiment was run twice for each experimental operating condition. For the second run

$$\int_0^\infty [t/\tau-1]^2 \, C(t)dt = 28.0 \text{ sec} \cdot \text{c.u.}$$

From Equation (A-37)

$$\sigma^2 = \frac{1}{\tau C_o} \int_0^\infty [t/\tau-1]^2 \, C(t)dt$$

Therefore

$$\sigma^2_{\text{1st Run}} = \frac{30.8 \text{ sec} \cdot \text{c.u.}}{70.5 \text{ sec} \cdot \text{c.u.}} = 0.436$$

$$\sigma^2_{\text{2nd Run}} = \frac{28.0 \text{ sec} \cdot \text{c.u.}}{70.5 \text{ sec} \cdot \text{c.u.}} = 0.398$$

From Figure 1, graphical solution of Equation (A-38) yields

$$Pe_{L_{\text{1st Run}}} = 2.95$$

$$Pe_{L_{\text{2nd Run}}} = 3.52$$

Using the average value of Pe_L for mass transfer calculations

$$Pe_L = \frac{2.95 + 3.52}{2} = 3.24$$

From Figure 2c, graphical solution of Equation (A-27) for $\Gamma_e = 0.518$ and

Pe_L = 3.24 yields

$$\beta = 1.389$$

From Equation (A-28) for Pe_L = 3.24 and β = 1.389, solution for R yields

$$R = 0.753$$

From Equation (A-21)

$$R = \frac{(K_L a)M_m Z}{L'} \quad ; \quad K_L a = \frac{RL'}{M_m Z}$$

$$K_L a = \frac{(0.753)(10.20 \times 10^4)}{(18.0)(1.78)} = 2400.\ \text{lbmole/hr-ft}^3\text{-}\Delta C$$

Therefore

$$(K_L a)_{DM} = 2400.\ \text{lbmole/hr-ft}^3\text{-}\Delta C$$

The preceding calculations are repeated for each type of fluidized bed as well as the plain bubble column, over the entire range of experimental operating conditions. The results are shown in Figure 4 through Figure 19.

VI. Fluidization Pressure Drop for a Three Phase Fluidized Bed.

From Equation (3-21) in Leva [9], the fluidization pressure drop for a two phase fluidized bed is given by

$$\Delta P = Z\varepsilon_p(\rho_p - \rho_F) \tag{A-40}$$

where

ΔP = pressure drop, lb_f/ft^2

Z = total fluidized bed length, ft

ε_p = volume fraction occupied by particles, dimensionless

ρ_p = particle density, lb_m/ft^3

ρ_p = fluid density, lb_m/ft^3

The total weight of the bed is

$$W = ZA\rho_p\varepsilon_p \tag{A-41}$$

where

W = weight of the particle bed, lb_f

A = fluidized bed cross sectional area, ft^2

Substitution of Equation (A-41) into Equation (A-40) yields

$$\Delta P = \left(\frac{W}{A}\right)\left(\frac{\rho_p - \rho_F}{\rho_p}\right) \tag{A-42}$$

For a three phase fluidized bed, the fluidization pressure drop will be a linear combination of the contributions of both gas and liquid phases. Application of this fact to Equation (A-42) yields

$$\Delta P = \left(\frac{W}{A}\right)\left(\frac{\rho_p - \rho_m}{\rho_p}\right)\left(\frac{\varepsilon_m}{\varepsilon_m + \varepsilon_g}\right) + \left(\frac{W}{A}\right)\left(\frac{\rho_p - \rho_g}{\rho_p}\right)\left(\frac{\varepsilon_g}{\varepsilon_m + \varepsilon_g}\right) \tag{A-43}$$

where

ε_m = volume fraction occupied by liquid, dimensionless

ε_g = volume fraction occupied by gas, dimensionless

We know that

$$\varepsilon_m + \varepsilon_g + \varepsilon_p = 1 \tag{A-44}$$

Substitution of Equation (A-44) into Equation (A-43) yields

$$\Delta P = \left(\frac{W}{A}\right)\left(\frac{\rho_p - \rho_m}{\rho_p}\right)\left(\frac{\varepsilon_m}{1-\varepsilon_p}\right) + \left(\frac{W}{A}\right)\left(\frac{\rho_p - \rho_g}{\rho_p}\right)\left(\frac{\varepsilon_g}{1-\varepsilon_p}\right) \tag{A-45}$$

Equation (A-45) gives the fluidization pressure drop for a three phase fluidized bed.

VII. Bed Expansion for a Three Phase Fluidized Bed.

According to Leva [9], the energy for fluidization (which constitutes bed expansion and particle movement) is given by

$$E_f = \frac{G_f W}{\rho_F} \tag{A-46}$$

where

E_f = energy for fluidization, lb_f.ft/hr

G_f = superficial fluid mass velocity, $lb_m/hr\text{-}ft^2$

W = weight of the particle bed, lb_f

ρ_F = fluid density, lb_m/ft^3

For a three phase fluidized bed, the energy for fluidization will be a linear combination of the contributions of both gas and liquid phases. Application of this fact to Equation (A-46) yields

$$E_{fT} = \left(\frac{L'W}{\rho_m}\right)\left(\frac{\varepsilon_m}{\varepsilon_m+\varepsilon_g}\right) + \left(\frac{G'W}{\rho_g}\right)\left(\frac{\varepsilon_g}{\varepsilon_m+\varepsilon_g}\right) \tag{A-47}$$

where

E_{fT} = total energy for fluidization, lb_f.ft/hr

L' = superficial liquid mass velocity, $lb_m/hr\text{-}ft^2$

G' = superficial gas mass velocity, $lb_m/hr\text{-}ft^2$

ρ_m = liquid density, lb_m/ft^3

ρ_g = gas density, lb_m/ft^3

ε_m = volume fraction occupied by liquid, dimensionless

ε_g = volume fraction occupied by gas, dimensionless

By using the fact that $\varepsilon_m + \varepsilon_p + \varepsilon_g = 1$, Equation (A-47) is readily reduced to the following form

$$E_{fT} = \left[\frac{W}{1-\varepsilon_p}\right]\left[\frac{L'\varepsilon_m}{\rho_m} + \frac{G'\varepsilon_g}{\rho_g}\right] \tag{A-48}$$

where

ε_p = volume fraction occupied by particles, dimensionless

According to Leva [9], the bed expansion is proportional to the energy for fluidization, thus, $\left(\frac{Z-Z_s}{Z_s}\right) \alpha E_{fT}$.

Therefore

$$\left(\frac{Z-Z_s}{Z_s}\right) = k\, E_{fT} \tag{A-49}$$

where

Z = total fluidized bed length, ft

Z_s = settled particle bed length, ft

k = proportionality constant, $hr/lb_f.ft$

Substitution of Equation (A-48) into Equation (A-49) yields

$$\left(\frac{Z-Z_s}{Z_s}\right) = \left[\frac{kW}{1-\varepsilon_p}\right]\left[\frac{L'\varepsilon_m}{\rho_m} + \frac{G'\varepsilon_g}{\rho_g}\right] \tag{A-50}$$

When k is known, Equation (A-50) gives the bed expansion for a three phase fluidized bed.

OXYGEN ABSORPTION IN THREE PHASE FLUIDIZED BEDS

by

MICHAEL PAUL NEWCOMER

B. S., Kansas State University, 1968

AN ABSTRACT OF A MASTER'S THESIS

submitted in partial fulfillment of the

requirements for the degree

MASTER OF SCIENCE

Department of Chemical Engineering

KANSAS STATE UNIVERSITY

Manhattan, Kansas

1971

ABSTRACT

The mass transfer characteristics of three phase fluidized beds for the absorption of oxygen in water were investigated in this work. Overall volumetric mass transfer coefficients were experimentally measured for the various types of three phase fluidized beds studied, and it was found that the mass transfer performance of three phase fluidized beds is very dependent on the particle properties of the bed. Large particles of high density material produce the best fluidized bed mass transfer performance.

Overall volumetric mass transfer coefficients were experimentally measured for an equivalent conventional bubble column, and it was found that the mass transfer performance of all types of three phase fluidized beds studied is superior to that of the conventional bubble column. It was concluded that the three phase fluidized bed may have considerable practicle value as a new efficient means of promoting oxygen transfer.

Overall volumetric mass transfer coefficients were determined based on two flow (mixing) models, the plug flow model and the dispersion model. The plug flow model assumes that axial liquid phase dispersion is zero, while the dispersion model relaxes this assumption. Therefore, for application of the dispersion model, axial liquid phase dispersion characteristics for the systems studied were experimentally determined. Mass transfer coefficients based on the plug flow and dispersion models were compared, with the expected result that dispersion model coefficients were larger than plug flow model coefficients.

Since it was determined experimentally that appreciable liquid dispersion existed in the systems studied, the mass transfer coefficient based on the dispersion model is a better approximation to the true mass transfer

coefficient than that based on the plug flow model. Thus, the empirical correlations obtained from the results of this work were developed from the dispersion model.

Empirical correlations were developed for the purpose of predicting liquid phase dispersion and mass transfer characteristics of three phase fluidized beds, and also for predicting mass transfer to pressure drop performance of three phase fluidized beds as compared to the conventional bubble column. The empirical correlations obtained were used for the hypothetical design of a three phase fluidized bed for the absorption of oxygen in water, and this design was compared to the hypothetical design of an equivalent conventional bubble column.